NTNU – Trondheim
Norwegian University of
Science and Technology

A novel hybrid flow cytometric approach to the Mussel micronucleus cytome assay

Tørris Sandsæter

August 15, 2023

Acknowledgments

This master's thesis in Environmental Toxicology was conducted as a part of the ENTRANS project (302378) at Sintef Ocean, Department of Climate and Environment.

For the completion of this work, I would like to thank my academic supervisor Julia Farkas for trusting me with this project, and for giving me the freedom to pursue the research questions that arose along the way.

I would like to thank my main supervisor professor Bjørn Munro Jenssen for giving me confidence in my project, and for invaluable help with the manuscript.

A special thanks goes to Chief Engineer Dag Altin, NTNU, for lending me state-of-the-art microscopy equipment, and for introducing me to techniques I didn't know I needed. Without your time and expertise, I would have settles for a lot less.

Lastly, I would like to send a my appreciation to Senior Researcher Bjørn Henrik Hansen; for making sport out of haemolymph sampling, and to Research Engineer Marianne Aas; for all the samples $>$ 95 % haemocyte events.

Abstract

In spite a widespread adoption of the Mussel micronucleus cytome assay in aquatic ecotoxicology (Bolognesi and Fenech, 2012), this protocol has several limitations or drawbacks; most of which has the potential to be addressed by flow cytometry. The manual scoring of cytogenic damage in defined subpopulations of bivalve haemocytes is a time-consuming and labor-intensive process with low throughput. The expanded scope of scoring subtle cytotoxic alterations and cell-types with a minimal reference material further aggravates this fact, and leaves too much room for subjectivity when the operator is faced with the complexity of haemocyte morphologies. Since certain cell types have been reported less sensitive to micronucleus (MN) induction (Venier et al., 1997), and others may exhibit morphological features deceptively similar cytotoxic alterations, confusions of this sort can possibly reduce the sensitivity and inter-lab comparability of the micronucleus cytome assay. For this reason, the overall aim of the present study was to develop a simple and reliable hybrid flow cytometric version of the Micronucleus cytome assay with haemocytes from the common blue mussel (*Mytilus edulis*). This approach would conserve the conventional scoring of genotoxic biomarkers and apoptosis by light microscopy, but was aimed to streamline the scoring of necrotic haemocytes and perform the differential haemocyte count with a novel flow cytometric methodology. Here we show that the three morphologically distinct cell types of *M. edulis* are distinguishable according to light-scatter measurements because of their inherent differences in granularity and/or size. By utilizing their dissimilarities in density, staining affinities and Calcein AM efflux rates, we were able to characterize and identify each cell type by isopycnic separation, an optimized Eosin Y staining procedure and staining with the cell permeable fluorescent probe with Calcein AM. From these insights, we propose a rapid and reliable flow cytometric differential haemocyte count employing log Calcein (533/15 nm) and log SSC as primary discriminators. As the proposed methodology employs Calcein AM – this procedure can be combined with TO-PRO-3 Iodide for simultaneous scoring of necrotic haemocytes by a Calcein AM/TO-PRO^{TM}-3 Iodide viability assay that was developed and validated for this protocol. These procedures are proposed as faster and more reliable approach to scoring necrotic haemocytes and cell types in the Mussel micronucleus cytome assay with *M. edulis*. By letting the flow cytometer take some of the load off the operators shoulders, the proposed methodology has potential to improve the power and efficiency of the existing assay.

Sammendrag

Til tross for den utbredte bruken av musling mikronukleus cytom-assayet innen akvatisk økotoksikologi(Bolognesi and Fenech, 2012), så har denne protokollen flere begrensninger og utfordringer ved seg; hvorav de fleste kan bli håndtert ved flow cytometri. Manuel scoring av cytogenisk skade i definerte subpopulasjoner av musling-hemocytter er en tidkrevende og arbeidsintensiv prosess med lav kapasitet. Den utvidede omfanget av å vurdere subtile cytotoksiske endringer og celletyper fra et veldig begrenset referanse-materiale forverrer dette ytterligere, og gir rom for subjektivitet når operatøren står overfor den overveldende kompleksiteten i hemocytt morfologi. Ettersom visse celletyper er rapportert å være mindre følsomme for mikronukleus (MN)-induksjon (Venier et al., 1997), og andre kan vise morfologiske trekk som er forvekslingsvis lik cytotoksiske endringer, kan slike forviklinger muligens redusere følsomheten og mellom-laboratoriums sammenlignbarheten av musling mikronukleus cytom assayrt. På bakgrunn av dette, var det overordnede målet med denne studien å utvikle en enkel og pålitelig hybrid flow-cytometrisk versjon av musling mikronukleus cytom assayet med hemocytter fra blåskjell (*Mytilus edulis*). Denne tilnærmingen vil beholde konvensjonell scoring av genotoksiske biomarkører og apoptose ved lysmikroskopi, men var rettet mot å forenkle scoringen av nekrotiske hemocytter og å utføre den differensielle hemocytt tellingen med en ny flow-cytometrisk metode. Her viser vi at de tre morfologisk distinkte celletypene i *M. edulis* kan skilles på grunnlag av lysspredningsmålinger på grunn av deres iboende forskjeller i granulæritet og/eller størrelse. Ved å utnytte ulikhetene deres i tetthet, fargestoff-affiniteter og Calcein AM-effluksrater, var vi i stand til å karakterisere og identifisere hver celletype ved tetthets-avhengif sentrifugering, en optimalisert Eosin Y farge-prosedyre og farging med den celle-permeable fluoriserende proben Calcein AM. Fra våre resultater foreslår vi en rask og pålitelig flow-cytometrisk differensiell hemocytt telling ved bruk av log Calcein (533/15 nm) og log SSC som primære diskriminatorer. Siden den foreslåtte metoden bruker Calcein AM - kan denne prosedyren kombineres med TO-PRO-3 Iodide for paralell scoring av nekrotiske hemocytter ved hjelp av en Calcein AM/TO-PRO^{TM}-3 Iodide vitalitetsanalys som ble utviklet og validert for denne protokollen. Disse prosedyrene blir foreslått som en raskere og mer pålitelig tilnærming til scoring av nekrotiske hemocytter og celletyper i musling mikronukleus cytom assayet med *M. edulis*. Ved å la flow-cytometeret ta noe av byrden av operatøren, har den foreslåtte metoden potensial til å forbedre

statistisk power og effektivitet til eksisterende analysen.

Contents

Figures

Tables

List of Code Listings

Acronyms

MeOH Methanol. 24, 26

7-AAD 7-Aminoactinomycin D. 9

ACB Anticoagulant Buffer. 15–18, 24–27, 29–33, 46, 47

Calcein AM Calcein AcetoxyMethyl. 7, 8, 10, 18, 21, 23, 37, 38, 47, 51, 65

DMSO Dimethyl Sulfoxide. 18, 45

dsDNA Double-Stranded DNA. 24, 25

EDTA Ethylenediaminetetraacetic acid. 15, 18, 31, 32, 47

Em$_{max}$ Emission Maximum. 8

Ex$_{max}$ Excitation Maximum. 8

FMO Fluorescence Minus One (control). 46

FSC Forward Scatter. 6, 20, 36, 37, 49

FSW Filtered Seawater. 13, 15, 16

MAS Modified Alserver's Solution. 15–18, 27, 29–32, 47

MFI Mean Fluorescent Intensity (arbitrary units). 25, 41, 44

MNi Micronuclei. 1, 9

MOA Mode Of Action. 1, 3

MPSS Marine Physiological Saline Solution. 16–21, 24, 27, 29–32, 47

N:C ratio Nuclear:Cytoplasmic ratio. 5, 19, 34

naMAS non-adjusted Modified Alsever's Solution (pH = 6.1). 19, 33

NBUDs Nuclear Buds. 2, 9

PAHs Polycyclic Aromatic Hydrocarbons. 3

SSC Side Scatter. 6, 20, 25, 36, 37, 48, 49

TBS Tris-Buffered Saline. 21, 22

TUNEL Terminal deoxynucleotidyl transferase (TdT) mediated dUTP Nick End Labeling. 9

Chapter 1

Introduction

1.1 The mussel micronucleus cytome Assay

Genetic toxicology is the study of substances that can cause damage to the genetic material of an organism (mutagens and genotoxicants), potentially leading to fixed mutations, chromosomal alterations and other potentially harmful nuclear anomalies. Allthough gene mutations form the genetic variation required for evolutionary adaptation (Harr, 2005), non-neutral changes to the genetic material more frequently result in detrimental effects to individuals and their offspring (Halligan, 2006). Genotoxic damage to somatic cells can contribute in cancer development (Hanahan and Weinberg, 2011), while damage to germ cells can lead to heritable genetic disorders in offspring (Mohrenweiser, 1991). Since these adverse outcomes represent long-term effects from chemical exposure, regulatory agencies must rely on early warning responses (biomarkers) from *in vivo* and *in vitro* bioassays for their risk assessments (ECHA, 2017). While the EU directive's mutagenicity testing is mainly focused on *in vivo* germ cell tests, genotoxicity testing of new substances serves an important role in the initial screening for potential carcinogenic effects (Broschinski et al., 1998 in: OSPAR, 2002) and for deciphering their mode of action (MOA) (Eastmond et al., 2009). In this context, the induction of micronuclei (MNi) represents a core biomarker of genotoxic effects in somatic test systems.

Micronuclei are small cytosolic membrane-enclosed chromatin bodies containing acentric chromosome fragments or whole lagging chromosomes, that remain outside the nucleus of daughter cells after cell division (Fenech et al., 2011). MNi with acentric fragments can originate from unrepaired or misrepaired DNA-breaks from interactions with clastogenic chemicals, while MNi containing whole chromosomes arise from indirect interactions of aneugenic chemicals with the replication apparatus during anaphase (Fenech et al., 2011). While the two structures may provide mechanistic information about the tested chemical, they are not readily distinguishable in standard cytological preparations (Natarajan, 1993). Without specific labeling of kinetochores or centromere-specific DNA, MNi provide general evidence for accumulated direct or indirect genotoxic damage during the

cell life (Lynch and Parry, 1993; Tucker and Preston, 1996).

These cytogenic damages are the major endpoints of micronucleus tests, which represent instrumental assays in the risk characterization of genotoxic compounds (UNEP, 2006; Davies and Vethaak, 2012; OECD, 2016a; OECD, 2016b; USEPA, 1998). Since there is a strong association between specific cytogenic alterations and tumorigenesis, the implementation of MN frequency as a biomarker in toxicological risk assessment is well justified (Zhang and Pellman, 2015, Mitelman, 1983 in: Tucker and Preston, 1996). Micronucleus tests are performed on dividing or newly divided cells, and are most typically used to assay genotoxic damage in cells from bone marrow samples and blood in the case of mammalian test systems (Heddle et al., 1983; Warheit, 2018). Since the marine environment represents the ultimate recipient and sink of toxicants from land-based sources (Davies and Vethaak, 2012), the deleterious effects of genotoxic compounds are not restricted to life on land.

Micronucleus tests were more recently extended for use in ecotoxicology, and represent one of the most prevalent biomarkers of genotoxicity in aquatic animals (Bolognesi and Hayashi, 2011). To date, such eco-genotoxicity assays have most notably been performed in fish erythrocytes (reviewed in D'Agostini and La Maestra, 2021) and in bivalve haemocytes (blood cells) and gill cells (reviewed in Bolognesi and Cirillo, 2014). Bivalve mussels have gained a central role as sentinels in marine ecotoxicology studies, and the widespread blue mussel (*Mytilus spp.*) has received a lot of attention in particular. Because of their sedentary lifestyle, limited biotransformation capacity (Beyer et al., 2017), low mortality (Ale et al., 2019; Costa et al., 2009) and ability to accumulate a wide range of pollutants as filter-feeders (Viarengo and Canesi, 1991); this hardy invertebrate has become the focal point of national monitoring programs for coastal pollution in more than 50 coastal nations (Cantillo, 1998 in: Beyer et al., 2017), including the Norwegian *Contaminants in coastal waters* program (Miljøgifter i kystområdene – MILKYS). In international marine pollution programs, micronucleus tests on caged mussels have been proposed as the only core biomarker of genotoxicity (Bolognesi and Fenech, 2012).

By following the cytome approach applied in mammalian systems (Fenech, 2007), Bolognesi and Fenech (2012) updated and refined the existing MN test for bivalve haemocytes and gill cells to include scoring of necrotic and apoptotic cells as endpoints of cytotoxicity. Nuclear buds (NBUDs) were also included as a biomarker of genotoxicity, although the mechanism leading to NBUD formation is not completely known (reviewed in Fenech et al., 2011). NBUDs are nuclear anomalies that are characterized by their morphological resemblance to MNi, except that they are connected to the main nucleus by a stalk of nucleoplasmic material (Fenech and Crott, 2002). In addition to scoring cytogenic damage (MNi and NBUDs) and cytotoxic alterations (necrosis and apoptosis), a differential count of the agranular and granular haemocytes cell types were included in the protocol presented by Bolognesi and Fenech. As these innate immune cells have been found to exhibit different immunocompetences with regard to phagocytic activ-

ity, encapsulation and the secretion of cytotoxic molecules in host defence (de la Ballina et al., 2022), changes in the circulating haemocyte cell types may possibly serve as indicators of stress and provide information on the immunological health status of mussels (Anderson, 1993).

Several contaminants have been shown to induce changes in the haemocyte profile of bivalves (Anderson, 1993). Among the tested contaminants, these include Cd^{2+} and Cd-based quantum dots (Rocha et al., 2014; Auffret and Oubella, 1994), Cu^{2+} (Pipe and Coles, 1995; Pipe et al., 1999), phenol (Fries and Tripp, 1980) and certain PAHs (Dyrynda et al., 1998; Dyrynda et al., 2000). Since the mussel micronucleus cytome assay includes a differential haemocyte count in combination with two biomarkers of cytotoxic damage, an integrated interpretation of these endpoints might provide mechanistic information about the immunomodulating effects of cytotoxic chemicals. Moreover, as increased hematopoiesis or regenerative hyperplasia from cytotoxic events increase the risk of neoplastic developments (Eastmond, 2012), the differential haemocyte count also has potential to indicate a non-receptor mediated MOA for substances that are not DNA-reactive. This possibility requires a differential haemocyte count that discriminates immature "pro-haemocytes" from mature cell types.

In spite the widespread adoption of the micronucleus cytome assay, this protocol has several limitations or drawbacks; most of which has the potential to be addressed by flow cytometry. First of all, the entire procedure is reported to take approximately 1 hour per individual mussel (Bolognesi and Fenech, 2012). If multiple sampling sites are employed with 10 individuals/site, the time required for a larger study can reach substantial proportions. Secondly, the added complexity of scoring cytotoxic alterations, genotoxic damages and performing differential counts in parallel might divert attention from the main endpoint. As MNi are rare events scored among a relatively small subset of cells ($>$ 1000 agranular haemocytes), a few false negatives can potentially have a significant effect on the MNi frequencies of mussels from sites with low contaminant levels. The third limitation is related to the complexity of the haemocyte cell types, and the operator's subjective interpretations or classification of these and their cytotoxic alterations in the haemocyte preparations.

The classification of bivalve haemocytes is a comprehensive literature that is dominated by a lack of scientific consensus (Hine, 1999). For operators that rely on the images provided by the protocol for their practical classification, the first inspection of a haemolymph preparation may not paint a picture that is all that intuitive. Bolognesi and Fenech (2012) proposed scoring of MNi in agranular haemocytes, which were characterized by their small size (3-4 µm), high nuclear:cytoplasmic (N:C) ratio and a lack or low abundance of cytoplasmic granules and organelles. As slight deviations from the staining protocol might produce striking differences in the overall staining result, the subjective interpretations of the observed cell types may produce large inter-operator variability in the scored cell population and the differential haemocyte count. This is highlighted by the fact that most operators fail to comment on the scored cell type (Bolognesi and Fenech,

2012), or erroneously score what they believe to be agranular haemocytes (e.g., Meng et al., 2020). Since the granular haemocytes of *M. galloprovincialis* are reportedly less sensitive to MN induction (Venier et al., 1997), confusion of this sort can possibly reduce the sensitivity and inter-lab comparability of the micronucleus cytome assay.

The difficulty of producing high quality preparations of haemolymph smears is another factor that might further complicate this issue. Haemolymph smears often have numerous staining artifacts and cells that are damaged during preparation. As a consequence, distinguishing cytotoxic alterations from staining artifacts may be challenging to operators without comprehensive training in histology or hematology. The identification of necrotic haemocytes based on extensive cytoplasmic vacuolation might be especially challenging in this context, as both granular cell types of *M. edulis* are phagocytic and often display numerous phagosomes in their cytoplasm (Moore and Lowe, 1977). Damaged cell membranes – and the paler cytoplasmic staining that results from it – may also be hard to distinguish from irrelevant staining artifacts.

In short, manual scoring of cytogenic damage in a defined population of bivalve haemocytes is a time-consuming and labor-intensive process with low throughput. The expanded scope of the micronucleus cytome assay further aggravates this fact, and a reference material consisting of a few microscope images leaves too much room for subjectivity in the identification of haemocyte cell types and cytotoxic alterations. As flow cytometers are permanent fixtures of contemporary cell biology labs, this high throughput cytologic instrument is availible to most ecotoxicologists involved in cellular work. With the capacity to differentiate single cells based on size, granularity and molecular markers, flow cytometry is a powerful tool for performing differential blood cells counts (Shapiro, 2004), as well as scoring necrotic and apoptotic cells (Shapiro, 2003). A hybrid flow cytometry/-microscopy protocol of the *Mussel micronucleus cytome assay* has therefore great potential to improve the power and efficiency of the existing methodology, while creating less room for subjectivity.

1.2 Classification of haemocyte subpopulations in *M. edulis*

Since the first written account on the subject of bivalve haemocyte classification (Cúenot, 1891, in: Cheng, 1980), several authors have devoted their attention to develop a unifying classification system for the amoebocytic blood cells of bivalve molluscs, more commonly known as haemocytes (Cheng, 1980; de la Ballina et al., 2022). The haemocytes of *Mytilus edulis*, *Mytilus galloprovincialis* and other commercially important species of the genus *Mytilus* have been encompassed by these efforts, which has created a substantial pool of literature on the haemocytes of this genus alone. Despite a lack of consensus for any unifying classification system for the haemocytes of this phylum at large, the literature that exists on the haemocytes of *M. edulis* generally agrees on the existence of three distinct subpopulations.

The first effort to classify the haemocytes of *M. edulis* was made by Moore and Lowe (1977). Much like other attempts to classify bivalve haemocytes at the time, this classification was based on the morphofunctional aspects of these cells – a system that has been extensively reviewed by Hine (1999). Moore and Lowe constructed a simple classification based on static morphological and ultrastructural characteristics of the haemocytes, combined with their phagocytic capacities (Moore and Lowe, 1977). From routine cytological staining, they identified three haemocyte subpopulations (or cell types): "(1) small basophilic hyaline cells or lymphocytes, (2) larger basophilic hemocytes with varying degrees of irregular cytoplasmic granulation and vacuolation, and (3) eosinophilic granular haemocytes or granulocytes" (Moore and Lowe, 1977). The small basophilic cells (4-6 μm) were generally spherical in outline, had a scant thin rim of basophilic hyaline (read: transparent) cytoplasm and a spherical nucleus – bearing resemblance to vertebrate lymphocytes. The larger granular basophils (7-10 μm) displayed less intense basophilic cytoplasm, lower nuclear:cytoplasmic (N:C) ratios and more irregularly shaped nuclei. The eosinophilic granulocytes were the largest cell type identified (7-12 μm). They had a regular spherical appearance, further characterized by a small round nucleus, low N:C ratio and a cytoplasm filled with spherical eosinophilic granules (0.5-1.0 μm).

Electron micrographs confirmed the existence of three ultrastructurally distinct morphologies. Except for a few mitochondria, the lymphocyte-like cells contained a scarcity of organelles and granules. This stood in sharp contrast to the larger granular basophils, which contained Golgi apparatus, phagosomes and smaller granular inclusions – possibly representing primary lysosomes. A phagocytosis assay with experimentally injected carbon particles revealed that both granular cell types displayed phagocytic properties, while the small lymphocyte-like cells did not show any evidence for this capacity (Moore and Lowe, 1977).

The morphological and ultrastructural findings of Moore and Lowe (1977) have since been confirmed by several investigators (Rasmussen et al., 1985; Renwrantz, 1990; Pipe, 1990; Nöel et al., 1994; Pipe et al., 1997; Wootton et al., 2003). From their stand-alone electron microscopical examinations, Pipe and colleagues (1990) made a distinction between granular haemocytes with small (0.2-0.3 μm) and large (0.5-1.5 μm) granules. By relating the two ultrastructural phenotypes to their cytological staining properties, investigators later demonstrated that the two cell types corresponded to the basophilic and eosinophilic granular haemocytes of Moore and Lowe (Pipe, 1990; Nöel et al., 1994). Thus, if reduced to its static morphological criteria, Moore and Lowe's classification of *M. edulis* haemocytes coincides with the original system of Cúenot (1891). This system generally recognized three types of haemocytes in bivalves: "(1) finely granular haemocytes, (2) coarsely granular haemocytes and (3) cells with very little cytoplasm surrounding the nucleus" (Cheng, 1984).

Leaning towards a phylum-wide two-categorical classification (hyalinocytes and granulocytes), Cheng (1981) argued that a distinction between the basophillic and eosinophilic granulocytes of *M. edulis* was artificial, as he saw them

as being immature and mature stages of the same cell type (granulocytes), respectively. From observations of what resembled (1) intermediate stages between the lymphocyte-like and larger basophilic cells and (2) a few smaller eosinophilic granulocytes (5-7 μm), Moore and Lowe (1977) had argued that the basophilic cells constituted a separate ontogenic lineage, with the larger phagocytic macrophages representing the final stage of maturation. This was further supported by observations of lymphocyte-like cells with mitotic figures, suggesting that it could be the stem cell of this lineage (Moore and Lowe, 1977). The notion that small lymphocyte-like basophils represented immature "prohemocyte" precursor cells was shared by Hine (1999), who argued that their basophilia indicated the presence of free ribosomes (immaturity), while their lack of cytoplasmic organelles precluded secretory or phagocytic functions.

Moore and Lowe's theory – as pointed out by Cheng (1984) – was primarily formulated through interpretive evaluations of morphological findings, rather than being based on direct ontogenic evidence. The classification of bivalve haemocytes should ideally be constructed on the basis of their ontogeny. However, mapping of ontogenic lineages among bivalve haemocytes has been tempered by the lack of availible molecular databases, no one unifying model species, combined with uncertainty regarding the hematompoietic tissue(s) and processes of bivalves (Hine, 1999; Smith et al., 2016; Pila et al., 2016; de la Ballina et al., 2022). With no real ontogenic evidence to work with, a careful assessment of availible morphological data may represent a better alternative, relative to a classification based solely on biochemistry and function (Hine, 1999).

1.2.1 Flow cytometric classification of *M. edulis* haemocytes

Almost two decades after flow cytometers became commercially availible in the 1970s (Shapiro, 2004), the application of these instruments started to gain traction within the field of invertebrate immunopathology (Fisher, 1988; Van Nguyen and Alfaro, 2019). Since the traditional characterization of bivalve haemocytes were largely based on morphological criteria such as size, granularity and staining affinities, the simultaneous measurement of forward scatter (FSC, ≈ size) and side scatter (SSC, internal complexity ≈ granularity) represented a far less subjective approach to their characterization (Ashton-Alcox and Ford, 1998; Allam et al., 2002; Mateo et al., 2009).

A detailed flow cytometric characterization of the haemocytes of *M. edulis* was undertaken by Le Foll et al., (2010), who were able to distinguish three subpopulations according to cell size and SSC. These comprised one population of small cells (7.14±0.05 μm) with low SSC, one population of larger cells (9.97±0.17 μm) with intermediate SSC and one population of large cells (10.08±0.24 μm) with high SSC. By running haemocytes stained with eosin – which is fluorescent in the green/yellow spectrum (Elfer et al., 2016; Koegl et al., 2020) – their results suggested that the latter subpopulation corresponded to eosinophilic granulocytes. However, these results were not visually verified by microscopy. The use of

flow cytometers equipped with cell sorting capabilities simplifies the process of verifying any classification derived from flow cytometric measurements (Shapiro, 2004). However, when extracting cells with known measured characteristics is not possible, the cells to be classified can be separated by other means prior to flow cytometric acquisition.

Since the three haemocyte cell types of *M. edulis* differ with regard to the size and density of their granules, researchers managed to physically separate the eosinophilic granulocytes from the two basophilic cell types by isopycnic centrifugation (Friebel and Renwrantz, 1995; Pipe et al., 1997). Depending on the fixative used, the whole haemocyte population separated into three or four distinct cell-bands in the interfaces of the gradient layers. The two basophillic cell types could be isolated in high purity from the upper cell band (lowest density), the eosinophilic granulocytes from the lower, while the intermediate fractions often consisted of varying proportions of all three cell types. Accompanied by the rapid growth of flow cytometric applications in invertebrate immunology, the progress made by Friebel and Renwrantz (1995) and Pipe, Farley and Coles (1997) meant that light scatter profiles could be assigned to specific cell types individually.

1.3 Cellular methods

The cytological alterations accompanied by necrotic and programmed cell death (e.g., apoptosis) can be detected and quantified at high throughput with contemporary flow cytometers. While the two mechanisms share the same faith, the cytotoxic alterations that characterize them can be distinguished by several parameters – individually or by discriminating assays (Shapiro, 2003). Since necrotic cell death is caused by damage to the cytoplasmic membrane, necrotic cells are primarily identified by loss of membrane integrity (Shapiro, 2003). Conversely, apoptosis can have several proximate causes (Bedoui et al., 2020), and the various structural and molecular alterations that proceed can be probed at different stages of the apoptotic process (Kari et al., 2022). Allthough laser scanning cytometry is the preferred method for detecting apoptotic cells (Darzynkiewicz et al., 2001), flow cytometric techniques have the advantage of being accessible, low-cost and highly versatile. In the present study, necrotic and apoptotic haemocytes were distinguished from viable cells by using the fluorescent dyes Calcein Acetoxymethyl ester (Calcein AM) and TO-PRO^{TM}-3 Iodide (ToPro3) and the fluorogenic peptide; Apo-15.

1.3.1 Calcein acetoxymethyl ester

Calcein acetoxymethyl ester (Calcein AM) is a cell-permeable esterase substrate commonly employed in viability assays and live cell imaging (Ramirez and Antczak, 2010). Similar to other electrically neutral fluorescein-derivatives, this small non-fluorescent molecule readily enters living cells through diffusion; where it is effectively trapped by intact cell membranes upon ester hydrolysis (Kaneshiro et

al., 1993). The retained poly-anionic Calcein molecule is highly fluorescent in the green spectrum (Ex_{max}/Em_{max}: 495/515 nm), and can be assayed by flow cytometry and epifluorescence microscopy (Wallach et al., 1959, in: Chiu and Haynes, 1977). Due to its insensitivity to pH in the physiological range, high photo-stability and superior cellular retention (Chiu and Haynes, 1977; Kaneshiro et al., 1993); Calcein AM is a versatile probe with several advantages over other commonly employed esterase substrates (Ramirez and Antczak, 2010).

One critical drawback of employing Calcein in standardized *in vitro* viability assays resides in the fact that the acetoxymethyl tetraester form is a substrate of mammalian P-glycoprotein (P-gp) efflux pumps (Liminga et al., 1995). Since different cell lines vary with regard to P-gp activity and hence the rate of Calcein accumulation, results may not be directly comparable across different cell lines (Ramirez and Antczak, 2010). On the other hand, this exact property has led to the utilization of Calcein AM as a fluorescent probe for assaying P-gp inhibitors (Di and Kerns, 2016). The inhibition of P-gp pumping activity results in an increased accumulation of hydrolyzed Calcein within cells, which can then be detected and quantified through its fluorescence (Tiberghien and Loor, 1996; Köhler and Stein, 2003).

Efflux pumps analogous to the mammalian P-gp and Multidrug Resistance-related protein (MRP) are also expressed in various bivalve tissues (Luckenbach and Epel, 2008; Luedeking et al., 2005), including haemocytes in *M. edulis* (Rioult et al., 2014). By using P-gp- and MRP-specific inhibitors, Rioult et al., (2014) demonstrated that a MRP-type transporter were responsible for pumping Calcein AM out of haemocytes in *M. edulis*, and that this activity was higher and more inducible in eosinophilic granulocytes compared to the other two cell types. While MRP-induction assayed through Calcein AM has been suggested as a potential biomarker for marine biomonitoring programs (Rioult et al., 2014; Minier and Moore, 1998), the resulting differential accumulation of Calcein might also represent a novel parameter for flow cytometric differential haemocyte counts in the common blue mussel.

1.3.2 Apo-15/TO-PRO-3 Iodide apoptosis assay

The Annexin-V/Propidium Iodide (PI) assay is considered a gold standard for monitoring cell death progression *in vitro* (reviewed in Van Engeland et al., 1998). This is a simple and feasible assay that is based on the differential (1) integrity of plasma membranes and (2) distribution of phosphatidylserine (PS) between bilipid layers of viable, necrotic and apoptotic cells (Jiang et al., 2016). In homeostasis, PS is actively translocated to the inner leaflet of the plasma membrane by flippases (Connor et al., 1992). As apoptotic cell death is induced, these flippases are cleaved by Caspases 3/7, and a PS-externalizing scramblase is irreversibly activated by the same mechanism (Verhoven et al., 1995; Suzuki et al., 2013). The consequent exposure of PS by apoptotic cells serves a ligand for phagocytic macrophages (Fadok et al., 1992) and persists throughout the whole apoptotic process

(Martin et al., 1995).

Annexin-V is a fluorogenic peptide that binds specifically to externalized PS in a Ca^{2+}-dependent manner (Andree et al., 1990; Martin et al., 1995). As the externalization of PS precludes the gradual loss of membrane integrity in early apoptotic cells, they are not stained by membrane impermeable dsDNA-binding dyes such as PI. But since internal PS is accessible through the permeabilized membranes of necrotic and late apoptotic cells, they are recognized as Annexin-V^+ PI^+ cells. Viable cells are double negative, while early apoptotic cells are stained with Annexin-V externally (Annexin-V^+ PI^-). To facilitate for multifluorescence measurements, PI can be replaced by other membrane impermeable dsDNA-binding dyes with far-red emission (e.g., ToPro3 or 7-AAD). (Jiang et al., 2016)

Apoptosis probes that bind extracellular target molecules have advantages over TUNEL assays and Caspase-binding probes, as they do not require cells to be permeabilized prior to staining (Del Bino et al., 1999). But, since Annexin-V requires extracellular Ca^{2+} (>1 mM) for optimal PS binding (Andree et al., 1990), this assay is not applicable with Ca^{2+}-free buffers or anticoagulant buffers containing divalent metal-chelators (e.g., EDTA). This property impairs the practical utility of Annexin-V in flow cytometric analyses of bivalve haemocytes, due to their rapid aggregation in the presence of free Ca^{2+} (Torreilles et al., 1999). On the bright side; a small fluorogenic peptide that binds PS in a Ca^{2+}-independent manner has recently been developed (Apo-15) (Barth et al., 2020). This new fluorogenic probe holds great potential for discriminating between viable, necrotic and early apoptotic haemocytes *in vitro*.

1.4 Objective

The overall aim of the present study was to develop a hybrid flow cytometric version of the Micronucleus cytome assay (Bolognesi and Fenech, 2012) with haemocytes from the common blue mussel (*Mytilus edulis*). This approach would conserve the conventional scoring of genotoxic biomarkers (MNi and NBUDs) and apoptosis by light microscopy, but was aimed to streamline the scoring of necrotic haemocytes and the differential haemocyte count with a novel flow cytometric methodology.

The overall aim was pursued by working towards the following objectives:

1. To develop a reliable sampling technique for the extraction of haemolymph from the posterior adductor muscle of *M. edulis*, such that the frequency of unsuccessful extractions and contaminating particles can be minimized.
2. To compare availible anticoagulant buffers/techniques with regard to their ability to inhibit haemocyte aggregation – without interfering with the targeted endpoints.
3. To characterize the different haemocyte cell types of *M. edulis* by conventional cytological criteria.

4. To test wether side scatter and the differential ability to efflux Calcein AM can be used to distinguish these cell types in suspensions of living haemocytes.
5. To develop a flow cytometric differential haemocyte count that estimates the relative proportions of haemocyte cell types discernible in haemocytes preparations stained with 3% Giemsa.
6. To develop and validate a flow cytometric assay for scoring necrotic haemocytes by Calcein AM/TO-PRO^{TM}-3 Iodide.

Chapter 2

Material and method

2.1 Material

2.1.1 Laboratory instruments

Instrument	Model	Manufacturer
Benchtop Flow Cytometer	BD Accuri^{TM} C6 Plus	BD Biosciences
Imaging Flow Cytometer	Cytosub	CytoBuoy
Upright microscope	Eclipse Ni-U	Nikon Corp
Upright microscope	Ecliplse 90i	Nikon Corp
Benchtop centrifuge	Centrifuge 5804 R	Eppendorf
Counting chamber	Bürker	Hirschmann-Laborgeräte

2.1.2 Chemicals

Chemicals	CAS-No.	Purity/grade	Supplier	State[a]
Calcium chloride dihydrate	10035-04-8	$\geq$ 99.0%	Sigma Aldrich	s
Dimethyl sulfoxide	67-68-5	$\geq$ 99.5%	Sigma Aldrich	l
D-(+)-Glucose	50-99-7	$\geq$ 99.5%	Sigma Aldrich	s
$Na_2EDTA{\cdot}2\,H_2O$	6381-92-6	98.5-101.5%	Sigma Aldrich	s
Ethanol	64-17-5	96%	VWR	l
$Na_2HPO_4{\cdot}2\,H_2O$	10028-24-7	$\geq$ 98.0%	Sigma Aldrich	s
Potassium phosphate monobasic	7778-77-0	$\geq$ 98.0%	Sigma Aldrich	s
Copper(II)sulfate pentahydrate	7758-99-8	$\geq$ 98.0%	Sigma Aldrich	s
Formaldehyde	50-00-0	37% wt	Sigma Aldrich	l
HEPES	7365-45-9	$\geq$ 99.5%	Sigma Aldrich	s
Magnesium sulfate heptahydrate	10034-99-8	$\geq$ 99.5%	Sigma Aldrich	s
Methanol	67-56-1	$\geq$ 99.9%	Sigma Aldrich	l
Potassium chloride	7447-40-7	$\geq$ 99.9%	Sigma Aldrich	s
Sodium chloride	7647-14-5	$\geq$ 99.5%	Merck	s
Trizma®base	77-86-1	ACS reagent	Merck	s
TRIS HCl	1185-53-1	$\geq$ 99.0%	Sigma Aldrich	s

[a] State: chemical state; l: liquid; s: solid.

2.1.3 Reagents for Flow Cytometry

Product name	Manufacturer	Supplier	Catalogue
TO-PRO^{TM}-3 Iodide	InVitrogen^{TM}	Thermo Fisher	T3605
BioTracker Apo-15	Millipore	Sigma Aldrich	SCT238
Calcein-AM	Invitrogen^{TM}	Thermo Fisher	C1430
CS&T RUO beads	BD Biosciences	BD Biosciences	661414
8-peak validation beads	Spherotech	BD Biosciences	653144
6-peak validation beads	Spherotech	BD Biosciences	653145

2.1.4 Microscopy kits and reagents

Product name	Manufacturer	Supplier	Catalogue
Giemsa staining solution	Merck	Sigma Aldrich	1.09204.0500
Hemacolor® staining kit	Merck	Sigma Aldrich	1.11661
Eukitt® mounting medium	Orsatec GmbH	Sigma Aldrich	03989
Immersion Oil Type N	Merck	VWR	1.03699.0100
Percoll^{TM}	Cytiva Sweden AB	VWR	17-0891-02

2.1.5 Microscope equipment and software

Equipment	Model	Manufacturer
Setup for Nikon 90i:		
Microscope controller software	iControl v.2.0.0.3	Nikon Corp
Light engine	EL6000	Leica Microsystems
Microscope camera	DS-Fi1	Nikon Corp
DS-Fi1 camera controller	DS-U2	Nikon Corp
DS-Fi1 digital imaging software	NIS Elements D v.3.22.15	Nikon Corp
Microscope camera	DS-Fi1c	Nikon Corp
DS-Fi1c camera controller	DS-U3	Nikon Corp
DS-Fi1c digital imaging software	NIS-Elements F v.4.60	Nikon Corp
Flat top microscope stage	Proscan H101/2	Prior Scientific
Microscope stage encoder	Lie5 1P N2KV	Numerik Jena
Microscope stage controller	Proscan II	Prior Scientific
Filtercube	Brightline® Led-Cy5-A	Semrock
Filtercube	Ex 470/20, DM 500, Em 515-	Nikon Corp
Stage micrometer cal. slide	2 mm, 0.01 mm interval	Leitz
Objective lens	Plan Apo 20X/0.75	Nikon Corp
Objective lens	Plan Apo 60XA/1.40 Oil	Nikon Corp
Objective lens	Plan Apo VC 100X/1.40 Oil	Nikon Corp

Continued on next page

– continued from previous page

Equipment	**Model**	**Manufacturer**
Setup for Nikon Ni-U:		
Light engine	Sola SM II 365	Lumencor Ink.
CMOS camera	MC170HD	Leica Microsystems
Microscope camera	4KHDMI	DeltaPix
Objective lens (Nikon Ni-U)	Plan Fluor 40X/0.75	Nikon Corp
Objective lens (Nikon Ni-U)	Plan Fluor 100X/1.30	Nikon Corp

2.1.6 Buffers and solutions

Buffer	**Composition**[a]
Modified Alsever's Solution (MAS)	375.6 mM NaCl, 28.97 mM Citric Acid·3Na·2H_2O, 2.6 mM Citric Acid·H_2O, 11.5 mM Na_2EDTA·2H_2O, 113.8 mM D-Glucose, 0.2 µm filtered, pH = 7.0
Anticoagulant buffer (ACB)	55.5 mM D-glucose, 171.1 mM NaCl, 13.4 mM Na_2EDTA·2H_2O, 0.05 M TRIS/HCl, 0.2 µm filtered, pH = 7.6
Phosphate Buffered Saline (PBS)	136.9 mM NaCl, 2.7 mM KCl, 10.1 mM Na_2HPO_4, 1.8 mM KH_2PO_4, 0.2 µm filtered, pH = 7.2
Sorensen Buffer	66.7 mM KH_2PO_4, 66.7 mM Na_2HPO_4·2H_2O, 0.2 µm filtered, pH = 6.8
Marine Physiological Saline Solution (MPSS)	470 mM NaCl, 10 mM KCl, 10 mM $CaCl_2$, 10 mM HEPES 47.7 mM $MgSO_4$, 0.2 µm filtered, pH = 7.4
Tris Buffered Saline (TBS)	44.5 mM Trizma®base, 5.5 mM TRIS/HCl, 450 mM NaCl, 0.2 µm filtered, pH = 7.00

[a]Buffer constituents were dissolved in ultrapure water (MilliQ, Milestone).

2.2 Methods

2.2.1 Animal housing

Adult blue mussels (*M. edulis*) of 56.5±3.4 mm shell length were obtained from Snadder og Snaskum AS (Indre Fosen, Norway). Upon arrival at the marine animal housing facilities of Sintef SeaLab, the mussels were transferred to 50 L flow-through tanks with continuous supply of filtered seawater (FSW, 11 L/min). FSW

was supplied by a direct inlet from the Trondheim Fjord at 80 m depth (7.5 °C). Mussels were fed sporadically with dried algae (*Chlorella vulgaris*).

2.2.2 Haemolymph sampling technique

To minimize the possibility of contaminating hemolymph samples during extraction, a simple and time-effective sampling technique was adapted from the non-lethal technique of Gustafson et al., (2005). "Blind" methods of withdrawal through a notch in the posterior dorsal shell or through the exhalant syphon frequently resulted in considerable contamination with debris from the pallial fluid (sea water). Therefore, the hemolymph sampling technique employed was based on having good visual control over the position of the needle within the posterior adductor muscle during hemolymph withdrawal.

(a) Placement of forceps between valves on the ventral side of the mussel.

(b) Posterior aspect of mussel with the connecting mantle intact (red arrow).

(c) Mussel with the posterior adductor muscle (red arrow) clearly visible with the connecting mantle cut.

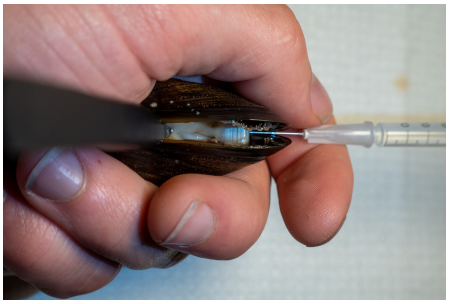

(d) The mussel grip and needle alignment employed, seen from the operators perspective.

Figure 2.1: Illustration of the method employed to extract hemolymph from the posterior adductor muscle of *M. edulis* in order to avoid off-target withdrawal of pallial fluid or spermatozoa. Images were captured using a Sony A6400 mirrorless digital camera with a Tamron 17-70mm F/2.8 lens, and were edited in Adobe® Lightroom Classic 12.0 image editing software.

In order to access and see the posterior adductor muscle, valves were prised apart ventrally by gently forcing a forceps between the valves midway of the mussel's length, or slightly posterior of the byssal mass (Figure 2.1a). When the pallial cavity opened, seawater was drained away from the muscle by positioning the mussel's umbo on a paper tissue for 15-30 seconds. Since the posterior adductor muscle is oblong in the anteroposterior direction, penetrating the muscle from the posterior end pointing straight anteriorly gave the operator better margins to avoid piercing the muscle.

To create a free path to the muscle from the posterior direction, the connecting mantle immediately surrounding the exhalant syphon were cut with a scalpel (Figure 2.1b and c), holding the blunt spine of the blade facing the posterior adductor muscle. Thus, when illuminating the pallial cavity from above with the ventral side facing upwards, the operator was able to supervise the position of the needle inside the posterior adductor muscle sinus through the slightly transparent muscle fibers, as seen in Figure 2.1d.

For haemolymph withdrawal, 1.0 mL syringes equipped with sterile 23 gauge hypodermic needles were used. Hemolymph samples were gently withdrawn at an approximate rate of 1.0 mL/min, in order to prevent negative pressure inside the muscle and drawing in pallial fluid between the muscle fibers.

2.2.3 Selection of haemocyte buffer for flow cytometry assays

The haemocytes of *M. edulis* have a tendency to form aggregates upon mechanical stress, e.g. when the hemolymph is withdrawn through a thin syringe needle. Since accurate flow cytometric analyses rely on single-cell measurements, there was a need to minimize haemocyte aggregation during staining procedures, until the samples could by analyzed on the flow cytometer.

In the literature, several authors have dealt with this challenge by aspirating hemolymph samples directly into slightly acidic EDTA-containing solutions buffered by citric acid (Söderhäll and Smith, 1983; Bachére and Grizel, 1988; Le Foll et al., 2010). Since haemocyte aggregation is a Ca^{2+}-dependent process (Torreilles et al., 1999; Chen and Bayne, 1995), withdrawal of hemolymph into buffers containing divalent metal-ion chelators effectively slows the rate of haemocyte aggregation, allthough it does not inhibit aggregation completely (Chen and Bayne, 1995). Another frequently reported method is to dilute the hemolymph in cold filtered seawater (FSW), while keeping samples on ice prior to analysis.

To determine the most effective method for this work, different "anticoagulant" or "antiaggregative" buffers (1:1) reported in the literature were tested. The degree of aggregation was initially evaluated by inspecting hemolymph smears prepared following the method of Bolognesi and Fenech (2012) under 10x magnification. After preliminary testing, the most promising buffers where the Modified Alsever's Solution (MAS, pH=7.0), and the similar Anticoagulant Buffer (ACB, pH=7.6) with EDTA reported by Pipe et al., (1997). To test their effects on haemocyte aggregation under the conditions intended for our flow cytometric analyses,

a more specific comparison was needed to arrive at the most suitable buffer for this work.

Haemocyte aggregation

An experiment was designed because singlet haemocyte counts was observed to decrease over time from withdrawal, presumably due to aggregation. The proportion of aggregated haemocytes in a sample at a given time could therefore be retraced from the initial haemocyte count when performing several counts of the same sample over time. Since the difference in density between buffers would be negligible, the sedimentation rates would be independent of the haemocyte medium. Any observed differences would thus be caused by differences in the buffers' ability to inhibit aggregation.

500 µL hemolymph was withdrawn from 24 individual mussels into syringes prefilled with either 500 µL MAS (n=8), ACB (n=8) or cold Marine Physiological Saline Solution (MPSS, n=8). Tris-buffered MPSS (pH=7.4) was used as a proxy for FSW, such that pH and osmolarity could be controlled. MAS and ACB were kept at room temperature, while MPSS was kept on ice during handling of the samples. The diluted hemolymph samples were transferred to 12×75 mm polystyrene tubes and the initial haemocyte counts were performed by acquiring 20 µL subsamples on the flow cytometer immediately thereafter. Each sample was run with identical acquisition and fluidics settings (Table A.1), and singlet haemocyte events were gated according to the two-step gating strategy presented in Figure A.1 (Appendix A). To account for any extra aggregation occurring from gentle mixing with flow cytometry reagents in the planned assay, each sample was gently pipetted up and down three times following the initial count. The second counts were performed precisely 15 minutes later to mimic the incubation periods of the flow cytometry reagents. Three more singlet haemocyte counts where performed per sample at 30, 45 and 60 minutes post-withdrawal.

Mixed logistic regression of the proportion of aggregated haemocytes

The buffers' ability to inhibit haemocyte aggregation was tested statistically by mixed effects logistic regression (Generalized Linear Mixed Model, GLMM), such that the within-individual correlation could be modelled as random effects to account for repeated measurements. The dataset consisted of 107 observations (y_{ij}, t_{ij}) from 24 individual mussels (i), $i = 1, ..., n_i$, where y_{ij} denotes the proportion of aggregated haemocytes from mussel i at timepoint t_{ij}, $j = 1, ..., n_j$, and j represents repeated measurements of mussel i at $t = (0, 60]$ minutes post-withdrawal. If we let N_{t0} represent the initial haemocyte count of mussel i at $t \approx 0$, the proportion of aggregated haemocyte at time t_{ij} was calculated according to eq. (2.1):

$$y_{ij} = \frac{N_{t0} - N_{ij}}{(N_{t0} - N_{ij}) + N_{ij}} = \frac{N_{t0} - N_{ij}}{N_{t0}} \tag{2.1}$$

where N_{ij} denotes the hemocyte count of mussel i at time t_{ij}.

The proportions were modelled as a function of log time, with buffer as a categorical explanatory variable. The mixed logistic regression model was fitted by maximum likelihood (Laplace approximation) using the *glmer* function of the R package *lme4* (Bates et al., 2015), with a binomial error distribution and logit link function, as shown in Code listing A.1 (Appendix A). However, instead of fitting the model with the calculated proportions (y_{ij}), the response variable was formatted as a two-column matrix of aggregated and singlet haemocyte counts for the response to be weighted by N_{t0}. The format of the response matrix is shown in eq. (2.2).

$$y_i := \begin{pmatrix} M_1 \\ \vdots \\ M_i \\ \vdots \\ M_{n_i} \end{pmatrix}, \quad M_i = \begin{pmatrix} N_{t0} - N_{i1} & N_{t0} \\ \vdots & \vdots \\ N_{t0} - N_{ij} & N_{t0} \\ \vdots & \vdots \\ N_{t0} - N_{in_j} & N_{t0} \end{pmatrix} \tag{2.2}$$

The factor levels of the categorical explanatory variable was defined as dummy variables (see eq. 2.3), where the MPSS buffer was set as reference level. Thus, the fitted proportion of aggregated haemocytes (y_{ij}) in a sample from mussel $i = [1, 24]$ at time t_{ij}, $j = (0, 60]$, can be written out on *logit* scale as in eq. (2.4), where $\alpha_1 + \beta_1 log(t_{ij})$ is the linear predictor of the reference level, α_2 and α_3 represents the difference in y-intercept for the ACB and MAS buffers, β_2 and β_3 represents the differences in slopes, while γ_{0i} and γ_{1i} represents the individual-specific deviation from the population intercept and slope, respectively. The linear predictors relate to the log proportions according to eq. (2.5), where the dummy variables D_2 and D_3 have been solved according to eq. (2.3).

$$D_2 = \begin{cases} 1, & \text{ACB} \\ 0, & \text{not ACB,} \end{cases} \qquad D_3 = \begin{cases} 1, & \text{MAS} \\ 0, & \text{not MAS} \end{cases} \tag{2.3}$$

$$y_{ij} = \frac{1}{1 + e^{-(\alpha_1 + \beta_1 log(t_{ij}) + D_2(\alpha_2 + \beta_2 log(t_{ij})) + D_3(\alpha_3 + \beta_3 log(t_{ij})) + \gamma_{0i} + \gamma_{1i} log(t_{ij}))}} \tag{2.4}$$

$$log \frac{P(y_{ij} = 1 \mid t_{ij}, \gamma_{0i}, \gamma_{1i})}{P(y_{ij} = 0 \mid t_{ij}, \gamma_{0i}, \gamma_{1i})} = \begin{cases} \alpha_1 + \gamma_{0i} + (\beta_1 + \gamma_{1i}) log(t_{ij}) & i \text{ in MPSS group,} \\ \alpha_1 + \alpha_2 + \gamma_{0i} + (\beta_1 + \beta_2 + \gamma_{1i}) log(t_{ij}) & i \text{ in ACB group,} \\ \alpha_1 + \alpha_3 + \gamma_{0i} + (\beta_1 + \beta_3 + \gamma_{1i}) log(t_{ij}) & i \text{ in MAS group} \end{cases} \tag{2.5}$$

Since generalized linear mixed models do not allow for a marginal interpretation of coefficients, the group-averaged proportions of aggregated haemocytes after 15 minutes post-withdrawal were compared by conventional two-sample Student's t-tests. This timepoint was chosen specifically, since the required incubation with flow cytometric viability dyes would most likely not surpass 15 minutes (Nescerecka et al., 2016).

EDTA cytotoxicity

One of the aims of this project was to score necrotic haemocytes present in the hemolymph of *M. edulis* by means of flow cytometry. Since the Mussel micronucleus cytome assay was developed for *in vivo* exposure regimes, the targeted endpoint is the number of necrotic haemocytes (‰) circulating the hemolymph at the timepoint of hemolymph extraction. Any acute effects on viability arising from the hemolymph extraction itself – or during incubation with the viability dyes (between extraction and FCM measurements) – serve to obscure the potential *in vivo* effect of test substances. Since high concentrations of EDTA has been reported to impair hemocyte viability (Grandiosa et al., 2018), a direct comparison of MAS (11.5 mM EDTA) and ACB (13.4 mM EDTA) with regards to acute effects on viability was required to ensure their suitability as anticoagulants for flow cytometric assays, i.e., to make sure that the buffers themselves do not interfere with the targeted endpoint.

To test wether haemocyte viability was reduced by EDTA during the 15 minute time-window required for staining, hemolymph samples were withdrawn into equal volumes of MAS (n=8), ACB (n=8) or MPSS (n=8) – where MPSS was used as negative EDTA-controls. The diluted hemolymph samples were transferred to 12×75 mm polystyrene tubes, where they were stored for 15 minutes prior to staining. Subsamples of 300 µL were stained with 1.0 µL 50 µM Calcein AM and 3.6 µL 100 µM TO-PRO^{TM}-3 Iodide dissolved in DMSO (see section A.2 for detailed staining procedure, Appendix A). The samples were incubated in darkness for 15 minutes, before 10.000 haemocyte events were recorded on the flow cytometer without washing steps.

488 nm-exited fluorescence from hydrolyzed Calcein was recorded on the FL1 detector (533/15 nm) of the BD Accuri C6 Plus flow cytometer (BD Biosciences, California, US), while 640 nm-exited far red fluorescence from dsDNA-bound TO-PRO^{TM}-3 Iodide was recorded on the FL4 detector (675/25 nm). Events were gated according to the strategy in presented Figure 3.14, obtaining counts of viable (Calcein^{+}ToPro3^{-}), necrotic (Calcein^{-}ToPro3^{+}) and double positive haemocytes (Calcein^{+}ToPro3^{+}), as well as non-cellular events (Calcein^{-}ToPro3^{-}) and a total count (n_{total}). In this particular experiment, double positive haemocytes were counted as necrotic, as newly damaged or lysed haemocytes might still retain a degree of non-specific esterase activity. Hence, the percentage of necrotic haemocytes were calculated according to eq. (2.6).

$$\text{Necrotic haemocytes (\%)} = \frac{n_{Calcein^{-}ToPro3^{+}} + n_{Calcein^{+}ToPro3^{+}}}{n_{total} - n_{Calcein^{-}ToPro3^{-}}} \times 100 \qquad (2.6)$$

The remaining sample material (700 µL) was stored for another 2 and 20 hours, and the same procedure was repeated at these timepoints. Because of considerable sedimentation after 20 hours, haemocytes were resuspended with a wide-bore pipette prior to the third round of staining.

Cytotoxicity of acidic buffer pH

The Modified Alsever's Solution (MAS) is an anticoagulant medium developed to inhibit aggregation among invertebrate haemocytes, while maintaining cell viability (Bachére and Grizel, 1988). The citric acid maintains an effective buffer range at pH = 6.1±0.2, where the acidic pH is thought to somehow contribute to the anticoagulant effect (Söderhäll and Smith, 1983; Renwrantz, 1990). The pH of MAS can be raised to 7.0, but the buffer capacity at this range negligible. Since pH-adjusted MAS (pH = 7.0) had proven as an effective tool for reducing haemocyte aggregation, there were obvious reasons for testing if it could be used within its intended pH-range.

However, since the pH of non-adjusted MAS (naMAS, pH = 6.1) is considerably lower than that of seawater and haemolymph, the acidic environment could potentially induce apoptosis and/or necrosis, and interfere with the endpoints of the planned flow cytometric Calcein AM/TO-PRO-3 Iodide assay (Worsley et al., 2022; Wang et al., 2016). To test wether the effective pH of haemolymph in naMAS (1:1) had any measurable effect on the percentage of early apoptotic and ($Apo15^+$ $ToPro3^-$) and necrotic ($Apo15^+$ $ToPro3^+$) haemocytes; haemolymph from 36 mussels were withdrawn into an equal volume of naMAS (n=18) and ACB (n=18). The slightly alkaline pH of ACB (pH = 7.6) is adapted to reflect that of *M. edulis* haemolymph (Pipe et al., 1997; Mangan et al., 2019), and was therefore used as a negative control for acidic buffer pH. The haemocytes were incubated in the media for 15 minutes prior to staining with Apo-15 (560 nM) and TO-PRO^{TM}-3 Iodide (1.2 μM). After 15 minutes incubation in darkness, 10.000 haemocyte events were acquired from each sample on the flow cytometer (see Table A.1 for FCM settings).

2.2.4 Cytological characterization of haemocyte subpopulations

For the purpose of characterizing and imaging the different haemocyte cell types of *M. edulis*, samples were withdrawn into an equal volume of ice-cold MPSS and transferred directly onto glass slides. The glass slides were kept in a humid chamber for up to 5 minutes before cells were fixed in ice cold methanol (5 × 1 sec dips). This assured haemocyte attachment, but prevented the profound morphological changes accompanied by the haemocytes' process of spreading. Slides were stained with the Hemacolor® kit (Merck, Darmstadt, DEU) according to the manufacturer's recommendations, air dried, mounted with Eukitt® and coverslipped. Stained haemocytes were examined and imaged under brightfield illumination on a Nikon Eclipse 90i upright microscope with a 100×/1.40 oil immersion objective and a Nikon DS-Fi1 microscope camera. Haemocyte morphology was characterized on the basis of cytoplasmic staining, granularity (granule size, abundance and staining affinities), N:C ratio, cell diameter and shape.

Determination of cell diameters

To establish wether haemocyte subpopulations differed with regard to size across a larger population of adult mussels, the cell diameters of 100 haemocytes were ascertained in haemolymph smears from 20 individual mussels (n=2000). Since the rate and degree of haemocyte spreading could be inherently different among cell types, all spreading was effectively impeded by collecting haemolymph samples into an equal volume of 5% formaldehyde in MPSS. The fixation was continued for one hour in suspension, before cells were pelleted by centrifugation (250G, 15 min, 10 °C) and resuspended in 100 µL 0.75 % eosin in Sorensen Buffer. After staining for 5 minutes, 1 mL 3% Giemsa was added and the staining was continued for an additional 15 minutes. Stained haemocytes were pelleted by centrifugation (180G, 12 min, 10 °C), resuspended in 100-200 µL Sorensen Buffer and transferred onto glass slides. The slides were air-dried in a fume hood until the smears were completely dry and transparent, before they were mounted with Eukitt® and coverslipped.

The slides were placed on the stage of a Nikon Eclipse 90i upright microscope, and 10-20 microscopic fields from each smear was photographed under DIC illumination with a 60x oil immersion objective. Cell diameter measurements were performed digitally with ImageJ (NIH, Bethesda, Maryland, US), using the *Straight line tool* of this image processing software. The size of the magnified haemocytes were determined by calibrating the software's pixel/µm scale with a stage micrometer calibration slide (Leitz Wetzlar, Buffalo, DEU). When haemocyte outlines deviated from an approximate spherical shape, diameters were estimated as the average length of the long and short axes, after Burkhard et al. (2009). The measurements were performed as differential counts, such that the number of measurements of each cell type reflected their average relative proportions (%) across all 20 mussels.

2.2.5 Flow cytometric characterization of haemocyte subpopulations according to light-scatter and MRP-mediated Calcein AM efflux

Light-scatter characterization

Suspensions of living haemocytes from 8 adult mussels were diluted in MPSS (1:1) and analyzed on a CytoSense-C imaging flow cytometer (CytoBuoy, Woerden, NLD). By inspecting 500 images per sample, regions containing debris, singlet haemocytes, doublets and larger aggregates could be positively identified in bivariate plots of FSC vs. SSC. In this way, debris, doublets and larger aggregates could be gated out of the analyses (Figure A.1, Appendix A), and the different subpopulations of singlet haemocytes could be characterized according to FSC vs. SSC. Further investigations were conducted on haemolymph diluted in ACB (1:1) with a BD Accuri C6 Plus flow cytometer. More than 500 adult mussels were sampled in the course of this thesis work. From this data material, the typical light scatter profiles of adult mussel haemocytes are presented. For an extensive

quantitative characterization, the reader is referred to LeFoll et al. (2010).

Characterization of haemocytes according to Calcein AM efflux and SSC

Since the eosinophilic granulocytes of *M. edulis* exhibit higher rates MRP-mediated efflux of Calcein AM compared to the basophilic cell types (Rioult et al., 2014), the differential accumulation of hydrolyzed Calcein could potentially serve as a discriminator in flow cytometric differential haemocyte in this species. To test the applicability of Calcein florescence (533/15 nm) in combination with SSC measurements for this purpose, the haemolymph of 22 untreated adult mussels were stained with 50 nM Calcein AM in ACB (15 min) prior to flow cytometric acquisition. The data was analyzed as bivariate plots of (1) Calcein fluorescence vs. log SSC and (2) FSC vs. log SSC, and the identity of the observed subpopulations were compared by backgating.

2.2.6 Relating cytologically defined cell types to light-scatter profiles

In developing a flow cytometric differential haemocyte count for *M. edulis*, the initial step involves identifying the different cell types that are differentiated in Giemsa-preparation by flow cytometry. This is typically accomplished by measuring light scatter (FSC vs. SSC) and fluorescently labelled markers that are specific to each cell type. Since the cytologically defined cell types of *M. edulis* were distinguishable according size and/or granularity, an attempt was made to identify them according to FSC (size) and SSC (granularity), individually. This involved separating the cell types by isopycnic centrifugation prior to flow cytometric analyses. A second approach was used to positively identify the eosinophilic granulocytes according to Eosin Y fluorescence. The experimental procedures are described in detail below.

Isopycnic separation and light-scatter characterization

Formaldehyde-fixed haemocytes were separated on discontinuous Percoll gradients according to the protocol by Friebel and Renwrantz (1995), with minor modifications. The separation was performed in duplicate with pooled haemocytes from a total of six adult mussels. For both gradients, the haemolymph of three individual mussels (1.5-2.0 mL/mussel) were withdrawn into an equal volume of 5% formaldehyde in MPSS, wherein the haemocytes were fixed for one hour after pooling. The fixed haemocytes were stained with 0.75 % Eosin and 3 % Giemsa according to the procedure in section 2.2.4. After pelleting, stained haemocytes were resuspended in Tris-Buffered Saline (TBS, 900 mOsm) to an approximate concentration of 9×10^6 cells/mL, before layering 2 mL suspension on top of both gradients. Discontinuous Percoll gradients consisted of 15%, 33%, 38%, 43% and 90% Percoll stock in TBS (vol/vol), and were constructed by carefully layering 2 mL of each Percoll concentration in 15 mL Falcon centrifuge tubes with conical bottoms (Corning, New York, US).

The centrifugation was started at 120G for 10 minutes (4 °C), followed by 40 minutes at 2500G. An Eppendorf 5804 R benchtop centrifuge equipped with an A-4-44 swing-bucket rotor was employed for the separation, with the brake ramp turned off. The separated cell fractions were collected into syringes by puncturing the tubes below the gradient interfaces with 23G hypodermic needles. According to the protocol by Bachére and Grizel (1988), the Percoll was eliminated from the 43/90% and 38/43% fractions by two consecutive dilutions in TBS (1:7) and a 10% sucrose cushions (1:1), followed by centrifugation (800G, 15 min, 4 °C). Haemocytes collected from the 15/33% interface were centrifuged directly after a seven-fold dilution in TBS (800G, 15 min, 4 °C).

The pelleted cell fractions were resuspended in Sorensen buffer and divided into two aliquots; one aliquot was used to prepare smears according to the procedure in section 2.2.4, while the remaining aliquots were further diluted in 1 mL Sorensen buffer for flow cytometric characterization. A total of 10.000 events were acquired from each cell fraction on the flow cytometer, in addition to 30.000 events from the unseparated pools (set aside prior to separation). The relative proportion (%) of cell types in each fraction was determined by 1000-cell microscopic differential counts.

Identification of eosinophilic granulocytes by Eosin Y fluorescence

Since Eosin Y is fluorescent in the green/yellow spectrum (${\lambda_{em}}^{max} = 543$ nm) (Koegl et al., 2020), it can be detected on the FL1 detector (533/15 nm) of the BD Accuri C6 Plus after 488 nm exitation. If the haemocytes of *M. edulis* are permeabilized and stained with Eosin Y prior to flow cytometric analyses, the fluorescent signal from Eosin Y can in theory be used to identify eosinophilic granulocytes (Le Foll et al., 2010). An attempt was therefore made to optimize a staining procedure flow cytometry; from which a practically applicable resolution between eosinophilic and basophilic granulocytes could be obtained.

After testing different fixatives (methanol, 5% formaldehyde and Carnoy's fixative), staining solutions (0.25, 0.5, 0.75, ..., 3% Eosin Y) and the duration of both fixation (15, 30, 45 and 60 min) and staining (5, 10 and 15 min) – the smears with the lowest degree unspecific staining were those fixed in 5% formaldehyde (1 hour) and stained with 0.5% Eosin Y (5 min). The events of these samples separated into two distinct populations according to log eosin fluorescence on the flow cytometer. When the eosin^{bright} events were back-gated to scatter-plots, the presumed light scatter profile of the eosinophilic granulocytes were obtained.

The test wether the eosin^{bright} (%) events from flow cytometric analyses corresponded the eosinophilic granulocytes exclusively, this methodology was combined with microscopic 1000-cell differential counts, where the percentage of eosinophilic granulocytes was determined relative to the basophilic haemocytes. Haemolymph samples from 10 individual mussels were withdrawn into an equal volume of 5% formaldehyde in MPSS and fixed for 1 hour. The fixed cells were pelleted by centrifugation (180G, 12 min, 20 °C) and resuspended in 0.5% eosin

in Sorensen buffer. The suspensions were divided into two aliquots, where one was pelleted and resuspended in 1 mL ACB after 5 minutes of staining, while the other was used to prepare Giemsa-smears according to the method described in section 2.2.4. Samples in ACB were analyzed on the flow cytometer, while the corresponding Giemsa smears were used for differential counts. The correlation between eosin^{bright} events (%) and the percentage of eosinophilic granulocytes in the samples was tested by simple linear regression. To determine the accuracy of the results, the mean percent error were calculated relative to the microscopic differential counts.

2.2.7 Performing differential haemocyte counts by flow cytometry

The investigations described in section 2.2.4 - 2.2.6 provided a sufficient data-material for the development of a flow cytometric differential haemocyte count in *M. edulis*. As the three cytologically defined cell types had been characterized and identified in scatter-plots, the remaining step was to implement these results into a final protocol and cross-validate the results by light microscopy. For this purpose, the haemolymph of 20 untreated mussels were sampled for parallel flow cytometric and microscopic differential haemocyte counts, i.e., twice subsequently.

Flow cytometric differential haemocyte count

The first round of samples were withdrawn into an equal volume of ACB and stained with 50 nM Calcein AM for 15 minutes. After staining, 10.000 singlet haemocyte events were recorded on the flow cytometer according to the gating strategy presented in Figure A.3 (Appendix A). By substituting log Calcein fluorescence (533/15 nm) for FSC, cluster 1-3 were gated indirectly according to log SSC vs. log Calcein (Figure 3.8). This allowed for better resolution between cluster 2 and 3 when they were partially overlapping with regard to SSC. The percentages of events in cluster 1, 2 and 3 were calculated from the total number of singlet haemocyte events per sample (9865±112 events/sample). These percentages were in turn used as estimates for the percentage of small blast-like basophils (cluster 1), basophilic granulocytes (cluster 2) and eosinophilic granulocytes (cluster 3) in each mussel.

1000-cell microscopic differential haemocyte count

Reference samples were withdrawn into an equal volume of 5% formaldehyde in MPSS and fixed for 1 hour. The fixed haemocytes were pelleted by centrifugation (250G, 15 min, 10 °C) and resuspended in 3% Giemsa to prepare smears according to the method described in section 2.2.4. The Giemsa smears were used for 1000-cell differential haemocyte counts, where the percentage of eosinophilic granulocytes, basophilic granulocytes and small blast-like basophils were determined under 400x magnification on a Nikon Ni-U microscope (Nikon Corp, Tokyo, JP).

To to assess the reliability of the flow cytometric methodology, the linearity of response was evaluated individually for each cell type within their observed ranges. The mean percent errors of the flow cytometric estimates are used to compare the accuracy between the three cell types.

2.2.8 Scoring of necrotic haemocytes by flow cytometry

To discriminate between viable and necrotic haemocytes by flow cytometry, a two-color fluorescence assay with the cell-permeant probe Calcein acetoxymethyl and the non-permeant dsDNA-binding dye TO-PRO^{TM}-3 Iodide (Molecular Probes, Eugene, OR) was chosen. This combination of probes was primarily selected for two reasons: (1) it enables simultaneous measurement of intracellular esterase activity and plasma membrane integrity – two recognized parameters of cell viability and (2) there is virtually no fluorescent spillover between the probes, such that the uncompensated raw data can be applied directly. Moreover, a complementary double staining methodology like this allows for discrimination between haemocytes and non-cellular particles. Since cells with intact plasma membranes retain esterase activity, double negative events (Calcein^{-} ToPro3^{-}) of cellular proportions must represent particles or cellular debris, since they do not contain dsDNA (ToPro3^{-}).

Since Calcein AM is commonly used in the LIVE/DEAD® kit for mammalian cells (Molecular Probes, Eugene, OR), the staining protocol of this kit was used as a guide for obtaining an adequate fluorescent signal from hydrolyzed Calcein on the FL1 detector (518-548 nm) . The manufacturer's recommendation of 50 nM Calcein AM mL^{-1} cell suspension (0.1-5 $\times 10^6$ cells) gave a bright fluorescent signal from living cells after 15 minute incubation, so no further optimization was required. Information on suitable concentrations of TO-PRO^{TM}-3 Iodide for flow cytometric dye exclusion tests was however sparse, such that this had to be determined experimentally.

Determination of optimal TO-PRO^{TM}-3 Iodide staining concentration

The optimal TO-PRO^{TM}-3 Iodide concentrations for a flow cytometric dye exclusion assay would ideally fulfill two requirements. The first would be to give the highest possible resolution between viable and necrotic cells in terms of fluorescent intensity. Secondly, and of equal importance; the concentration cannot be acutely cytotoxic to haemocytes within the time-frame of staining and flow cytometric acquisition. To determine a suitable range of concentrations for this assay, a pool of dead (70% MeOH, 30 min) and freshly withdrawn haemocytes were prepared. Methanol-killed hameocytes were washed three times in MPSS, resuspended ACB and gently mixed with freshly withdrawn heamocytes in ACB. The suspension was divided into 11 aliquotes of 1 mL, and all but one was stained with TO-PRO^{TM}-3 in the range of 30 nM to 8 µM. After 15 minutes incubation, 10 000 events were acquired from each sample on the flow cytometer. To determine wether the fluorescent signal intensity increased with further incubation, the

same samples were incubated for another 15 minutes before the measurement was repeated.

Red laser-exited fluorescence from dsDNA-bound TO-PRO^{TM}-3 Iodide was collected on the FL4 detector (675/25 nm) of the BD Accuri C6 Plus flow cytometer. A histogram representation of the fluorescence revealed two distinct populations of events: one population of ToPro3^{-} events and one population of ToPro3^{+} events. The mean fluorescent intensity (MFI) of the two populations were calculated for each aliquot, and their difference was plotted against the staining-concentrations of TO-PRO^{TM}-3 Iodide.

In order to predict a suitable range of concentrations from the data, the differences in MFI were regressed on the TO-PRO^{TM}-3 concentration using a log-logistic model. Since the data required a model range bound by 0 and some unknown positive integer (0, a), a four-parameter log-logistic function from the R package *drc* was used (v3.0-1; Ritz et al., 2015). This function allowed the lower asymptote to be fixed to 0, as shown in code listing A.2 (Appendix A). The general function is seen in eq. (2.7), where b and e represents the slope parameter and inflection point, while d and c represents the upper and lower asymptotes, respectively.

$$y_i = c + \frac{d-c}{1+(x_i/e)^b} \tag{2.7}$$

Potential cytotoxicity at high concentrations was evaluated by examining the ToPro3^{-} populations (SSC vs. FL4), to see wether any of the freshly withdrawn haemocytes were starting to loose their ability to exclude TO-PRO^{TM}-3 Iodide.

Gating Strategy

To establish a quadrant gating strategy for scoring necrotic and viable haemocytes according to Calcein and dsDNA-bound TO-PRO^{TM}-3 Iodide fluorescence, three pools of haemocytes were prepared: (1) MeOH-killed (70% MeOH, 30 min), (2) newly withdrawn (ACB, 1:1) and (3) a 1:1 mixture of both. Each pool was divided into four aliquots of 1 mL, where three of them were stained with either Calcein AM (50 nM), TO-PRO^{TM}-3 Iodide (1.2 µM) or both, and the fourth was kept as an unstained (US) control. After incubating for 15 minutes, 10.000 events were acquired from each sample on the flow cytometer.

Method validation

A flow cytometer is a very sensitive instrumentation for measuring fluorescent signals, and with a throughput of up to 10.000 events s^{-1}, these instruments represent a far superior technology for counting fluorescent cells compared to epifluorescent microscopy. However, the result obtained from a flow cytometric assay is entirely dependent on the gating strategy employed to generate the results. An effort was therefore made to cross-validate the gating strategy presented in the previous section by epifluorescent microscopy.

Methanol-killed (70% MeOH, 30 min) and freshly withdrawn haemocytes (ACB, 1:1) were mixed in semi-random proportions to prepare 10 samples with 0-100% necrotic haemocytes. Samples were stained with Calcein AM (50 nM) and TO-PRO^{TM}-3 Iodide (1.2 µM) for 15 minutes, and 10.000 events were acquired from each sample on the BD Accuri C6 Plus flow cytometer. Events were gated according to the strategy presented in Figure 3.14.

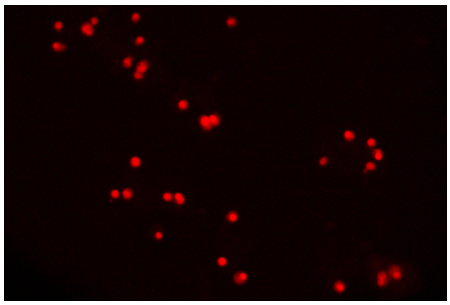

(a) TO-PRO^{TM}-3 Iodide fluorescence collected from microscopic field with a LED-Cy5-A filter cube.

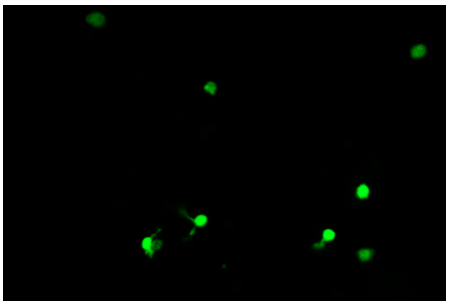

(b) Calcein fluorescence collected from the same microscopic field with a B-2A filter cube.

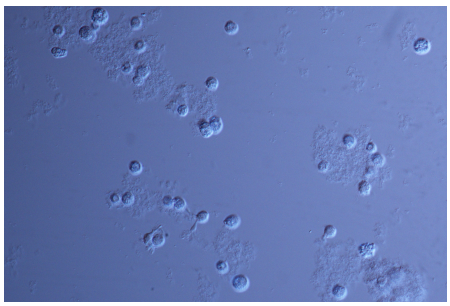

(c) Microscopic field imaged by DIC microscopy to verify cellular identities of fluorescent signals.

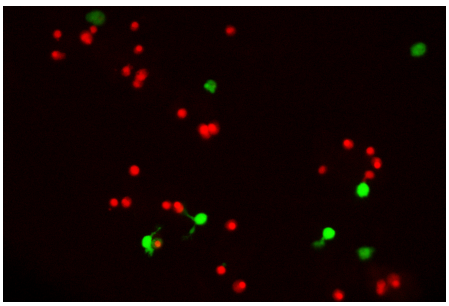

(d) Merged RGB image from the red and green color planes of image *a* and *b*, respectively.

Figure 2.2: An illustration of the image analysis used to score necrotic and viable haemocytes by epifluorescence and DIC microscopy at 20x magnification.

Following flow cytometric acquisition, the 10 samples were transferred onto glass slides, coverslipped and put on the stage of a Nikon 90i upright microscope equipped with a DS-Fi1c microscope camera (Nikon, Tokyo, JP). Ten microscopic fields were imaged per slide at 20x magnification, and each field was imaged in three subsequent steps (see Figure 2.2): (1) Epifluorescence microscopy with a LED-Cy5-A filter cube, 6 s exposure and 4.8 gain (2) epifluorescent microscopy with a B-2A filter cube, 400 ms exposure and 2.0 gain, followed by (3) DIC microscopy. The red and green color planes of the two epifluorescence images were merged into an RGB image in NIS Elements D software (v.3.22.15), and the percentages of necrotic, viable and doubly stained haemocytes were scored using the merged image (see Figure 2.2d). The DIC images were used to confirm the iden-

tity of the fluorescent signals, such that only cellular signals were included in the counts.

The validity of the flow cytometric assay was evaluated by linearity of response after Ericson et al., 2021, while the accuracy was determined from the mean percent error relative to the epifluorescence microscopy data. The percentage of necrotic haemocytes (Calcein$^-$ ToPro3$^+$) from flow cytometric and epifluorescence microscopy analyses were analyzed by simple linear regression. The percentage of necrotic haemocytes (%) were calculated according to eq. (2.8), such that double positive haemocytes were counted as viable. The imaging process took up to one 1 hour per slide, so any double positive haemocytes had most likely become necrotic during the course of microscopy. It should be noted that samples were prepared and scored one at a time to minimize the occurrence of *in vitro* necrosis.

$$\text{Necrotic haemocytes (\%)} = \frac{n_{Calcein^-ToPro3^+}}{n_{total} - n_{Calcein^-ToPro3^-}} \times 100 \qquad (2.8)$$

Statistical analyses

All statistical analyses were performed using R (R Core Team, 2021) in RStudio (v2023.06.1 RStudio Team, 2021). Mixed logistic regression was performed using the *glmer* function of the *lme4* R-package (Bates et al., 2015), while four-parameter log-logistic regression was performed with the *drc*-package (v3.0-1; Ritz et al., 2015). The mean percentage of necrotic haemocytes in MPSS, ACB and MAS were compared by one-tailed two-sample Student's t-tests at the three different timepoints. Since the group variances (s^2) differed by more than a factor of 2 at the last timepoint, these comparisons were bade by Welch two-sample t-tests. Paired t-tests were used to assess wether the percentages of necrotic haemocytes increased with incubation time within each group. The mean percentage of necrotic and early apoptotic haemocytes in naMAS and ACB were compared by Welch two-sample t-tests.

Chapter 3

Results

3.1 Haemocyte medium

The following section presents results from three experiments that were conducted to explore the suitability of three anticoagulant buffers for flow cytometric applications. They are evaluated with regard to their ability to inhibit haemocyte aggregation – without affecting the viability of haemocytes.

3.1.1 Inhibition of haemocyte aggregation

The proportions of aggregated haemocytes in MPSS, ACB and MAS are plotted against time post-withdrawal in Figure 3.1, together with their predicted mean proportions, or more accurately: the predicted proportion of aggregated haemocytes in mussels with random effects γ_{0i} and $\gamma_{1i} = 0$. Predictions were made from the estimated fixed effects in order to address the marginal effect of "Buffer" on the population-averaged proportions. The estimated regression coefficients of the generalized linear mixed model (GLMM) is presented in Table 3.1, while the fixed effect submodels are shown in eq. (3.1).

$$y_{ij} = \begin{cases} \dfrac{1}{1+e^{-(-1.7192+0.5516\times log(t_{ij}))}} & i \text{ in MPSS group,} \\ \dfrac{1}{1+e^{-(-6.9842+1.8400\times log(t_{ij}))}} & i \text{ in ACB group,} \\ \dfrac{1}{1+e^{-(-7.7198+2.0138\times log(t_{ij}))}} & i \text{ in MAS group} \end{cases} \tag{3.1}$$

Figure 3.1 unambiguously demonstrates that both ACB and MAS exerted an immediate decelerating effect on the rate of haemocyte aggregation. This inhibitory effect is evident from the estimated differences in slopes and intercepts from the MPSS sub-model, which were significantly different from zero (see Table 3.1). Since the effect sizes are challenging to interpret from the isolated coefficients, the linear predictors of the three sub-models are evaluated on link scale in Figure 3.2, i.e. as log odds of the proportion of aggregated haemocytes ($logP(y_{ij} = 1)/P(y_{ij} = 0)$).

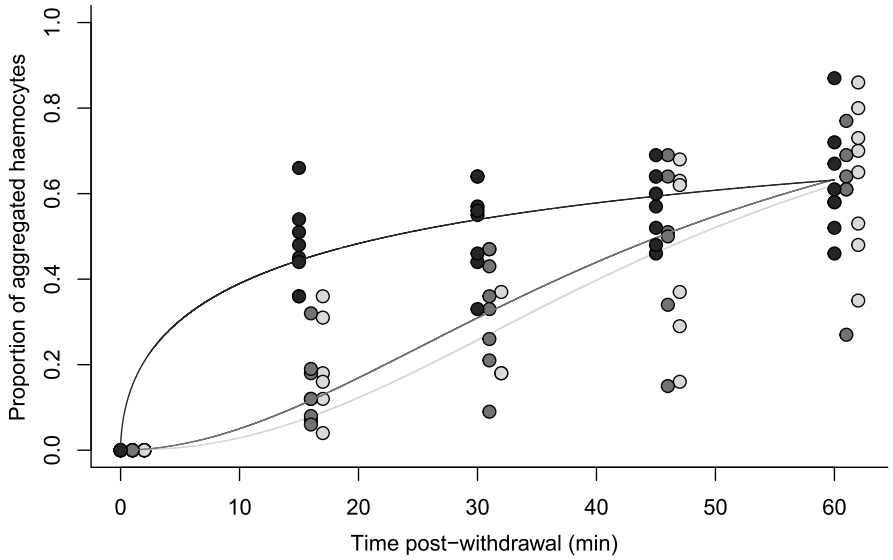

Figure 3.1: Anticoagulant effect of withdrawing haemolymph samples into equal volumes of MAS, ACB or cold MPSS. The proportion of aggregated haemocytes is plotted against time from haemolymph withdrawal after diluting samples in an equal volumes Marine Physiological Saline Solution (MPSS, n=8), Modified Alsever's Solution (MAS, n=8) or Anticoagulant Buffer (ACB, n=8). **D)** Regression curves represent the mean proportion of aggregated haemocytes in MPSS (●), MAS (◉) and ACB (◉), as predicted from the submodels presented in eq. (3.1). Data-points have been jittered on the x-axis to prevent overlapping values.

Table 3.1: Parameter estimates of the fitted Generalized linear mixed model (GLMM) presented in Figure 3.1, and their belonging 95% confidence intervals (CI) and standard errors (S.E.) Marginal and conditional R^2 is included as measures of model fit, together with the conditional model's residual deviance.

Parameter	**Symbol**	**Estimate**[b]	**95% CI**[a]	**S.E.**
Intercept	α_1	-1.72*	[-3.24, -0.202]	0.740
log(t)	β_1	0.552**	[0.189, 0.915]	0.177
$Buffer_{ACB}$	α_2	-5.27***	[-7.41, -3.11]	1.05
$Buffer_{MAS}$	α_3	-6.00***	[-8.18, -3.86]	1.06
$log(t) \cdot Buffer_{ACB}$	β_2	1.29***	[0.775, 1.80]	0.251
$log(t) \cdot Buffer_{MAS}$	β_3	1.46***	[0.950, 1.98]	0.253
$SD(\gamma_{0i})$	τ_0^2	2.09	[1.57, 2.91]	–
$SD(\gamma_{1i})$	τ_1^2	0.500	[0.379, 0.694]	–
Marginal $R^2 = 0.87$[c]				
Conditional $R^2 = 0.98$[c]				
Residual deviance: 13498 on 98 degrees of freedom				

[a] Computed 95% confidence intervals based on Likelihood Ratio Test of the profile likelihood.

[b] *, **, *** indicate significance on 95%, 99% and 99.9% confidence levels, respectively. Confidence levels were obtained from z-statistics of the asymptotic Wald test.

[c] Calculated according to the method proposed by Nakagawa and Schielzeth, 2013.

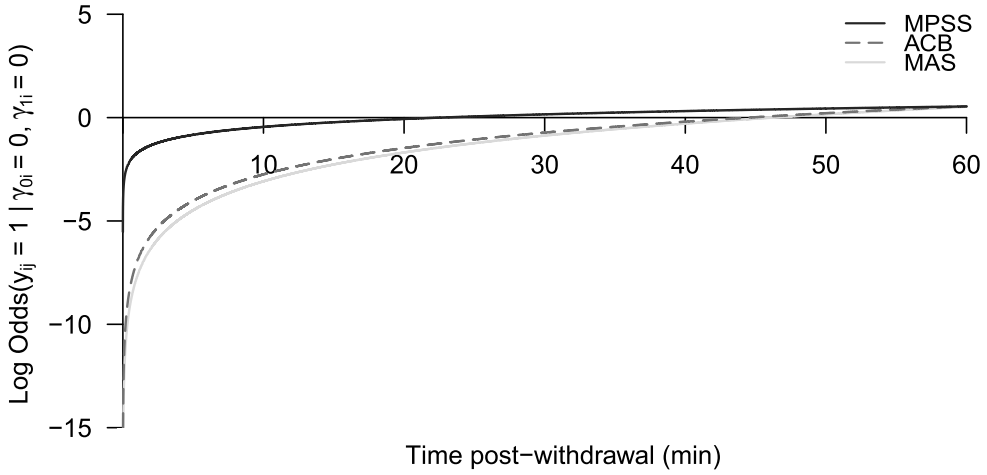

Figure 3.2: Logit-scaled predictions of GLMM aggregation model. The log odds of the proportion of aggregated haemocytes ($logP(y_{ij} = 1)/P(y_{ij} = 0)$) is plotted against time (min) after haemolymph withdrawal, when samples were withdrawn into an equal volume of Marine Physiological Saline Solution (MPSS), Anticoagulant Buffer (ACB) or Modified Alsever's Solution (MAS).

Given the that the predicted proportion of aggregated haemocytes is 0.50 when the log odds is equal to zero, Figure 3.2 shows that 50% of the haemocytes withdrawn into MPSS had aggregated within 23 minutes post-withdrawal. This interpretation is valid when the random effects of individual mussels (γ_{0i} and γ_{1i}) are equal to zero. For samples withdrawn into ACB or MAS on the other hand, the haemocytes did not aggregate to this degree until 45 and 46 minutes post-withdrawal, respectively. The three log odds curves depicted in Figure 3.2 shows that the inhibitory effects of ACB and MAS were modelled through their significantly lower y-intercepts compared to the MPSS sub-model (Table 3.1). These differences were significant after accounting for within-mussel correlations (Table 3.1).

The inhibitory effects of ACB and MAS were greatest during the initial 15-20 minutes, before the degree of aggregation slowly approached that of MPSS around 60 minutes post-withdrawal. In haemolymph samples withdrawn into ACB or MAS, the mean proportions of aggregated haemocytes after 15 minutes were 0.14 (95% CI [0.07, 0.22]) and 0.20 (95% CI [0.07, 0.32]), respectively. There was no significant difference between the two EDTA-containing buffers, but both ACB and MAS had significantly lower proportions of aggregated haemocytes at this timepoint compared with samples withdrawn into cold MPSS (0.48, 95% CI [0.39, 0.56]).

3.1.2 EDTA cytotoxicity

The mean percentages of necrotic hemocytes in MPSS, ACB and MAS after 15 min, 2 hours and 20 hours incubation are presented in Figure 3.3, with error

bars representing 95% confidence intervals around group means. Within group differences in means at the three incubation periods are presented Table 3.2.

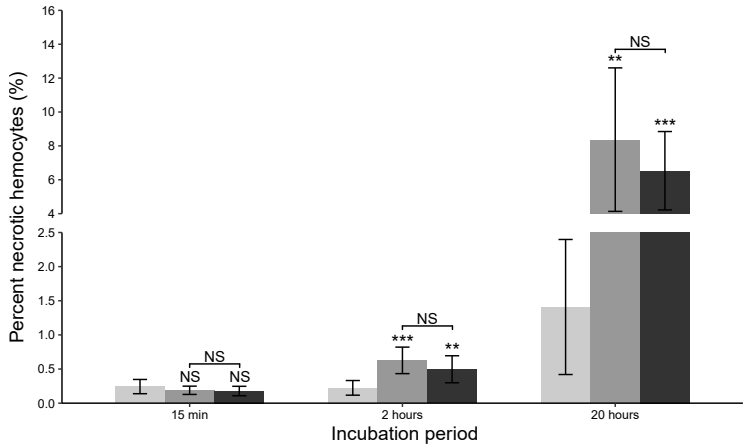

Figure 3.3: Cytotoxicity of EDTA in anticoagulant buffers. The mean percentages of necrotic hemocytes after 15 min, 2 hours and 20 hours incubation in Marine Physiological Saline Solution (, n=8), Anticoagulant Buffer (, n=8) and Modified Alsever's Solution (, n=8). Error bars represent 95% confidence intervals around group means, *, **, *** above error bars denotes confidence level of one-tailed two sample t-test comparisons with the MPSS control group, while asterisks above horizontal lines represent ACB vs. MAS comparisons. NS: Not Significant.

The difference between the negative control group (cold MPSS) and the two EDTA-containing buffers were not significantly different from zero after 15 min incubation. But as the incubation period was increased to 2 and 20 hours, the percentages of necrotic haemocytes in ACB and MAS increased relative to cold MPSS. After 2 hours of incubation, there were 0.40% and 0.27% more necrotic haemocytes in ACB ($t(14) = 4.29$, $p<0.001$) and MAS ($t(14) = 2.86$, $p=0.006$) compared to cold MPSS, respectively. After 20 hours of incubation, these differences had increased to 6.96% ($t(14) = 3.78$, $p=0.003$) and 5.12% ($t(14) = 4.82$, $p<0.001$) for ACB and MAS, respectively.

Table 3.2: Paired two-tailed Student's t-tests were used to assess wether the percentages of necrotic haemocytes increased with incubation time within each group. The difference between means at t = 15 min, 2 hours and 20 hours are presented with 95% confidence intervals (CI) and the belonging p-value (Pr(T > | t |)).

Buffer	**Paired t-test comparison** Incubation *t*	Incubation *t - 1*	Difference (%)	95% CI	Pr(T > | t |)
MPSS	2 hours	15 min	-0.018	[-0.023, -0.015]	0.78
	20 hours	2 hours	1.184	[1.157, 1.211]	0.026
ACB	2 hours	15 min	0.438	[0.433, 0.444]	0.00187
	20 hours	2 hours	7.742	[7.627, 7.857]	0.00324
MAS	2 hours	15 min	0.319	[0.313, 0.324]	0.00690
	20 hours	2 hours	6.037	[5.970, 6.105]	<0.001

The mean percentage of necrotic haemocytes increased significantly with the incubation period in both MAS and ACB (Table 3.2). There was significant increase in the percentage of necrotic haemocytes in MPSS between 15 minutes and 2 hours of incubation, however, a significant increase of 1.18% was observed after 20 hours (p=0.026).

3.1.3 Cytotoxicity of acidic haemocyte buffer pH

The mean percentages of necrotic and early apoptotic haemocytes after 15 minutes incubation in non-adjusted Modified Alsever's Solution (naMAS, pH = 6.1) and ACB (pH = 7.6) are presented as bargraphs in Figure 3.4, with error bars representing 95% confidence intervals around group means.

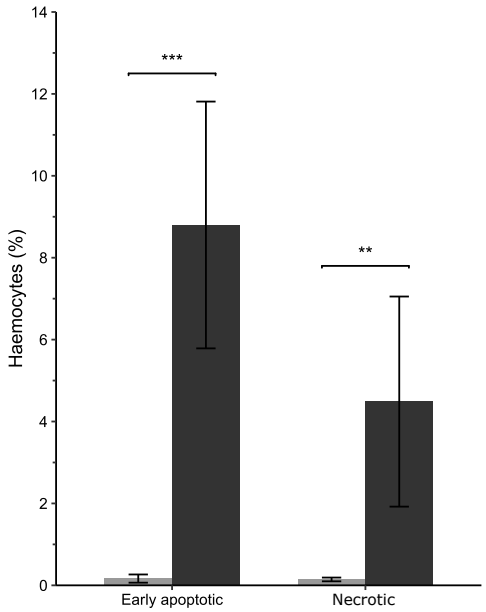

Figure 3.4: Haemocytes are sensitive to buffer pH. The mean percentage of early apoptotic (Apo15$^+$ ToPro3$^-$) and necrotic haemocytes (Apo15$^+$ ToPro3$^+$) after 15 minutes incubation in Anticoagulant Buffer (, n=18) and non-adjusted Modified Alsever's Solution (, n=18). Error bars represent 95% confidence intervals around group means. Asterisks *, **, *** denotes confidence level of one-tailed two sample t-test comparisons.

Haemocytes that were incubated in the acidic MAS buffer showed a significant induction of apoptosis relative to samples kept in ACB. The mean percentage of early apoptotic haemocytes in naMAS were 53 times higher than in ACB ($t(17) = 6.04$, $p<0.001$), while that of necrotic haemocytes were 31 times higher ($t(17) = 3.57$, $p=.00117$). The percentages of necrotic and early apoptotic haemocytes in ACB were consistently low, with mean percentages of 0.144±0.09% and 0.165±0.2%, respectively.

3.2 Development of a flow cytometric differential count

This section presents results from the experiments that were conducted in order to develop and validate a flow cytometric differential count of the cell types present in the haemolymph of *M. edulis*. Section 3.2.1 presents a cytological characterization of the haemocytes according to i.a., cell size, granularity and staining affinities in accordance with the current scientific practice in invertebrate immunology. The flow cytometric characterization in section 3.2.2 presents the subpopulations of haemocytes that were separated according to FSC (relative size) and side scatter (internal complexity), and put these results in context of the cytologically defined cell types. The next section (3.2.3) presents results from two experiments that aimed to uncover the relationship between the cytologically defined cell types and the subpopulations discernible by light scatter measurements. Lastly, the gating strategy for the differential haemocyte count is presented with proof of concept.

3.2.1 Cytologic characterization of *M. edulis* hemocyte cell types

The hemolymph of *M. edulis* comprised a mixed population of cells differing in size, granularity, morphometrics and staining affinities. If the haemocytes were allowed to spread prior to fixation and staining, the diversity further expanded as cells took on a variety of shapes and/or developed cytoplasmic extensions. From these morphological criteria, a total of three distinct cell types could be identified by light microscopy.

Based on the basophilic or eosinophilic nature of their granules and other cytoplasmic contents, cytologic staining with 3 % Giemsa or the Hemacolor® kit gave rise to two distinct staining profiles: basophilic and eosinophilic haemocytes. The cytoplasm of eosinophilic hemocytes (Figure 3.5, A-E) were densely packed with pink to dark purple granules of varying size and abundance. Hence, they are referred to as eosinophilic granulocytes herein. Their individual granules were usually not distinguishable in a non-spread state, but instead gave their cytoplasm an irregular pink color (Figure 3.5, A and E). These haemocytes had cell diameters in the range of 6-16 μm, with a mean of 9.06±1.25 μm (n=1030). Two strikingly homogeneous features of this cell type is a small acentrically located nucleus, and a regular spherical outline in a non-spread state. With abundant pink cytoplasm making up the majority of the cells' surface area – even in the smallest specimens – the eosinophilic granulocytes could also be characterized by a low N:C ratio.

Compared to the eosinophilic granulocytes, the basophilic hemocytes encompassed a more heterogeneous population. Common to all basophils were a larger nucleus that occupied more of the cells' total surface area (higher N:C ratio). The shape of which varied from spherical to oval, or had a distinct bean-shaped or irregular outline. But judged from the morphological criteria of cell size, granularity and N:C ratio, there were essentially two distinct subpopulations of basophilic haemocytes. These comprised one subpopulation of small blast-like basophils (5.63 ±0.72 μm, n=154) displaying only a marginal rim of dove blue

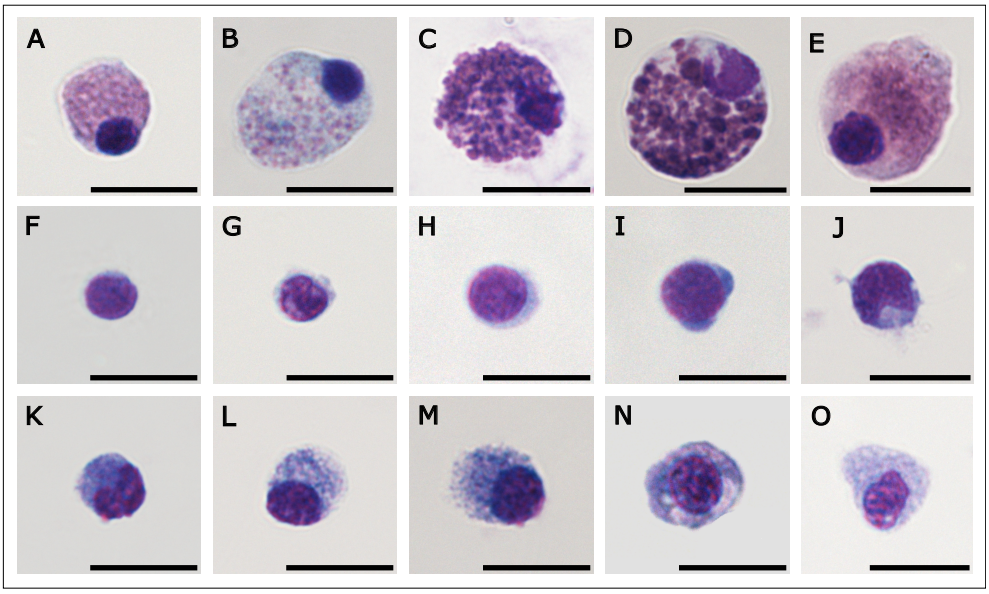

Figure 3.5: 1000x brightfield micrographs of the three haemocyte cell types found in the haemolymph of *M. edulis*. Samples were fixed and stained on glass slides with the Hemacolor® kit according to the manufacturers recommendations. **(A-E)** Eosinophilic granulocytes. **(F-J)** Small blast-like basophils. **(K-O)** Basophilic granulocytes. Scale bars = 10 µm.

cytoplasm and no apparent cytoplasmic granules (Figure 3.5, F-J), and one subpopulation of larger basophils (8.07 ±1.25 µm, n=821) – displaying abundant basophilic cytoplasm with varying degrees of cytoplasmic granulation and vacuolation (Figure 3.5, K-O).

The basophillic granules appeared much smaller than those of the eosinophilic granulocytes, and were usually not very conspicuous – unless haemocytes were subjected to osmotic swelling prior to fixation and staining. However, under differential interference contrast (DIC) illumination, their granules created highly irregular surface topographies in spread cells that could be observed without such treatment. On the basis of these morphological differences, the basophilic haemocytes were subdivided into small blast-like basophils (Figure 3.5 F-J) and basophilic granulocytes (Figure 3.5 K-O), herein.

The size distributions of the three haemocyte types are shown as three kernel-smoothened density plots in Figure 3.6, together with that of the total haemocyte population. The densities have been scaled to the number of observations of each cell type, such that their relative proportions can be visualized. In the 20 adult mussels examined here, the small blast-like basophils were the least abundant cell type, making up 7.9 ±5.6% of the total haemocyte population. In 14 out of 20 mussels, the small blast-like basophils were followed by the basophilic granulocytes, with a mean relative proportion of 40.7 ±12.9%. In spite of constituting similar proportions to the basophilic granulocytes in several mussels, the eosinophilic granulocytes were the most abundant cell type in the haemolymph of *M.*

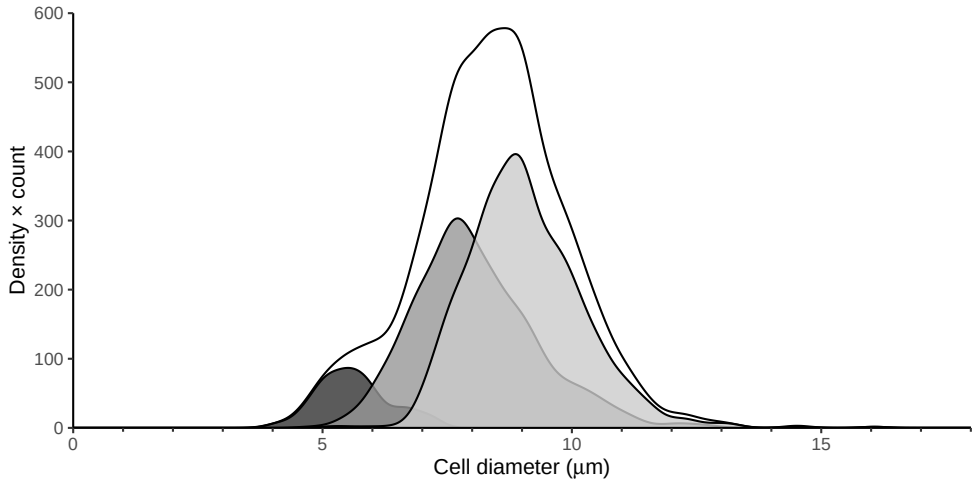

Figure 3.6: Size distribution of ■ small blast-like basophils (n=154), ■ basophilic granulocytes (n=821), ■ eosinophilic granulocytes (n=1030) and □ the total undifferentiated haemocyte population of *M. edulis* (n=2005). The diameters of 100 formaldehyde-fixed haemocytes were measured in each of 20 individual mussels, and the density was scaled to the number of observations of each cell type.

edulis, constituting 51.5 ±15.3% of the total haemocyte population, on average. The relative proportions of basophilic and eosinophilic granulocytes did however vary to a large extent between individual mussels, as reflected by their standard deviations.

3.2.2 Flow cytometric characterization of haemocyte subpopulations

Light-scatter characteristics

A maximum of three distinct subpopulations could be separated according to forwards scatter (FCS) vs. side scatter (SSC) in suspensions of living haemocytes from *M. edulis*. These subpopulations correspond to clusters 1, 2 and 3 in Figure 3.7, where the haemocytes of three representative mussels are displayed with SSC on logarithmic and linear scales. Cluster 1 consisted of events with low FSC- and SSC-values, cluster 2 of events with high FSC-values and intermediate SSC-values, while cluster 3 consisted of events with both high FSC- and SSC-values.

The adjunct histograms in Figure 3.7A and B clearly illustrates that the three clusters of events were separated according to log SSC, while there was substantial overlap between cluster 2 and 3 with regard to FSC. The latter feature was consistent across all mussels, while the degree of separation according to log SSC was subject to individual variation. In this regard, the haemolymph sample presented in 3.7B represents a typical mussel, i.e., with cluster 2 and 3 incompletely separated according to log SSC. The samples presented in 3.7A and C represents the extreme ends of this variation, with complete separation and complete overlap, respectively.

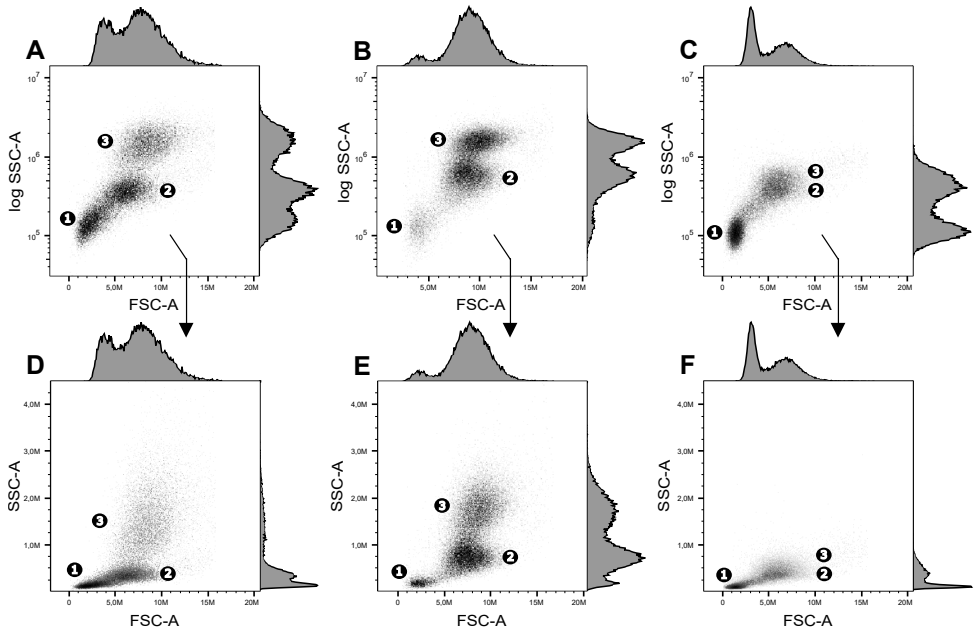

Figure 3.7: Haemocyte subpopulations distinguishable according to FSC and SSC measurements on the BD Accuri C6 Plus flow cytometer. The light-scatter profiles of three representative adult mussels are displayed with SSC on logarithmic **(A-C)** and linear **(D-F)** scales. Adjunct histograms are included to illustrate the degree of separation contributed from by each parameter individually.

Since FSC and SSC can be interpreted as relative measures of cell size and internal complexity, these results suggests that the haemolymph of *M. edulis* are comprised of three cell types that are distinguishable according to size and internal complexity. The events populating cluster 1 exhibited low FSC- and SSC-values relative to cluster 2 and 3, indicating that it is populated by haemocytes that are both smaller and less complex than the rest of the haemocytes. If SSC is interpreted more specifically in terms of haemocyte characteristics, the events populating cluster 2 and 3 most likely correspond to large semi-granular haemocytes and large granulocytes, respectively.

Calcein AM efflux and SSC

After staining with 50 nM Calcein AM prior to flow cytometric analyses, suspensions of living haemocytes separated into three distinct subpopulations according to log Calcein fluorescence (533/15 nm) vs. log SSC in 90% of adult mussels (n=22). The gating strategy is presented in Figure 3.8 (A-D), where the aforementioned subpopulations are displayed in subplot 3.8C. These corresponded to one subpopulation of Calcein^{dim} events with low SSC-values (Calcein^{dim} SSC^{low}), one subpopulation of Calcein^{bright} events with intermediate SSC-values (Calcein^{bright} SSC^{mid}) and one subpopulation of Calcein^{dim} events with high SSC-values (Calcein^{dim} SSC^{high}).

The two Calcein^{dim} clusters were gated according to the regions in Figure 3.8C, and were shown to correspond to cluster 1 and 3 in bivariate plots of FSC vs. log SSC (see Figure 3.8D). Calcein bright events with intermediate SSC-values were gated as events not present in the two aforementioned regions, and were invariably corresponding to cluster 2 when back-gated to bivariate plots of FSC vs. log SSC.

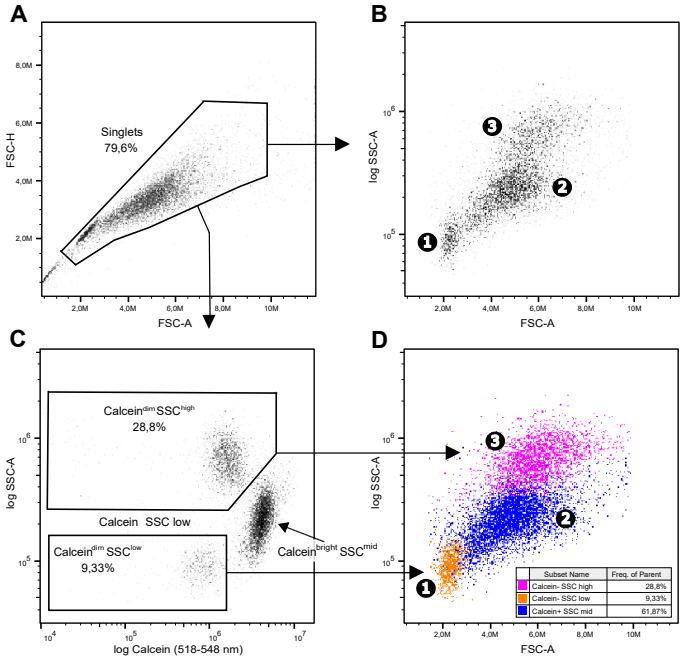

Figure 3.8: Haemocyte subpopulations distinguishable by Calcein AM efflux and SSC. Haemolymph samples were stained with 50 nM Calcein AM for 15 minutes prior to flow cytometric analysis. **(A)** Events were gated according to FSC-A vs. FSC-H to eliminate doublet haemocytes, debris and larger aggregates from the analysis. **(B)** The singlet events populated three distinct clusters according to FSC-A vs. log SSC-A (cluster 1-3). **(C)** By exchanging FSC-A for log Calcein fluorescence on the x-axis, cluster 1 and 3 could be gated without considerable overlap with cluster 2, due to their lower fluorescent intensity of hydrolyzed Calcein AM. **(D)** The events in the Calcein^{dim}/SSC^{low} and Calcein^{dim}/SSC^{high} gates are shown to correspond to cluster 1 and 3, respectively.

As shown in the previous section (3.2.2), the degree of separation between clusters 1-3 were subject to individual variation with regard to SSC. Since cluster 2 and 3 are distinguished solely on the basis of this parameter, the events populating these regions cannot be completely resolved in mussels where these clusters are partly overlapping with regard to SSC. However, by employing Calcein fluorescence as a second discriminator in place of FSC, the haemocytes of cluster 3 could be gated indirectly on the basis of their lower accumulation of hydrolyzed Calcein. As the events of cluster 1 also exhibited a lower fluorescent intensity of Calcein, the substitution Calcein fluorescence for FSC did not present a compromise for the resolution of cluster 1.

3.2.3 Relating cytologically defined cell types to light-scatter profiles

Flow cytometric characterization of haemocytes pre-separated by isopycnic centrifugation

Formaldehyde-fixed haemocytes separated into three distinct cell-bands on the 15/33%, 38/43% and 43/90% gradient interfaces of the discontinuous Percoll gradients. As shown in Figure 3.9, the two upmost bands exhibited a similar blue coloration, while the band located on the 43/90% interface had a darker purple color. The latter consisted of 96.9±0.9% eosinophilic granulocytes (n=2), with a few basophillic granulocytes scattered among them. From the cell-bands located at the 15/33% interface, populations of 96.3±0.2% basophillic haemocytes were isolated (n=2). The majority of these cells were basophilic granulocytes (87.5±1.2%), with a lesser fraction of small blast-like basophils (8.8±1.5%). The middle bands did not yield any of the cell types in high purity, but were predominantly populated by basophilic granulocytes (72.7±1.5%, n=2). The light scatter profiles of the three isolated cell fractions are depicted in Figure 3.10 – together with that of the unseparated haemocytes.

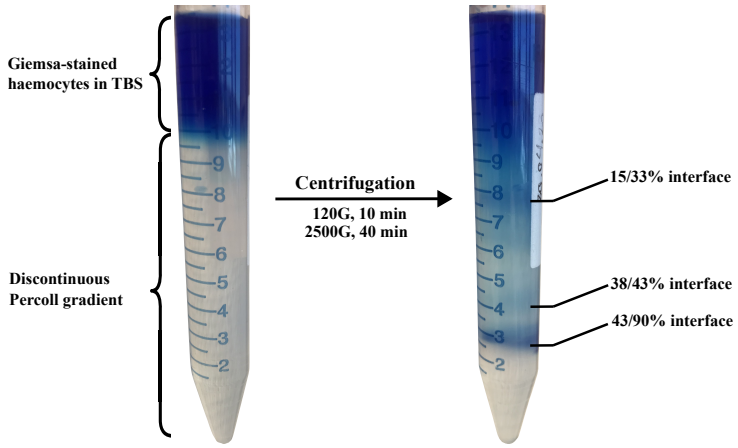

Figure 3.9: Percoll gradients before and after isopycnic separation. Formaldehyde-fixed haemocytes pre-stained with 3% Giemsa were separated by isopycnic centrifugation on discontinuous Percoll gradients. The haemocytes settled into three distinct cell bands on the 15/33%, 38/43% and 43/90% gradient interfaces.

As shown in Figure 3.10A, the pooled haemocytes were not readily distinguishable as three separate subpopulations prior to ispycnic separation. Since the relative size and complexity of the three cell types vary slightly between individual mussel, this is expected when haemolymph from two or more mussels are pooled together. However, as the pooled haemocytes were separated into enriched fraction of eosinophilic and basophilic haemocytes, a more distinct and non-overlapping clustering was seen among these subpopulations.

The eosinophilic granulocytes (>97%) that were isolated from the bottom layer formed a dense cluster of events with high FSC- and SSC-values (Figure

3.10B). This is consistent with the expected light scatter profile of this cell type, as they represent highly granulated cells with large cell diameters. In relation to the three clusters observed in suspensions of living haemocytes (section 3.2.2), the purified fraction of eosinophilic granulocytes populated a region corresponding to cluster 3.

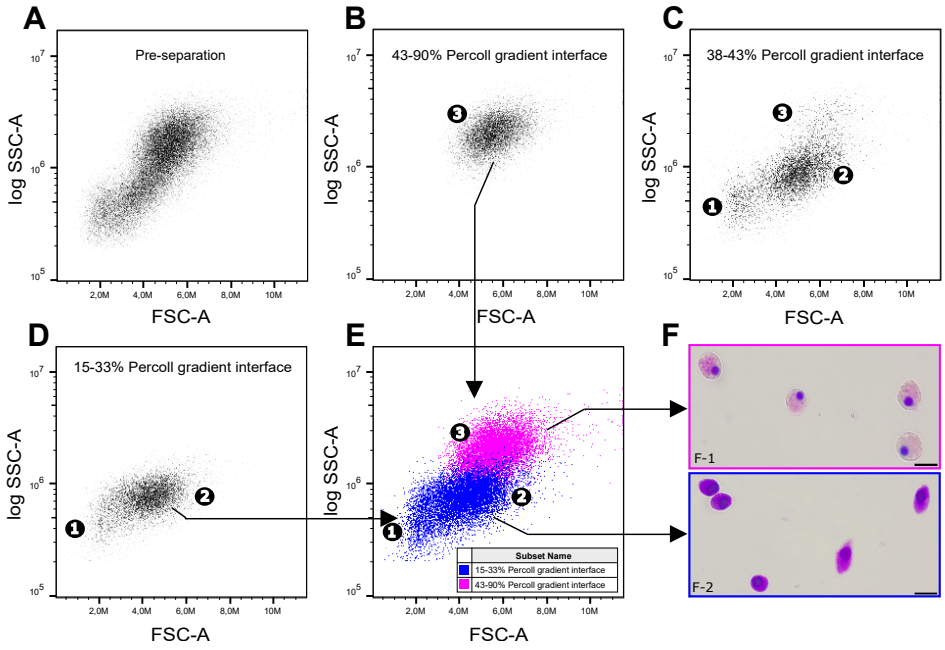

Figure 3.10: Flow cytometric analysis of the isolated cells types of *M. edulis* haemolymph after separation by isopycnic centrifugation. Two pools of formaldehyde-fixed haemocytes were separated by density-dependent centrifugation after the method of Friebel and Renwrantz (1994), and the isolated fractions were analyzed by flow cytometry and light microscopy. FSC vs. log SSC plots depict one of the pools prior to centrifugation **(A)** and after separating into three distinct cell-bands on the gradient interfaces **(B-D)**. The enriched fractions (>97%) of eosinophilic granulocytes **(B)** and basophilic haemocytes (>96%) **(D)** are overlayed in **(E)**, with 400x haemocyte micrographs from the respective layers presented in **(F)**. F-1: eosinophilic granulocytes; F-2: basophilic granulocytes; scale bars = 10 µm.

Since the middle cell band was populated by all three cell types, the scatter-plot in Figure 3.10C contains three clusters of events. Even though the haemocytes were permeabilized prior to flow cytometric acquisition, these clusters clearly corresponded to clusters 1-3 in samples of living haemocytes. With just 18.4% eosinophilic granulocytes, the region corresponding to cluster 3 was only sparsely populated. The predominant basophilic fraction (81.6%) must therefore represent most or all of the events in cluster 2, and all of the events in cluster 1. This was further supported by the scatter-plot in Figure 3.10D, where the purified fraction of basophilic haemocytes (>96%) populated the regions of cluster 1 and 2, exclusively. Because of their significantly smaller size, the small blast-like basophils must be confined to cluster 1.

The two basophilic cell types from the upper cell band were unambiguously separated from the eosinophilic granulocytes according to log SSC. This is clearly demonstrated by the overlayed dotplot in Figure 3.10E, where the haemocytes of the two fractions barely overlap. Micrographs (400x) of the most predominant cell types found in these layers are shown in Figure 3.10F.

Identification of eosinophilic granulocytes by Eosin Y fluorescence

Formaldehyde-fixed haemocytes stained with 0.5% Eosin Y were separated into distinct eosin^{bright} and eosin^{dim} populations by flow cytometric measurements of Eosin Y fluorescence (Figure 3.11, A-D). The degree of separation varied to a large extent between individual mussels, but the MFI of eosin^{bright} events were 11±9 times higher than that of eosin^{dim} events, on average. The difference in fluorescent intensity between eosinophilic and basophilic granulocytes is illustrated in Figure A.2 (Appendix A.5), where Giemsa-stained haemocytes have been imaged by epifluorescence microscopy ($\lambda \geq 515$ nm).

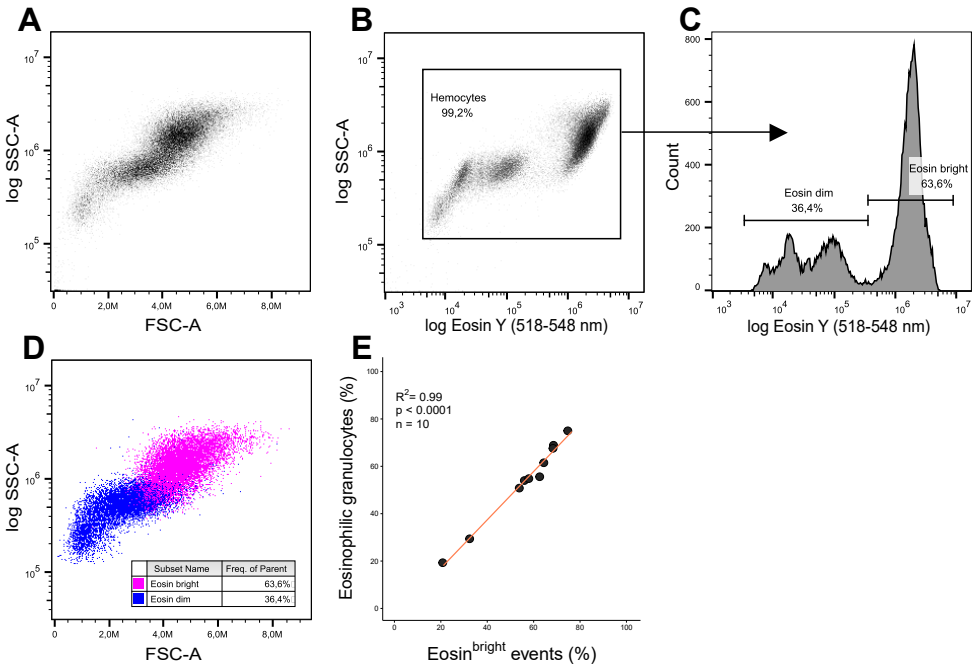

Figure 3.11: Identification eosinophilic granulocytes on FSC vs. SSC dotplots according to log eosin fluorescence (533/15 nm). Ten formaldehyde-fixed haemolymph samples were stained with 0.5% eosin and recorded on the flow cytometer right thereafter **(A)**. Haemocyte events were gated according to log eosin fluorescence vs. SSC-A **(B)** and the eosin^{bright} events were gated univariately **(C)**. The eosin^{bright} events were back-gated to show their light scatter profile relative to eosin^{dim} events **(D)**. The simple regression of eosin^{bright} events (%) vs. eosinophilic granulocytes (%) determined from 1000-cell differential counts are shown in **(E)**, regression line: $y_i = -3.20042 + 1.06656x_i$.

The pooled sample depicted in Figure 3.11A were unambiguously separated

into three distinct haemocyte subpopulations according to FSC and SSC. These subpopulations were equivalent to cluster 1-3 in samples of living haemocytes (see Figure 3.7). When the eosin^{bright} events were back-gated to bivariate plots of FSC vs. log SSC, they invariably corresponded to the subpopulation with high FSC- and SSC-values, i.e., cluster 3. (see Figure 3.11D). This is clearly demonstrated by comparing Figure 3.11A and D, where the eosin^{bright} events are shown in pink.

In the 10 Giemsa-preparations that were prepared, the percentage of eosinophilic granulocytes were significantly predicted by the percentage of eosin^{bright} events (%) in the parallel flow cytometric analyses ($\beta = 1.06656$, t(8) = 23.3, p<0.001). The data is presented in Figure 3.11E, together with the fitted linear regression model ($R^2 = 0.99$, F(1, 8) = 541, p<0.001). With a mean percent error of 3.08±2%, about 97% of the pink events shown Figure 3.11D would represent eosinophilic granulocytes, on average.

3.2.4 Flow cytometric differential haemocyte count: validation

The estimated percentages of small blast-like basophils (events in cluster 1), basophilic granulocytes (events in cluster 2) and eosinophilic granulocytes (events in cluster 3) exhibited close linear relationships with the results obtained by light microscopy. The flow cytometric estimates are presented individually for each cell-type in Figure 3.12 (A-C), where they are regressed on the percentages calculated from the 1000-cell microscopic differential counts. To reveal any potential bias along the observed range of values, the best-fitted lines are evaluated in relation to an ideal linear relationship, which is described by a linear function with y-intercept = 0 and slope = 1.

The percentages of eosinophilic granulocytes in Giemsa-smears were significantly predicted by the percentages of events in cluster 3 ($\beta = 1.0576$, t(18) = 23.8, p<0.001), with a mean percent error of 6.42±4%. The linearity of the response was close to ideal, with a slight underestimation bias in the flow cytometric estimates. As shown in Figure 3.12A, this tendency was more pronounced in mussels with high proportions of eosinophilic granulocytes. Aside from this, a significant correlation was observed between results obtained by the two methods ($R^2 = 0.97$, F(1, 18) = 566.2, p<0.001).

The percentages of events in cluster 2 significantly predicted the percentages of basophilic granulocytes from the microscopic counts ($\beta = 1.0540$, t(18) = 22.0, p<0.001). While the correlation between the flow cytometric estimates and the microscopy counts ($R^2 = 0.96$, F(1, 18) = 481.9, p<0.001) were similar to that of the eosinophilic granulocytes; the accuracy were comparatively lower (mean percent error = 9.80±12%). As the y-intercept of the best fitted line was marginally lower than zero (α = -5.2120, 95% CI [-10.2416, -0.1825]), the regression analysis showed that the percentages of basophilic granulocytes were slightly overestimated in the lower end of the observed range. This tendency can be seen from the data depicted in Figure 3.12B.

The linearity plot presented in Figure 3.12C shows that the flow cytometric

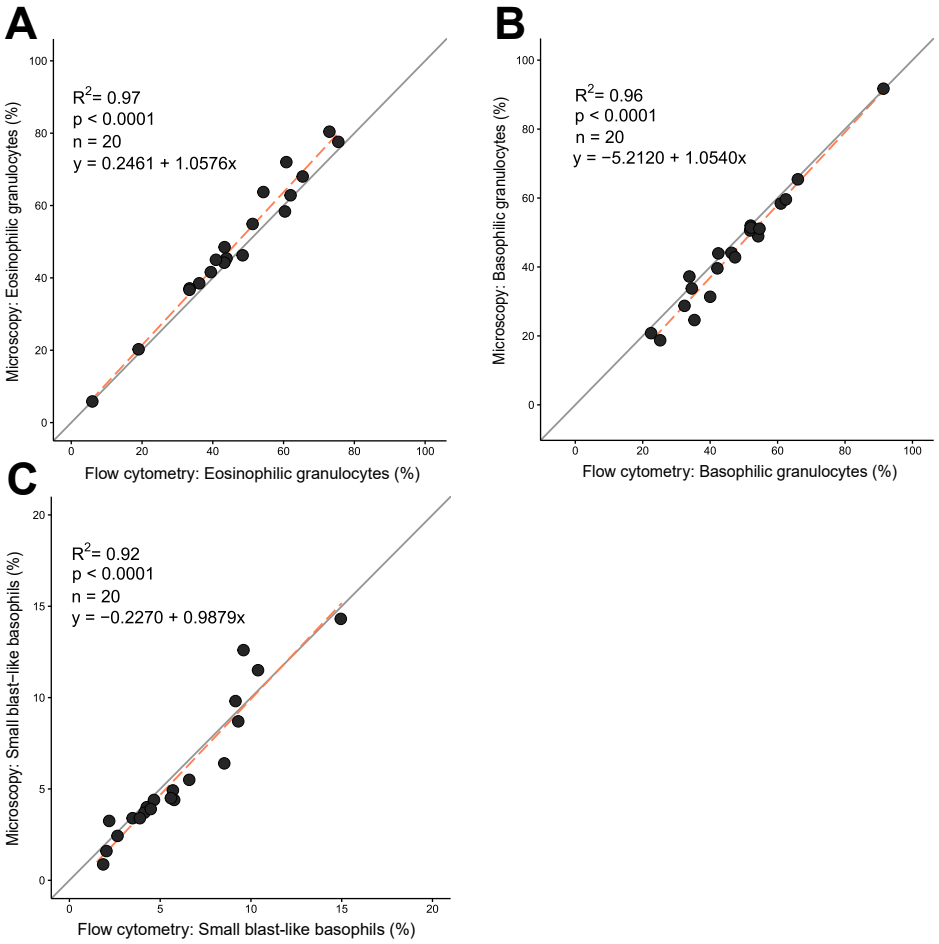

Figure 3.12: Linearity of response validation of flow cytometric differential haemocyte count. Simple linear regression of the percentages of eosinophilic granulocytes **(A)**, basophilic granulocytes **(B)** and small blast-like basophils **(C)** from differential haemocyte counts performed by microscopy and flow cytometry (n=20). The three cell types were differentiated as clusters 1-3 (1: small blast-like basophils; 2: basophilic granulocytes; 3: eosinophilic granulocytes), which were gated indirectly according log Calcein fluorescence (518-538 nm) vs. log SSC-A as shown in Figure 3.8.

differential haemocyte count was less accurate in predicting the percentages of small blast-like basophils compared to the granular cell types. This is evident from the mean percent error of 20.72±24%, which is more than three times higher than that observed for the eosinophilic granulocytes. Despite having similar absolute errors to the two granular cell types, the small blast-like haemocytes presented relatively higher percentage errors due to their lower proportions in haemolymph (5.68±4%). In spite of this, the percentages of events in cluster 1 was a significant and almost entirely unbiased predictor in the tested mussels ($\beta = 1.0501$, $t(18) = 14.1$, $p<0.001$).

3.3 Scoring of necrotic haemocytes by flow cytometry

3.3.1 Determination of optimal TO-PRO-3 Iodide staining concentration

Viable and MeOH-killed haemocytes could be separated according to TO-PRO-3 Iodide fluorescence in the whole range of tested concentrations (30 nM - 8 µM). As shown in Figure 3.13, the resolution between $ToPro3^{-}$ and $ToPro3^{+}$ events increased with the TO-PRO^{TM}-3 Iodide concentration according to the log-logistic function shown in (3.2), with a marked stagnation > 1.2 µM. The model explained almost all the variation in the dataset (Pseudo-R^2 = 0.99, see table A.2), and should therefore be a good predictor of the expected resolution between necrotic and viable haemocytes in the tested range of TO-PRO^{TM}-3 Iodide.

$$y_i = \frac{9890700}{1 + (x_i/0.41655)^{-0.94088}} + \epsilon_i \tag{3.2}$$

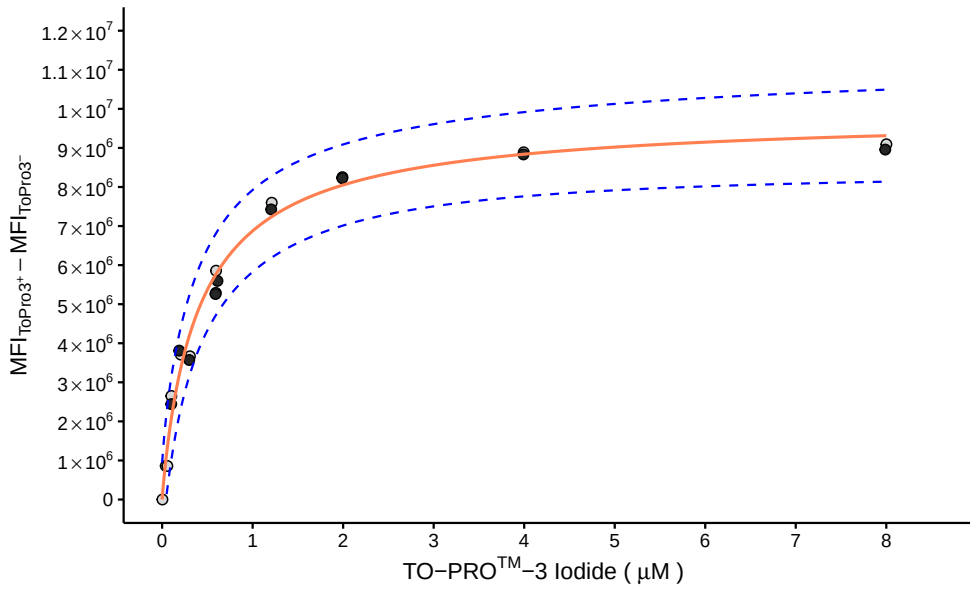

Figure 3.13: Experimental determination of the optimal TO-PRO^{TM}-3 Iodide concentration for dye exclusion tests. 10 aliquots of pooled methanol-killed (70% MeOH, 30 min) and viable haemocytes (1:1) were stained with different concentrations of TO-PRO^{TM}-3 Iodide (30 nM - 8 µM) for 15 and 30 minutes, and analyzed on the flow cytometer (FL4 detector, 675/25 nm). The difference in mean fluorescent intensity (MFI) between viable ($ToPro3^{-}$) and methanol-killed haemocytes ($ToPro3^{+}$) after 15 (◎) and 30 minutes (●) is plotted against the staining concentration of TO-PRO^{TM}-3 Iodide. Red line: fitted log-logistic regression model; blue dashed lines: prediction intervals.

The predicted difference in MFI at 1.2 µM was 7.220.000 (95% PI[6.170.000, 8.260.000]). Since the slope of function (3.2) decreased rapidly for x > 0.6 µM,

the predicted difference in MFI at x = 1.2 μM was contained within the prediction intervals for the rest of the function's range. Furthermore, the MFI of the ToPro3^{-} populations increased abruptly at concentrations ≥ 2 μM (see Table B.4, Appendix B), indicating a potential cytotoxic effect of either TO-PRO^{TM}-3 Iodide or the DMSO solvent at the three highest concentrations.

The results were also unambiguous regarding the incubation period. According to Figure 3.13, the resolution between viable and necrotic cells did not increase after the initial 15 minute incubation period. The MFI of necrotic haemocytes did increase somewhat in the extended incubation period, but the resolution remained unchanged due to a concurrent proportional increase among the viable haemocytes (see table B.4, Appendix B).

3.3.2 Gating strategy

The finalized quadrant gating strategy for the Calcein AM/TO-PRO^{TM}-3 Iodide membrane integrity assay is presented in Figure 3.14. The four plots (A-D) represent samples of viable and methanol-killed haemocytes in equal proportions (A, unstained control; B, Calcein FMO; C, TO-PRO^{TM}-3 Iodide FMO; D, Calcein/TO-PRO^{TM}-3 Iodide). Unstained controls were used to establish a tentative lower left quadrant gate (Calcein^{-} ToPro3^{-}) for non-cellular events (Figure 3.14A). This quadrant was expanded in both directions to include all Calcein^{-} events of the Calcein FMOs and all the ToPro3^{-} events of the TO-PRO^{TM}-3 Iodide FMOs (Figure 3.14B and C). When the double stained samples were run, the viable and methanol-killed haemocytes populated the upper left and lower right quadrants, exclusively (Figure 3.14D).

3.3.3 Method validation

Simple linear regression was used to examine the correlation between results obtained by epifluorescent microscopy and the flow cytometric gating strategy presented in Figure 3.14. It was found that the established quadrant gating strategy significantly predicted the the percentage of ToPro3^{+} haemocytes in samples scored by epifluorescent microscopy ($\beta = 0.9882$, t(8) = 32.5, p<0.001), with a mean absolute error of 2.37±2% and a mean percent error of 21.8±35%. The data is presented in Figure 3.15, together with the fitted linear regression model ($R^2 = 0.99$, F(1, 8) = 1059, p<0.001). By comparing the best fitted line to the "ideal" linear response line in Figure 3.15, this method was completely free of bias in the whole range of MeOH-killed haemocytes tested .

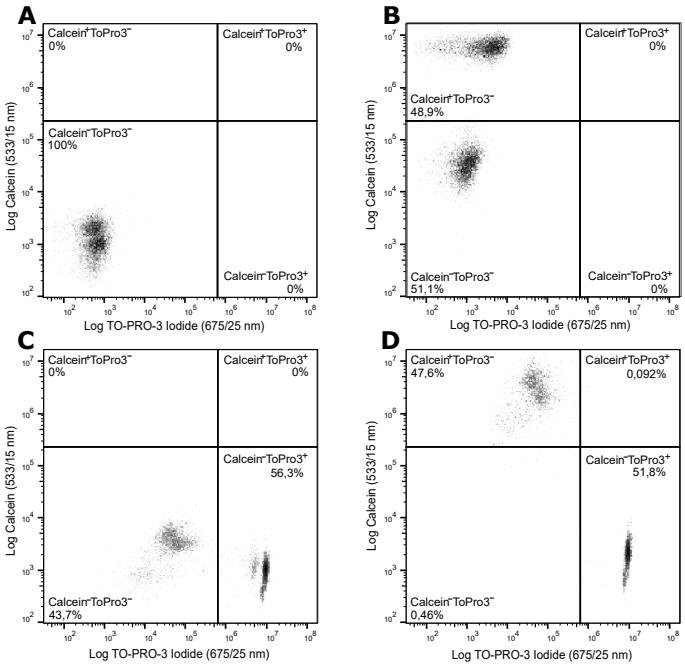

Figure 3.14: Quadrant gating strategy for scoring necrotic (Calcein$^-$ ToPro3$^+$) an viable (Calcein$^+$ ToPro3$^-$) haemocytes. By preparing a 1:1 pool of MeOH-killed and newly withdrawn haemocytes in (ACB), gates were drawn according to the florescent profiles of **A)** Unstained controls, **B)** Calcein FMOs, **C)** TO-PRO^{TM}-3 Iodide FMOs and **D)** aliquotes stained with both probes.

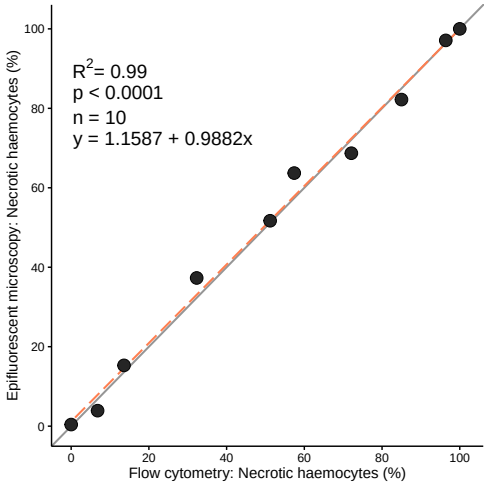

Figure 3.15: Correlation between necrotic haemocyte percentages scored by flow cytometry and epifluorescent microscopy. 10 samples of freshly withdrawn haemocytes (ACB, 1:1) were mixed with methanol-killed haemocytes in semi-random proportions (0-100%), stained with Calcein AM (50 nM) and TO-PRO^{TM}-3 Iodide (1.2 µM) and the percentage of necrotic haemocytes (%) were scored by both flow cytometry and epifluorescent microscopy. Each datapoint represents one scored sample. Red line: fitted linear regression model.

Chapter 4

Discussion

4.1 Selection of haemocyte medium for flow cytometric analyses

Even though the aggregation model was slightly over-dispersed, the estimates provide some insight into the three buffers relative abilities to prevent hemocyte aggregation within the first hour post-withdrawal. The Ca^{2+}-free EDTA-containing buffers were effective inhibitors of hemocyte aggregation compared to simply diluting samples in cold in MPSS. When the latter method was used, visible aggregates were usually formed within the syringes immediately after hemolymph aspiration – even when the MPSS was pre-chilled on ice. This observation shows that a two-fold dilution in MPSS is less than sufficient, such that a further dilution may be required for satisfactory effect. A many-fold dilution would be inconvenient in the preparation of haemolymph smears with a certain desired density, and too time-consuming for the acquisition of 10.000 events on a flow cytometer. This method was therefore excluded as a potential approach.

By comparing the inhibitory effects of MAS and ACB on haemocyte aggregation, our data suggests that the slightly higher concentration of EDTA in ACB compensates for the lack of citrate. Since high concentrations of EDTA have been reported to impair haemocyte viability (Grandiosa et al., 2018; Burkhard et al., 2009), a direct comparison of MAS and ACB with regards to acute effects on viability was required to identify the most suitable buffer of the two.

Our results suggest that EDTA is cytotoxic to haemocytes at the concentrations used in both ACB (13.4 mM) and MAS (11.5 mM), since these buffers caused a significant dose-dependent increase in the percentage of necrotic haemocytes across the three timepoints (Table 3.2). However, since there was no significant differences between the EDTA-containing buffers and the negative EDTA-control after 15 minutes of incubation, this cytotoxic effect had no detectable manifestation within the time-frame of the planned flow cytometric assay. As long as haemolymph samples are stained and processed within 30 minutes of sampling, a flow cytometric dye exclusion/inclusion assay with TO-PRO^{TM}-3 Iodide and Calcein

AM will not have time to detect *in vitro* necrosis caused by the buffers themselves.

The apoptosis assay with non-adjusted MAS (pH = 6.1) showed that 15 minutes was more than enough for haemocytes to enter programmed cell death. The percentage of early apoptotic cells suggests that an abrupt decrease in pH is an efficacious inducer of apoptosis, and that the haemocytes of *M. edulis* are very sensitive to their environmental pH. This has been demonstrated by several recent studies investigating the effects of ocean acidification on the immune system of bivalves (see e.g., Wang et al., 2016; Dang et al., 2023). Maintaining the pH of MAS at 6.1 was therefore not an option for flow cytometric analyses of apotosis or necrosis.

Our analyses did not detect any differences between ACB and MAS with regard to their anticoagulant effects or cytotoxicity within the time-frame of the planned assays. The data does however demonstrate the importance of a carefully regulated haemocyte medium pH. As the buffer capacity of MAS is negligible at pH = 7.0, ACB appears as the most suitable haemocyte medium of the two. The Anticoagulant Buffer (ACB) of Pipe et al. (1997) was therefore chosen to contain the degree of haemocyte aggregation during our flow cytometric analyses.

4.2 Development of a flow cytometric differential count

The haemolymph of *M. edulis* were found to contain three morphologically distinct cell types according to traditional cytological criteria. These comprised (1) small agranular basophilic cells (small blast-like basophils), (2) larger basophilic cells with small inconspicuous granules (basophilic granulocytes) and (3) large eosinophilic cells with cytoplasm densely populated by larger eosinophilic granules (eosinophilic granulocytes). This finding corroborates the early work by Moore and Lowe (1977), and what several other investigators have found since (Rasmussen et al., 1985; Renwrantz, 1990; Pipe, 1990; Nöel et al., 1994; Pipe et al., 1997; Wootton et al., 2003). Allthough, there has been scientific dispute regarding the classification of basophilic and eosinophilic granulocytes as two distinct cell-types (Cheng, 1980), this distinction was made for purely descriptive purposes herein.

Similar to the cytological characterization, a maximum of three distinct subpopulations could be separated according to relative size (FSC) and internal complexity (SSC) in suspensions of living haemocytes. These comprised one subpopulation of small cells with low internal complexity (cluster 1), one subpopulation of larger cells with intermediate internal complexity (cluster 2) and one subpopulation of large cells with high internal complexity (cluster 3). These subpopulations correspond to those described by Le Foll et al., (2010), who characterized the haemocytes of *M. edulis* according to cell diameter (µM) and SSC with a flow cytometer equipped with Coulter-type cell-volume determination. The apparent correlation between these subpopulations and the three cytologically defined cell types were striking with regard to their relative size and granularity.

The small blast-like basophils (5.63 ±0.72 µm) were considerably smaller than the basophilic and eosinophilic granulocytes, and exhibited no apparent granulation. One would therefore expect them to be unambiguously separated from the

larger granulocytes according to both FSC and SSC. The size distributions in Figure 3.6 does however indicate an overlap in size between the largest blast-like basophils and the smallest basophillic granulocytes in some mussels. But, since they are uncomplex cells, they should be separated according to SSC regardless. The events populating cluster 1 in Figure 3.7 were therefore expected to represent small blast-like basophilic haemocytes.

Both eosinophilic and basophilic granulocytes were granulated in the formal definition of the word. But this discussion requires a more nuanced interpretation of what is meant by granulocyte herein. The cytoplasm of eosinophilic granulocytes were packed with pink to dark purple granules to the extent that their cytoplasm appeared pink in a non-spread state (see Figure 3.5, K-O). This is in sharp contrast to the granulation of basophilic granulocytes, which were more sparse, variable and much less conspicuous. Consequently, there was little doubt that cluster 3 was expected to correspond to eosinophilic granulocytes, while the semi-granular events of cluster 2 aligned with the size and complexity of basophilic granulocytes.

Le Foll et al., (2010) suggested that the events of cluster 2 could corresponded to a cell type which they referred to as hyalinocytes. These were larger agranular cells (10 µm) with pale staining cytoplasm (Hemacolor®), and were often observed as spread cells with vacuoles. This distinct morphology was occasionally observed in our Hemacolor® preparations too, but not in preparations stained with 3% Giemsa - regardless of the fixative used. They where also not observed if haemocytes were fixed before they had sufficient time to spread extensively onto glass slides. For that reason, the pale cytoplasmic staining was regarded as a result of extensive spreading and technicalities pertaining to the Hemacolor® staining protocol. Several electron microscope studies have shown ultrastructural variability among the larger semi-granular to agranular basophils (Carballal et al., 1997; Rasmussen et al., 1985; Pipe, 1990), such that a definite distinction is hard to infer from light microscopy examinations alone. Because of the inconsistency in observations of the "hyalinocyte" morphology, it did not represent a separate cell type distinct from the basophilic granulocytes in our view.

As seen from the size distributions in Figure 3.6, the basophilic and eosinophilic granulocytes were not readily distinguishable according to cell diameter. This was further substantiated by the fact that cluster 2 and 3 were more or less completely overlapping with regard to FSC. The haemolymph samples depicted in Figure 3.7 did however show that the FSC of cluster 3 was slightly right-shifted relative to cluster 2, which was expected since the eosinophilic granulocytes were found to be 0.92 µM larger than basophilic granulocytes on average.

Even thought there was an apparent correlation between cluster 1-3 and the size and internal complexity of the cytologically defined cell types; these interpretations required visual verification before a potential gating strategy could be implemented from these results. The ispycnic separation of eosinophilic granulocytes from the two basophilic cell types allowed for these cell types to be characterized by FSC vs. SSC separately.

The eosinophilic granulocytes (> 96%) formed a dense cluster of events with high SSC relative to the two basophilic cell types, and were thus positively identified as the cells populating cluster 3 in figure 3.7. This observation was further supported by the fact that eosin^{bright} events populated the same cluster when formaldehyde-fixed cells stained with 0.5% Eosin Y were back-gated to bivariate plots of FSC vs. SSC. Since there was a strong correlation between eosin^{bright} events (%) and the percentage of eosinophilic granulocytes (R^2=0.99), this finding provided additional compelling evidence for this hypothesis. The same conclusion was reached by Le Foll et al., (2010), from which the latter experiment originated. The original methodology failed to produce well-defined eosin^{bright} and eosin^{dim} peaks, such that the lower bound of the eosin^{bright} gate had to be drawn more or less arbitrarily (Le Foll et al., 2010, Figure 4A). It could therefore not be used to pinpoint the exact region populated by eosinophilic granulocytes. In this context, the Eosin Y staining procedure described in section 2.2.6 of the present study represents a significant improvement to this flow cytometric approach.

Similar to the findings of previous investigators (Friebel and Renwrantz, 1995; Pipe et al., 1997; Carballal et al., 1997), the basophilic granulocytes and small blast-like basophils of *M. edulis* were not separated according to density by the discontinuous Percoll gradient. This finding demonstrated that the granule density of basophilic granulocytes was too low to produce a measurable difference in the overall cell density compared to small blast-like basophils. However, the basophilic cells that populated the middle fraction of the Percoll gradient were separated into two subpopulations according to FSC vs. SSC in the subsequent flow cytometric analyses (Figure 3.10C). These two subpopulations occupied the regions corresponding to cluster 1 and cluster 2 in suspensions of living haemocytes, and eosin^{dim} events in measurements of Eosin Y fluorescence. Based on the relative size and granularity of these cell types, cluster 2 should intuitively correspond to larger basophilic granulocytes, while cluster 1 to that of small blast-like basophils. Allthough this working hypothesis had not been verified by visual inspection, there was no compelling evidence against it, either. If it turned out to be correct, this would become apparent during the validation of the flow cytometric differential haemocyte count.

As pointed out in section 3.2.2, light-scatter analyses of haemolymph from *M. edulis* did not always result in three well defined subpopulations, i.e., cluster 1-3. This was mainly due to a substantial overlap between the two granular cell types (cluster 2 and 3) according to FSC, which made it difficult to gate these cell types accurately when they were not completely separated according to SSC. In the context of developing a flow cytometric differential haemocyte count for *M. edulis*, this fact presented a challenge for the application of FSC vs. log SSC as the only discriminators. Careful staining with Eosin Y represented a potential candidate, as the percentage of eosin^{bright} events had proven to be a good predictor for the percentage eosinophilic granulocytes in formaldehyde-fixed samples. The two centrifugation steps and fixation (1 hour) did however render this methodology

rather time-consuming, such that a cell-permeable or external fluorescent marker would be more preferable.

The cell-permeable fluorescent probe Calcein AM were shown to produce dimmer signals in eosinophilic granulocytes (cluster 3) and small blast-like basophils (cluster 1) compared to the basophilic granulocytes (cluster 2). This phenomenon was explained by the work of Rioult et al., (2014), who demonstrated that Calcein AM is a substrate of the Multidrug Resistance-related Protein (MRP) in *M. edulis*, which has higher expression and inducibility in eosinophilic granulocytes. The lower fluorescent intensity of hydrolyzed Calcein observed in the small blast-like basophils can possibly be explained by their smaller size (cell volume), as the fluorescent signals were not normalized to FSC. This is a likely explanation, as Rioult et al., (2014) showed that the two basophilic cell types exhibited similar Calcein AM efflux activity after normalizing fluorescent signals to electronic volume.

By gating the small blast-like basophils (Calcein^{dim} SSC^{low}), basophilic granulocytes (Calcein^{bright} SSC^{mid}) and eosinophilic granulocytes (Calcein^{dim} SSC^{high}) of cluster 1-3 according to log SSC and their differential accumulation of hydrolyzed Calcein, the three cell types could be distinguished by flow cytometry in 90% of the mussels tested (n=22). Although SSC constituted the primary discriminator between the three cell types, the higher rates of Calcein AM efflux from eosinophilic granulocytes resulted in a practically applicable resolution between cluster 2 and 3. This approach allowed the events of cluster 1-3 to be gated spite of partial or substantial overlaps according to SSC. For this reason, Calcein fluorescence (533/15 nm) was substituted with FSC for performing differential haemocyte counts of *M. edulis* by flow cytometry. By performing parallel flow cytometric and microscopic differential counts in 20 adult mussels, the validity of this approached could be assessed.

The percentages of small blast-like basophils, basophilic granulocytes and eosinophilic granulocytes in Giemsa-smears were significantly predicted by the percentages of events in cluster 1 (Calcein^{dim} SSC^{low}), 2 (Calcein^{bright} SSC^{mid}) and 3 (Calcein^{dim} SSC^{high}), respectively. This suggests that the established gating strategy is counting the same cell types as those differentiated by microscopy. Linearity of response assessments revealed a marginal underestimation bias in the upper range for eosinophilic granulocytes, while a slight overestimation bias was observed for the basophilic granulocytes in their lower range. As these estimates are expressed as percentages of a whole, they are all closely interlinked. Since the percentages of events in cluster 1 was a nearly unbiased predictor for small blast-like basophils, the systematic error must originate from the eosinophilic granulocyte predictor (cluster 3) - since this subpopulation is gated first.

In practical terms, these biases do not produce substantial deviance from the true values - unless mussels have very high proportions of eosinophilic granulocytes, and consequently lower proportions of basophilic granulocytes. E.g., a mussel containing 80% eosinophilic granulocytes in circulation would be estimated to contain 75.5% on average, while a mussel with 20% eosinophilic granulocytes in

circulation would be estimated to contain 18.7%. However, this deviance can be corrected for once the bias is estimated. Compared to a similar attempt to estimate haemocyte cell types by flow cytometry (Allam et al., 2002), the accuracy and reliability of the proposed differential haemocyte count is superior. Given that microscopic differential counts are performed from a total 1000 cells per mussel, this flow cytometric methodology can potentially perform more accurate estimates from 10.000 events, in a fraction of the time.

4.3 Scoring of necrotic haemocytes by flow cytometry

From the observations that the resolution between ToPro3^{-} and ToPro3^{+} events stagnated $>$ 1.2 µM TO-PRO^{TM}-3 Iodide, and that subtle cues of cytotoxicity was evident at concentrations $\geq$ 2.0 µm, the potential gain from increasing the staining concentration above 1.2 µM was limited – and not completely free of risk. The resolution between viable and necrotic haemocytes was for all practical purposes sufficient in the range of 300 nM - 1.2 µM, but the resolution achieved at 1.2 µM would simplify gating on a logarithmic scale. 1.2 µM TO-PRO^{TM}-3 Iodide was therefore preferred for scoring necrotic haemocytes by flow cytometry, together with 50 nM Calcein AM. Since the degree of separation between ToPro3^{-} and ToPro3^{+} events did not increase after the first 15 minutes of incubation, there was little use of extending the incubation period further. The latter result is in line with an optimization experiment that was performed with Propidium Iodide (Nescerecka et al., 2016), where the fluorescent intensity of PI-positive cells where stable between 10-25 minutes after onset of staining. As the occurrence of false positive cells normally increase with the incubation period (Nescerecka et al., 2016), staying close to the shortest required incubation period is advisable.

The quadrant gating strategy for scoring of necrotic haemocytes (‰) were established such that all viable (Calcein^{+} ToPro3^{-}) and methanol-killed haemocytes (Calcein^{-} ToPro3^{+}) populated the upper left and lower right quadrants respectively. By validating flow cytometric estimates from linearity of response with epifluorescence microscopy, this method was found to be highly accurate and unbiased. Compared to commercial kits validated for use in invertebrate studies, the reliability and accuracy of the proposed Calcein AM/TO-PRO^{TM}-3 Iodide viability assay is comparable or better (Ericson et al., 2021; Zeng et al., 2021).

Chapter 5

Conclusion

The present study proposes a rapid and reliable method for performing differential haemocyte counts in *M. edulis* by flow cytometry. The methodology relies on the inherent difference in granularity between small blast-like basophils, basophilic granulocytes and eosinophilic granulocytes to differentiate them according to SSC, and demonstrates that their differential accumulation of Calcein AM can be used to further distinguish subpopulations that are not separated completely according to SSC. As the proposed methodology employs Calcein AM as a second discriminator – this procedure can be combined with TO-PRO-3 Iodide for simultaneous scoring of necrotic haemocytes by a Calcein AM/TO-PRO^{TM}-3 Iodide viability assay. This assay was developed and validated herein. As accurate flow cytometric assays are more attainable with pure haemolymph samples, an effective haemolymph sampling technique was described. The withdrawal of haemolymph samples into equal volumes of the Anticoagulant Buffer (ACB) by Pipe et al., (1997) serves to slow the rate of haemocyte aggregation for the differential haemocyte count, and has been validated for use with the Calcein AM/TO-PRO^{TM}-3 Iodide viability. These procedures are proposed as faster and more reliable scoring of necrotic haemocytes and cell types in the Mussel micronucleus cytome assay by Bolognesi and Fenech (2012).

Bibliography

Ale, A., G. Giberatori, M.L. Vannuccini et al. (2019). 'Exposure to a nanosilver-enabled consumer product results in similar accumulation and toxicity of silver nanoparticles in the marine mussel Mytilus galloprovincialis'. *Aquatic Toxicology* 211, pp. 46–56. DOI: https://doi.org/10.1016/j.aquatox.2019.03.018.

Allam, B., K.A. Ashton-Alcox and S.E. Ford (2002). 'Flow cytometric comparison of haemocytes from three species of bivalve molluscs'. *Fish and Shellfish Immunology* 13 (2), pp. 141–158. DOI: https://doi.org/10.1006/fsim.2001.0389.

Anderson, A. (1993). 'Pathobiology of Marine and Estuarine Organisms'. Advances in fisheries science. CRC Press. Chap. 17.

Andree, H.A., C.P. Reutelingsperger, R. Hauptmann et al. (1990). 'Binding of vascular anticoagulant alpha (VAC alpha) to planar phospholipid bilayers.' *Journal of Biological Chemistry* 265 (9), pp. 4923–4928. DOI: https://doi.org/10.1016/S0021-9258(19)34062-1.

Ashton-Alcox, K.A. and S.E. Ford (1998). 'Variability in molluscan hemocytes: a flow cytometric study'. *Tissue & Cell* 30 (2), pp. 195–204. DOI: https://doi.org/10.1016/S0040-8166(98)80068-2.

Auffret, M. and R. Oubella (1994). 'Cytometric parameters of bivalve molluscs: effect of environmental factors'. *Modulators of fish immune responses* 1, pp. 23–32. URL: https://apps.dtic.mil/sti/pdfs/ADA276524.pdf.

Bachére, E. and H. Grizel (1988). 'Separation of Crassostrea gigas hemocytes by density gradient centrifugation and counterflow centrifugal elutriation'. *Developmental and Comparative Immunology* 12, pp. 549–559. DOI: https://doi.org/10.1016/0145-305X(88)90071-7.

Barth, N.D., R. Subiros-Funosas, L. Mendive-Tapia et al. (2020). 'A fluorogenic cyclic peptide for imaging and quantification of drug-induced apoptosis'. *Nature Communications* 11 (1). DOI: https://doi.org/10.1038/s41467-020-17772-7.

Bates, D., M. Mächler, B. Bolker et al. (2015). 'Fitting Linear Mixed-Effects Models Using lme4'. *Journal of Statistical Software* 67 (1), pp. 1–48. DOI: 10.18637/jss.v067.i01.

Bedoui, S., M.J. Herold and A. Strasser (2020). *Emerging connectivity of programmed cell death pathways and its physiological implications*. DOI: 10.1038/s41580-020-0270-8.

Beyer, J., N.W. Green, S. Brooks et al. (2017). 'Blue mussels (Mytilus edulis spp.) as sentinel organisms in coastal pollution monitoring: A review'. *Marine Environmental Research* 130, pp. 338–365. DOI: https://doi.org/10.1016/j.marenvres.2017.07.024.

Bolognesi, C. and S. Cirillo (2014). 'Genotoxicity biomarkers in aquatic bioindicators'. *Current Zoology* 60 (2), pp. 273–284. DOI: 10.1093/czoolo/60.2.273.

Bolognesi, C. and M. Fenech (2012). 'Mussel micronucleus cytome assay'. *Nature Protocols* 7 (6), pp. 1125–1137. DOI: https://doi.org/10.1038/nprot.2012.043.

Bolognesi, C. and M. Hayashi (2011). 'Micronucleus assay in aquatic animals'. *Mutagenesis* 26 (1), pp. 205–213. DOI: 10.1093/mutage/geq073.

Broschinski, L., S. Madle and C. Hensel (1998). 'Genotoxicity tests for new chemicals in Germany: routine in vitro test systems'. *Mutation Research/Genetic Toxicology and Environmental Mutagenesis* 418 (2), pp. 121–129. DOI: https://doi.org/10.1016/S1383-5718(98)00119-3.

Burkhard, M.J., S. Leavell, R.B. Weiss et al. (2009). 'Analysis and cytologic characterization of hemocytes from freshwater mussels (Quadrula sp.)' *Veterinary Clinical Pathology* 38 (4), pp. 426–436. DOI: https://doi.org/10.1111/j.1939-165X.2009.00148.x.

Cantillo, A.Y. (1998). 'Comparison of results of Mussel Watch Programs of the United States and France with Worldwide Mussel Watch Studies'. *Marine Pollution Bulletin* 36 (9), pp. 712–717. DOI: https://doi.org/10.1016/S0025-326X(98)00049-6.

Carballal, M.J., M.C. López, C. Azevedo et al. (1997). 'Hemolymph cell types of the mussel Mytilus galloprovincialis'. *Diseases of Aquatic Organisms* 29, pp. 127–135. URL: https://www.int-res.com/articles/dao/29/d029p127.pdf.

Chen, J.H. and C.J. Bayne (1995). 'Bivalve Mollusc Hemocyte Behaviors: Characterization of Hemocyte Aggregation and Adhesion and Their Inhibition in the California Mussel (Mytilus californianus)'. *Biological Bulletin* 188 (3), pp. 255–266. DOI: https://doi.org/10.2307/1542303.

Cheng, T.C. (1984). 'A Classification of Molluscan Hemocytes Based on Functional Evidences'. *Invertebrate Blood: Cells and Serum Factors*. Ed. by T.C. Cheng. Springer US, pp. 111–134.

Cheng, T.C. (1980). 'Bivalves'. *Invertebrate Blood Cells*. Ed. by Ratcliffe, N.A. and Rowley, A.F. Vol. 1. Academic Press, pp. 233–300.

Chiu, V.C. and D.H. Haynes (1977). 'High and low affinity Ca2+ binding to the sarcoplasmic reticulum: use of a high-affinity fluorescent calcium indicator.' *Biophys J* 18 (1), pp. 3–22. DOI: 10.1016/S0006-3495(77)85592-6.

Connor, J., C.H. Pak, R.F. Zwaal et al. (1992). 'Bidirectional transbilayer movement of phospholipid analogs in human red blood cells. Evidence for an ATP-dependent and protein-mediated process.' *Journal of Biological Chemistry* 267 (27), pp. 19412–19417. DOI: https://doi.org/10.1016/S0021-9258(18)41791-7.

Costa, M.M., M. Prado-Alvarez, C. Gestal et al. (2009). 'Functional and molecular immune response of Mediterranean mussel (Mytilus galloprovincialis) haemocytes against pathogen-associated molecular patterns and bacteria'. *Fish and Shellfish Immunology* 26 (3), pp. 515–523. DOI: 10.1016/j.fsi.2009.02.001.

Cúenot, L. (1891). 'Etudes sur le sang et les glandes lymphatiques dans la serie animale (2e partie: Invertebres)'. *Archives de zoologie expérimentale et générale* 19 (1), pp. 19–54.

D'Agostini, F. and S. La Maestra (2021). 'Micronuclei in Fish Erythrocytes as Genotoxic Biomarkers of Water Pollution: An Overview'. *Reviews of Environmental Contamination and Toxicology Volume 258*. Ed. by P. de Voogt. Springer International Publishing. Chap. 7, pp. 195–240. DOI: 10.1007/398_2021_76.

Dang, X., Q. Huang, Y.Q. He et al. (2023). 'Ocean acidification drives gut microbiome changes linked to species-specific immune defence'. *Aquatic Toxicology* 256 (106413). DOI: https://doi.org/10.1016/j.aquatox.2023.106413.

Darzynkiewicz, Z., B. Bedner and F. Traganos (2001). 'Difficulties and pitfalls in analysis of apoptosis'. *Cytometry*. Vol. 63. Methods in Cell Biology. Academic Press. Chap. 24, pp. 527–546. DOI: https://doi.org/10.1016/S0091-679X(01)63028-0.

Davies, I.M. and D. Vethaak (2012). *Integrated marine environmental monitoring of chemicals and their effects*. ICES Cooperative Research Report (CRR) 315. ICES, pp. 71–83. DOI: https://doi.org/10.17895/ices.pub.5403.

de la Ballina, N.R., F. Maresca, A. Cao et al. (2022). 'Bivalve Haemocyte Subpopulations: A Review'. *Frontiers in Immunology* 13, pp. 1–28. DOI: 10.3389/fimmu.2022.826255.

Del Bino, G., Z. Darzynkiewicz, C. Degraef et al. (1999). 'Comparison of methods based on annexin-V binding, DNA content or TUNEL for evaluating cell death in HL-60 and adherent MCF-7 cells'. *Cell Proliferation* 32 (1), pp. 25–37. DOI: https://doi.org/10.1046/j.1365-2184.1999.3210025.x.

Di, L. and E.H. Kerns (2016). 'Chapter 27 - Transporter Methods'. *Drug-Like Properties (Second Edition)*. Ed. by L. Di and E.H. Kerns. Second Edition. Boston: Academic Press, pp. 339–350.

Dyrynda, E.A., R.J. Law, P.E.J. Dyrynda et al. (2000). 'Changes in immune parameters of natural mussel Mytilus edulis populations following a major oil spill ('Sea Empress', Wales, UK)'. *Marine Ecology Progress Series* 206, pp. 155–170. DOI: 10.3354/meps206155.

Dyrynda, E.A., R.K. Pipe, G.R. Burt et al. (1998). 'Modulations in the immune defences of mussels (Mytilus edulis) from contaminated sites in the UK'. *Aquatic Toxicology* 42 (3), pp. 169–185. DOI: https://doi.org/10.1016/S0166-445X(97)00095-7.

Eastmond, D.A. (2012). 'Factors influencing mutagenic mode of action determinations of regulatory and advisory agencies'. *Mutation Research/Reviews in Mutation Research* 751 (1), pp. 49–63. DOI: https://doi.org/10.1016/j.mrrev.2012.04.001.

Eastmond, D.A., A. Hartwig, D. Anderson et al. (2009). 'Mutagenicity testing for chemical risk assessment: update of the WHO/IPCS Harmonized Scheme'. *Mutagenesis* 24 (4), pp. 341–349. DOI: 10.1093/mutage/gep014.

ECHA (2017). *Guidance on Information Requirements and Chemical Safety Assessment*. Endpoint specific guidance. Version 6.0. European Chemical Agency. Chap. R.7a, pp. 575, 606. DOI: 10.2823/337352.

Elfer, K.N., A.B. Sholl, M. Wang et al. (2016). 'DRAQ5 and eosin ('D&E') as an analog to hematoxylin and eosin for rapid fluorescence histology of fresh tissues'. *PLoS ONE* 11 (10). DOI: https://doi.org/10.1371/journal.pone.0165530.

Ericson, J.A., N.L.C. Ragg and A. Rolton (2021). 'Flow cytometric validation of a commercial kit to assess the concentration and viability of bivalve hemocytes'. *Fish and Shellfish Immunology* 119, pp. 452–455. DOI: 10.1016/j.fsi.2021.10.030.

Fadok, V., D.R. Voelker, P.A. Campbell et al. (1992). 'Exposure of phosphatidylserine on the surface of apoptotic lymphocytes triggers specific recognition and removal by macrophages.' *Journal of immunology* 148 7, pp. 2207–16.

Fenech, M. (2007). 'Cytokinesis-block micronucleus cytome assay'. *Nat Protoc* 2, pp. 1084–1104. DOI: https://doi.org/10.1038/nprot.2007.77.

Fenech, M. and J.W. Crott (2002). 'Micronuclei, nucleoplasmic bridges and nuclear buds induced in folic acid deficient human lymphocytes—evidence for breakage–fusion-bridge cycles in the cytokinesis-block micronucleus assay'. *Mutation Research/Fundamental and Molecular Mechanisms of Mutagenesis* 504 (1), pp. 131–136. DOI: https://doi.org/10.1016/S0027-5107(02)00086-6.

Fenech, M., M. Kirsch-Volders, A.T. Natarajan et al. (2011). 'Molecular mechanisms of micronucleus, nucleoplasmic bridge and nuclear bud formation in mammalian and human cells'. *Mutagenesis* 26 (1), pp. 125–132. DOI: 10.1093/mutage/geq052.

Fisher, W.S. (1988). 'Flow cytometry: a tool for cell research in bivalve pathology'. *Disease processes in marine bivalve molluscs*. Ed. by W.S. Fisher. Vol. 18. Bethesda, Maryland: American Fisheries Society, pp. 286–292.

Friebel, B. and L. Renwrantz (1995). 'Application of density gradient centrifugation for separation of eosinophilic and basophilic hemocytes from Mytitus edulis and characterization of both cell groups'. *Comp. Biochem. Physiol* 112 (1), pp. 81–90. DOI: https://doi.org/10.1016/0300-9629(95)00086-M.

Fries, C.R. and M.R. Tripp (1980). 'Depression of phagocytosis in mercenaria following chemical stress'. *Developmental & Comparative Immunology* 4, pp. 233–244. DOI: https://doi.org/10.1016/S0145-305X(80)80027-9.

Grandiosa, R., M.L. Bouwman, T. Young et al. (2018). 'Effect of antiaggregants on the in vitro viability, cell count and stability of abalone (Haliotis iris) haemocytes'. *Fish & Shellfish Immunology* 78, pp. 131–139. DOI: https://doi.org/10.1016/j.fsi.2018.04.038.

Gustafson, L.L., M. Stoskopf, A.E. Bogan et al. (2005). 'Evaluation of a nonlethal technique for hemolymph collection in Elliptio complanata, a freshwater bi-

valve (Mollusca: Unionidae)'. *Diseases of aquatic organisms* 65 (2), pp. 159–165. DOI: 10.3354/dao065159.

Halligan, D.L. (2006). 'Ubiquitous selective constraints in the Drosophila genome revealed by a genome-wide interspecies comparison'. *Genome Res* 16 (7), pp. 875–884. DOI: 10.1101/gr.5022906.

Hanahan, D. and R.A. Weinberg (2011). 'Hallmarks of cancer: the next generation'. *Cell* 144 (5), pp. 646–74. DOI: 10.1016/j.cell.2011.02.013.

Harr, H. (2005). 'The genetic theory of adaptation: a brief history'. *Nat Rev Genet* 6, pp. 119–127. DOI: https://doi.org/10.1038/nrg1523.

Heddle, J.A., M. Hite, B. Kirkhart et al. (1983). 'The induction of micronuclei as a measure of genotoxicity: A report of the U.S. environmental protection agency Gene-Tox program'. *Mutation Research/Reviews in Genetic Toxicology* 123 (1), pp. 61–118. DOI: https://doi.org/10.1016/0165-1110(83)90047-7.

Hine, P.M. (1999). 'The inter-relationships of bivalve haemocytes'. *Fish & Shellfish Immunology* 9 (5), pp. 367–385. DOI: https://doi.org/10.1006/fsim.1998.0205.

Jiang, L., R. Tixeira, S. Caruso et al. (2016). 'Monitoring the progression of cell death and the disassembly of dying cells by flow cytometry'. *Nature Protocols* 11 (4), pp. 655–663. DOI: 10.1038/nprot.2016.028.

Kaneshiro, Edna S., Michael A. Wyder, Yi-Ping Wu et al. (1993). 'Reliability of calcein acetoxy methyl ester and ethidium homodimer or propidium iodide for viability assessment of microbes'. *Journal of Microbiological Methods* 17 (1), pp. 1–16. DOI: https://doi.org/10.1016/S0167-7012(93)80010-4.

Kari, S., K. Subramanian, I.A. Altomonte et al. (Aug. 2022). *Programmed cell death detection methods: a systematic review and a categorical comparison*. DOI: 10.1007/s10495-022-01735-y.

Koegl, M., C. Weiß and L. Zigan (2020). 'Fluorescence spectroscopy for studying evaporating droplets using the dye eosin-y'. *Sensors (Switzerland)* 20 (21), pp. 1–16. DOI: 10.3390/s20215985.

Köhler, S. and W.D. Stein (2003). 'Optimizing chemotherapy by measuring reversal of P-glycoprotein activity in plasma membrane vesicles'. *Biotechnology and Bioengineering* 81 (5), pp. 507–517. DOI: https://doi.org/10.1002/bit.10488.

Le Foll, F., D. Rioult, S. Boussa et al. (2010). 'Characterisation of Mytilus edulis hemocyte subpopulations by single cell time-lapse motility imaging'. *Fish and Shellfish Immunology* 28 (2), pp. 372–386. DOI: https://doi.org/10.1016/j.fsi.2009.11.011.

Liminga, G., P. Nygren, S. Dhar et al. (1995). 'Cytotoxic effect of calcein acetoxymethyl ester on human tumor cell lines: drug delivery by intracellular trapping'. *Anti-cancer Drugs* 6 (4), pp. 578–585. DOI: 10.1097/00001813-199508000-00011.

Luckenbach, T. and D. Epel (2008). 'ABCB- and ABCC-type transporters confer multixenobiotic resistance and form an environment-tissue barrier in bivalve

gills'. *American Journal of Physiology-Regulatory, Integrative and Comparative Physiology* 294 (6), pp. 1919–1929. DOI: 10.1152/ajpregu.00563.2007.

Luedeking, A., C.J.F. Van Noorden and A. Koehler (2005). 'Identification and characterisation of a multidrug resistance-related protein mRNA in the blue mussel Mytilus edulis'. *Marine Ecology Progress Series* 286, pp. 167–175.

Lynch, A.M. and J.M. Parry (1993). 'The cytochalasin-B micronucleus/kinetochore assay in vitro: Studies with 10 suspected aneugens'. *Mutation Research/Fundamental and Molecular Mechanisms of Mutagenesis* 287 (1), pp. 71–86. DOI: https://doi.org/10.1016/0027-5107(93)90146-7.

Mangan, S., R.W. Wilson, H.S. Findlay et al. (2019). 'Acid-base physiology over tidal periods in the mussel Mytilus edulis: size and temperature are more influential than seawater pH'. *Proc. Biol. Sci.* 1897 (286), p. 20182863. DOI: 10.1098/rspb.2018.2863.

Martin, S.J., C.P. Reutelingsperger, A.J. McGahon et al. (1995). 'Early redistribution of plasma membrane phosphatidylserine is a general feature of apoptosis regardless of the initiating stimulus: inhibition by overexpression of Bcl-2 and Abl.' *Journal of Experimental Medicine* 182 (5), pp. 1545–1556. DOI: 10.1084/jem.182.5.1545.

Mateo, D.R., A. Spurmanis, A. Siah et al. (2009). 'Changes induced by two strains of Vibrio splendidus in haemocyte subpopulations of Mya arenaria, detected by flow cytometry with LysoTracker'. *Diseases of Aquatic Organisms* 86 (3), pp. 253–262. DOI: 10.3354/dao02121.

Meng, X., F. Li, X. Wang et al. (2020). 'Toxicological effects of graphene on mussel Mytilus galloprovincialis hemocytes after individual and combined exposure with triphenyl phosphate'. *Marine Pollution Bulletin* 151, p. 110838. DOI: https://doi.org/10.1016/j.marpolbul.2019.110838.

Merck (2020). *Hemacolor Rapid staining of blood smear*. URL: https://www.sigmaaldrich.com/deepweb/assets/sigmaaldrich/product/documents/384/887/111956-en.pdf (visited on 15/04/2023).

Minier, C. and M.N. Moore (1998). 'Calcein accumulation in mussel blood cells'. *Marine Environmental Research* 46 (1), pp. 425–428. DOI: https://doi.org/10.1016/S0141-1136(97)00076-7.

Mitelman, F. (1983). 'Catalogue of chromosome aberrations in cancer'. *Cytogenet. Cell Genet.* 36 (1-2), pp. 1–515. DOI: 10.1159/000131930.

Mohrenweiser, H.W. (1991). 'Germinal mutations and human genetic disease'. *Genetic Toxicology*. Ed. by A.P. Li and R.H. Heflich. Boca Raton: CRC Press. Chap. 4, pp. 67–92.

Molecular Probes (2005). *LIVE/DEAD Viability/Cytotoxicity Kit *for mammalian cells**. URL: https://tools.thermofisher.com/content/sfs/manuals/mp03224.pdf (visited on 23/07/2022).

Moore, M.N. and D.M. Lowe (1977). 'The cytology and cytochemistry of the hemocytes of Mytilus edulis and their responses to experimentally injected carbon particles'. *Journal of Invertebrate Pathology* 29 (1), pp. 18–30. DOI: https://doi.org/10.1016/0022-2011(77)90167-7.

Nakagawa, S. and H. Schielzeth (2013). 'A general and simple method for obtaining R2 from generalized linear mixed-effects models'. *Methods in Ecology and Evolution* 4 (2), pp. 133–142. DOI: https://doi.org/10.1111/j.2041-210x.2012.00261.x.

Natarajan, A.T. (1993). 'An overview of the results of testing of known or suspectec aneugens using mammalian cells in vitro'. *Mutation Research/Fundamental and Molecular Mechanisms of Mutagenesis* 287 (1), pp. 113–118. DOI: https://doi.org/10.1016/0027-5107(93)90150-E.

Nescerecka, A., F. Hammes and T. Juhna (Dec. 2016). 'A pipeline for developing and testing staining protocols for flow cytometry, demonstrated with SYBR Green I and propidium iodide viability staining'. *Journal of Microbiological Methods* 131, pp. 172–180. DOI: 10.1016/j.mimet.2016.10.022.

Nöel, D., R. Pipe, R. Elston et al. (1994). 'Antigenic characterization of hemocyte subpopulations in the mussel Mytilus edulis by means of monoclonal antibodies'. *Marine Biology* (119), pp. 549–556. DOI: https://doi.org/10.1007/BF00354317.

OECD (2016a). *Test No. 474: Mammalian Erythrocyte Micronucleus Test*, p. 21. DOI: https://doi.org/https://doi.org/10.1787/9789264264762-en. URL: https://www.oecd-ilibrary.org/content/publication/9789264264762-en.

OECD (2016b). *Test No. 487: In Vitro Mammalian Cell Micronucleus Test*, p. 29. DOI: https://doi.org/https://doi.org/10.1787/9789264264861-en. URL: https://www.oecd-ilibrary.org/content/publication/9789264264861-en.

OSPAR (2002). *Survey on genotoxicity test methods for the evaluation of waste water within whole effluent assessment*. Tech. rep. OSPAR Comission.

Pila, E.A., J.T. Sullivan, X.Z. Wu et al. (2016). 'Haematopoiesis in molluscs: A review of haemocyte development and function in gastropods, cephalopods and bivalves'. *Developmental and Comparative Immunology* 58, pp. 119–128. DOI: 10.1016/j.dci.2015.11.010.

Pipe, R.K, J.A. Coles, F.M.M Carissan et al. (1999). 'Copper induced immunomodulation in the marine mussel, Mytilus edulis'. *Aquatic Toxicology* 46 (1), pp. 43–54. DOI: https://doi.org/10.1016/S0166-445X(98)00114-3.

Pipe, R.K. (1990). 'Differential binding of leetins to haemocytes of the mussel Mytilus edulis'. *Cell Tissue Res* (261), pp. 261–268. DOI: https://doi.org/10.1007/BF00318667.

Pipe, R.K. and J.A. Coles (1995). 'Environmental contaminants influencing immune function in marine bivalve molluscs'. *Fish & Shellfish Immunology* 1995, pp. 581–595. DOI: https://doi.org/10.1016/S1050-4648(95)80043-3.

Pipe, R.K., S.R. Farley and J.A. Coles (1997). 'The separation and characterisation of haemocytes from the mussel Mytilus edulis'. *Cell tissue Res.* 289 (3), pp. 537–545. DOI: 10.1007/s004410050899.

R Core Team (2021). *R: A Language and Environment for Statistical Computing*. R Foundation for Statistical Computing. Vienna, Austria. URL: https://www.R-project.org/.

Ramirez, C.N. and C. Antczak (2010). 'Cell viability assessment: toward content-rich platforms'. *Expert Opinion on Drug Discovery* 5 (3), pp. 223–233. DOI: 10.1517/17460441003596685.

Rasmussen, L.P.D., E. Hage and O. Karloc (1985). 'An Electron Microscope Study of the Circulating Leucocytes of the Marine Mussel, Mytilus edulis'. *JOURNAL OF INVERTEBRATE PATHOLOGY* 45, pp. 158–167. DOI: https://doi.org/10.1016/0022-2011(85)90005-9.

Renwrantz, L. (1990). 'Internal defence system of Mytilus edulis'. *Neurobiology of Mytilus edulis*. Ed. by GB Stefano. Manchester and New York: Manchester University Press. Chap. 15, pp. 256–275.

Rioult, D., J. Pasquier, C. Boulangé-Lecomte et al. (2014). 'The multi-xenobiotic resistance (MXR) efflux activity in hemocytes of Mytilus edulis is mediated by an ATP binding cassette transporter of class C (ABCC) principally inducible in eosinophilic granulocytes'. *Aquatic Toxicology* 153, pp. 98–109. DOI: https://doi.org/10.1016/j.aquatox.2013.11.012.

Ritz, C, F Baty, J.C Streibig et al. (2015). 'Dose-Response Analysis Using R'. *PLOS ONE* 10 (e0146021) (12). DOI: https://doi.org/10.1371/journal.pone.0146021.

Rocha, T.L., T. Gomes, C. Cardosa et al. (2014). 'Immunocytotoxicity, cytogenotoxicity and genotoxicity of cadmium-based quantum dots in the marine mussel Mytilus galloprovincialis'. *Marine Environmental Research* 101, pp. 29–37. DOI: https://doi.org/10.1016/j.marenvres.2014.07.009.

RStudio Team (2021). *RStudio: Integrated Development Environment for R*. RStudio, PBC. Boston, MA. URL: http://www.rstudio.com/.

Shabenberger, O. and F.J. Pierce (2001). 'Contemporary Statistical Models for the Plant and Soil Sciences'. 1st ed. Boca Raton: CRC Press. Chap. 5.

Shapiro, H.M. (2003). *Practical Flow Cytometry*. John Wiley & Sons, Inc. Chap. 10, pp. 462–464. DOI: 10.1002/0471722731.

Shapiro, H.M. (2004). 'The Evolution of Cytometers'. *Cytometry Part A* 58 (1), pp. 13–20. DOI: https://doi.org/10.1002/cyto.a.10111.

Smith, V.J., A. Accorsi and D. Malagoli (2016). 'Hematopoiesis and Hemocytes in Pancrustacean and Molluscan Models'. *The Evolution of the Immune System: Conservation and Diversification*. Ed. by Davide Malagoli. Elsevier Inc., pp. 1–28.

Söderhäll, K. and V.J. Smith (1983). 'Separation of the haemocyte populations of Carcinus Maenas and other marine decapods, and prophenoloxidase distribution'. *Developmental & Comparative Immunology* 7 (2), pp. 229–239. DOI: 10.1016/0145-305x(83)90004-6.

Suzuki, J., D.P. Denning, E. Imanishi et al. (2013). 'Xk-Related Protein 8 and CED-8 Promote Phosphatidylserine Exposure in Apoptotic Cells'. *Science* 341 (6144), pp. 403–406. DOI: 10.1126/science.1236758.

Tiberghien, F. and F. Loor (1996). 'Ranking of P-glycoprotein substrates and inhibitors by a calcein-AM fluorometry screening assay'. *Anti-cancer Drugs* 7 (5), pp. 568–578. DOI: 10.1097/00001813-199607000-00012.

Torreilles, J., M.C. Guérin and P. Roch (1999). 'Modified Alsever's solution is not a good medium for reactive oxygen metabolite study in bivalves'. *Fish & Shellfish Immunology* 9 (1), pp. 65–69. DOI: https://doi.org/10.1006/fsim.1998.0167.

Tucker, J.D. and R.J. Preston (1996). 'Chromosome aberrations, micronuclei, aneuploidy, sister chromatid exchanges, and cancer risk assessment'. *Mutation Research/Reviews in Genetic Toxicology* 365 (1), pp. 147–159. DOI: https://doi.org/10.1016/S0165-1110(96)90018-4.

UNEP (2006). 'Manual on the biomarkers reccomended for the MED POL biomonitoring programme'. URL: https://api.semanticscholar.org/CorpusID:32084494.

USEPA (May 1998). *Health Effects Test Guidelines OPPTS 870.5395 Mammalian Erythrocyte Micronucleus Test*. Tech. rep. 712C98226. Washington, D.C.: Office of Prevention, Pesticides and Toxic Substances. URL: https://nepis.epa.gov/Exe/ZyPURL.cgi?Dockey=P100IRUF.txt.

Van Engeland, M., L.J.W. Nieland, F.C.S. Ramaekers et al. (1998). 'Annexin V-Affinity Assay: A Review on an Apoptosis Detection System Based on Phosphatidylserine Exposure'. *Cytometry* 31, pp. 1–9.

Van Nguyen, T. and A.C. Alfaro (2019). 'Applications of flow cytometry in molluscan immunology: Current status and trends'. *Fish & Shellfish Immunology* 94, pp. 239–248. DOI: https://doi.org/10.1016/j.fsi.2019.09.008.

Venier, P., S. Maron and S. Canova (1997). 'Detection of micronuclei in gill cells and haemocytes of mussels exposed to benzo[a]pyrene'. *Mutation Research/-Genetic Toxicology and Environmental Mutagenesis* 390 (1), pp. 33–44. DOI: https://doi.org/10.1016/S0165-1218(96)00162-0.

Verhoven, B., R.A. Schlegel and P. Williamson (1995). 'Mechanisms of phosphatidylserine exposure, a phagocyte recognition signal, on apoptotic T lymphocytes.' *Journal of Experimental Medicine* 182 (5), pp. 1597–1601. DOI: 10.1084/jem.182.5.1597.

Viarengo, A. and L. Canesi (1991). 'Mussels as biological indicators of pollution'. *Aquaculture* 94 (2), pp. 225–243. DOI: https://doi.org/10.1016/0044-8486(91)90120-V.

Wallach, D.F.H., D.M. Surgenor, J. Soderberg et al. (1959). 'Preparation and Properties of 3,6-Dihydroxy-2,4-bis-[N-N´-di-(carboxymethyl)-aminomethyl] fluoran'. *Anal. Chem.* 31 (2), pp. 456–460. DOI: https://doi.org/10.1021/ac60147a041.

Wang, Q., R. Cao, X. Ning et al. (2016). 'Effects of ocean acidification on immune responses of the Pacific oyster Crassostrea gigas'. *Fish & Shellfish Immunology* 49, pp. 24–33. DOI: https://doi.org/10.1016/j.fsi.2015.12.025.

Warheit, D.B (2018). 'Genetic toxicology'. *Casarett and Doull´s Toxicology: The basic science of poisons (9th ed.)* Ed. by C. Klaasen. New York: McGraw-Hill Education. Chap. 9, pp. 1381–1429.

Wootton, E.C., E.A. Dyrynda and N.A. Ratcliffe (2003). 'Bivalve immunity: comparisons between the marine mussel (Mytilus edulis), the edible cockle (Cerastoderma edule) and the razor-shell (Ensis siliqua)'. *Fish & Shellfish Immunology* 15 (3), pp. 195–210. DOI: https://doi.org/10.1016/S1050-4648(02)00161-4.

Worsley, C.M., R.B. Veale and E.S. Mayne (2022). 'Inducing apoptosis using chemical treatment and acidic pH, and detecting it using the Annexin V flow cytometric assay'. *PLOS ONE* 17 (6). DOI: 10.1371/journal.pone.0270599.

Zeng, Yangqing, Yuanzi Huo and Huiping Yang (2021). 'Immunological assays of hemocytes in the Northern Quahog Mercenaria mercenaria'. *Fish & Shellfish Immunology* 118, pp. 261–269. ISSN: 1050-4648. DOI: https://doi.org/10.1016/j.fsi.2021.09.006.

Zhang, C.Z. and D. Pellman (2015). 'From Mutational Mechanisms in Single Cells to Mutational Patterns in Cancer Genomes'. *Cold Spring Harb Symp Quant Biol* 80, pp. 117–137. DOI: 10.1101/sqb.2015.80.027623.

Appendix A

Additional Material

A.1 R Code listings from statistical models

Code Listing A.1: R source code run to fit the proportion aggregation GLMM in RStudio.

```
model = glmer(data = df, formula = y ~ log(t)*Buffer + (log(t)|ID),
                 family = binomial(link = "logit"))
```

Code Listing A.2: R source code run to fit the four-parameter log-logistic regression model in RStudio.

```
model = drm(y ~ x, data = df, fct = LL.4(fixed = c(NA, 0, NA, NA),
names = c("b", "c", "d", "e")))
```

A.2 Staining procedure for flow cytometric dyes

During all staining procedure with Calcein AM, TO-PRO^{TM}-3 Iodide and Apo-15, the dyes were transferred to 1.5 mL Eppendorf tubes with conical bottoms prior to mixing with diluted haemolymph samples. In this way, the dyes were mixed faster with haemolymph samples upon transfer of the latter to Eppendorf tubes. While transferring haemolymph to Eppendorf tubes, the whole suspension (haemolymph + dyes) was pipetted gently back up and down three times to ensure thorough and fast mixing. 1000 µL pipette tips where used for this purpose, since they are relatively wide-bored.

A.3 Haemocyte gating strategy

The two-step gating strategy for identification of singlet heamocytes are presented in Figure A.1. This gating strategy were used in all flow cytometric assays, where

subsequent analyses of fluorescence markers (Eosin Y, Calcein AM, Apo-15 and TO-PRO^{TM}-3 Iodide) were continued with events included in the haemocyte gate (see Figure A.1C).

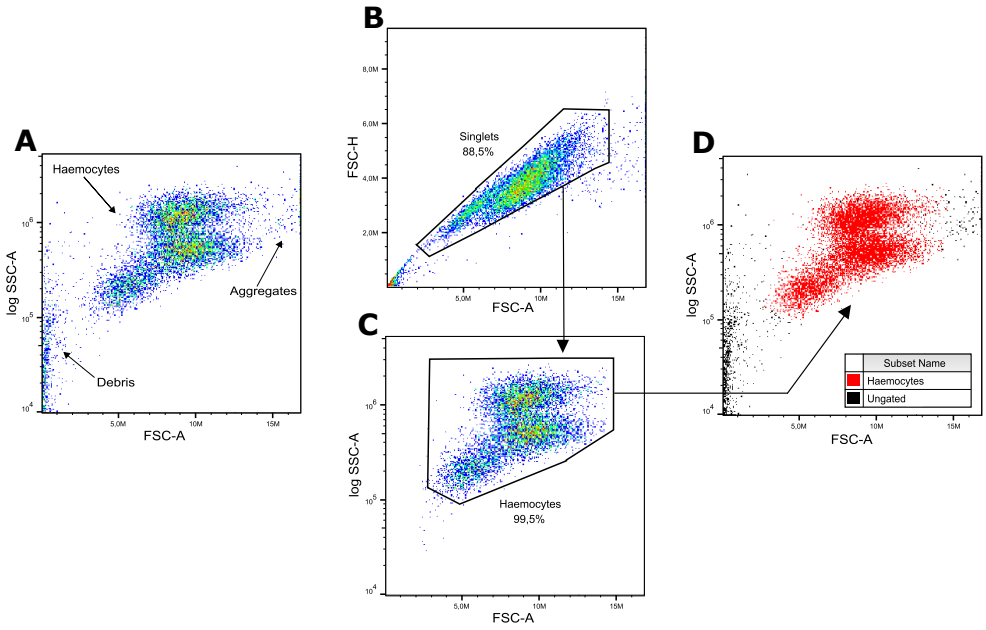

Figure A.1: Gating strategy for identification of haemocytes according to FSC-A vs. vs. log SSC-A. (A) Ungated sample with debris, haemocytes and aggregates.**(B)** Debris and aggregates were excluded from analysis by gating on haemocytes according to a doublet exclusion gate (FSC-A vs. FSC-H). **(C)** Remaining debris were separated from singlet heamocytes according a haemocyte gate (FSC-A vs. log SSC-A). **(D)** Singlet heamocytes are displayed in red.

A.4 Flow cytometry software and instrument settings

Table A.1: Acquisition and fluidics settings specified with the BD Accuri C6 Plus acquisition software during flow cytometric assays.

Assay	**Trigger threshold**	**Acquisition stop-condition**	**Flow rate** (µL/min)	**Core size** (µm)
Aggregation	80.000 FSC-H	acquired volume, 20 µL	30	10
Calcein/ToPro3	80.000 FSC-H	Haemocyte events, 10.000	36	16
Apo-15/ToPro3	80.000 FSC-H	Haemocyte events, 10.000	36	16

A.5 Epifluorescence imaging of haemocytes stained with Eosin Y

Since Eosin Y is fluorescent in the green/yellow spectrum, eosinophilic granulocytes were distinguished from the two basophilic cell types according to 488-nm exited fluorescence and SSC. To illustrate what the flow cytometer "sees", haemocyte preparations stained with 0.5% Eosin Y and 3% Giemsa were imaged by epifluorescence microscopy with a long-pass B2A filtercube (exposure: 250 msec; gain: 3.4). As demonstrated in Figure A.2, the eosinophilic granulocytes emitted bright fluorescent signals ($\lambda \geq 515$ nm), while the basophilic cells are barely visible in the epifluorescence image (A.2).

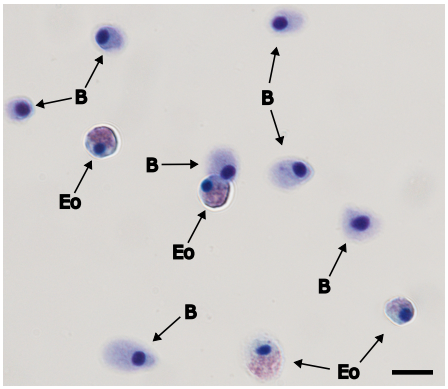

(a) Hemocytes imaged under brightfield illumination.

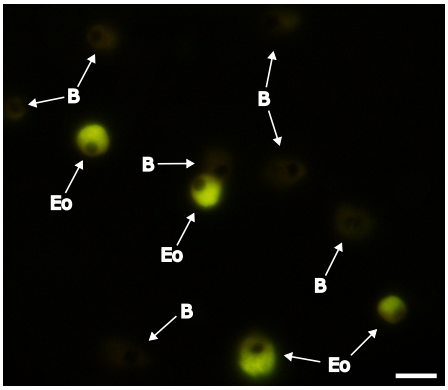

(b) Haemocytes imaged by epifluorescence microscopy with a B-2A filtercube.

Figure A.2: Eosinophilic granulocytes are distinguished from the two basophilic cell types according to eosin fluorescence ($\geq$ 515 nm). Formaldehyde-fixed haemocytes stained in 0.5% eosin and 3% Giemsa were imaged at ×60 magnification under **a)** brightfield illumination and **b)** by epifluorescence microscopy with a B-2A filter cube. The slide was mounted with Eukitt® and coverslipped prior to microscopy. Eo: eosinophilic granulocyte; B: basophilic haemocyte; scale bars = 10 µm.

A.6 4-parameter log-logistic model parameter estimates

Table A.2: Log-logistic regression analysis of the relationship between TO-PRO^{TM}-3 Iodide concentration and the difference in median fluorescent intensity (MFI) between ToPro3^{-} and ToPro3^{-} populations. Parameter estimates with 95% CI, standard errors, t-value and the belonging p-value.

Parameter	**Estimate**	**95% CI**	**S.E.**	**t-value**	**Pr(T > | t |)**
b	-0.94088	[-1.182762, -0.6989903]	0.11	-8.7992	< 0.0001
d	9890700	[8701569, 11079860]	530000	18.8155	< 0.0001
e	0.41655	[0.2622887, 0.5708113]	0.068	6.10085	0.0001

Pseudo $R^2 = 0.99^a$
Residual standard error: 416074.3 on 9 degrees of freedom

[a]Calculated according to Shabenberger and Pierce, 2001.

Appendix B

Raw data

Table B.1: Haemocyte proportion of aggregation raw data.

Mussel ID	Buffer	t (min)	N_{tx}	N_{t0}
1	MAS	0.000001	36877	36877
1	MAS	15	23728	36877
1	MAS	45	13479	36877
1	MAS	60	5209	36877
2	MAS	0.000001	25544	25544
2	MAS	15	17570	25544
2	MAS	45	8195	25544
2	MAS	60	5060	25544
3	MAS	0.000001	24381	24381
3	MAS	15	21462	24381
3	MAS	45	9347	24381
3	MAS	60	8525	24381
4	MAS	0.000001	27327	27327
4	MAS	15	26100	27327
4	MAS	30	22529	27327
4	MAS	60	8333	27327
5	MAS	0.000001	12889	12889
5	MAS	15	10605	12889
5	MAS	30	8146	12889
5	MAS	60	3450	12889
6	MAS	0.000001	2519	2519
6	MAS	45	2107	2519
6	MAS	60	1627	2519
7	MAS	0.000001	4131	4131
7	MAS	45	2622	4131
7	MAS	60	2149	4131
8	MAS	0.000001	43469	43469

Continued on next page

Table B.1 – continued from previous page

Mussel ID	Buffer	t (min)	N_{tx}	N_{t0}
8	MAS	15	36442	43469
8	MAS	30	35465	43469
8	MAS	45	30743	43469
8	MAS	60	20399	43469
9	ACB	0.000001	14829	14829
9	ACB	15	13764	14829
9	ACB	30	8520	14829
9	ACB	60	4579	14829
10	ACB	0.000001	48859	48859
10	ACB	15	44741	48859
10	ACB	30	31079	48859
10	ACB	60	11281	48859
11	ACB	0.000001	10140	10140
11	ACB	15	8912	10140
11	ACB	30	5353	10140
11	ACB	45	3681	10140
12	ACB	0.000001	16736	16736
12	ACB	15	11449	16736
12	ACB	30	8935	16736
12	ACB	45	5145	16736
13	ACB	0.000001	31027	31027
13	ACB	15	25305	31027
13	ACB	30	22889	31027
13	ACB	45	15348	31027
13	ACB	60	12203	31027
14	ACB	0.000001	25449	25449
14	ACB	15	22438	25449
14	ACB	30	20068	25449
14	ACB	45	16712	25449
14	ACB	60	9246	25449
15	ACB	0.000001	5117	5117
15	ACB	15	4128	5117
15	ACB	30	3415	5117
15	ACB	45	2541	5117
15	ACB	60	2016	5117
16	ACB	0.000001	22176	22176
16	ACB	15	20947	22176
16	ACB	30	20189	22176
16	ACB	45	18893	22176
16	ACB	60	16102	22176
17	MPSS	0.000001	2447	2447

Continued on next page

Table B.1 – continued from previous page

Mussel ID	Buffer	t (min)	N_{tx}	N_{t0}
17	MPSS	15	823	2447
17	MPSS	30	887	2447
17	MPSS	45	972	2447
17	MPSS	60	798	2447
18	MPSS	0.000001	2645	2645
18	MPSS	15	1693	2645
18	MPSS	30	1779	2645
18	MPSS	45	1438	2645
18	MPSS	60	1419	2645
19	MPSS	0.000001	2377	2377
19	MPSS	15	1318	2377
19	MPSS	30	1064	2377
19	MPSS	45	862	2377
19	MPSS	60	659	2377
20	MPSS	0.000001	2879	2879
20	MPSS	15	1624	2879
20	MPSS	30	1617	2879
20	MPSS	45	1049	2879
20	MPSS	60	1120	2879
21	MPSS	0.000001	3151	3151
21	MPSS	15	1445	3151
21	MPSS	30	1125	3151
21	MPSS	45	984	3151
21	MPSS	60	414	3151
22	MPSS	0.000001	1699	1699
22	MPSS	15	1080	1699
22	MPSS	30	733	1699
22	MPSS	45	811	1699
22	MPSS	60	715	1699
23	MPSS	0.000001	3309	3309
23	MPSS	15	1634	3309
23	MPSS	30	1453	3309
23	MPSS	45	1415	3309
23	MPSS	60	1393	3309
24	MPSS	0.000001	2822	2822
24	MPSS	15	1460	2822
24	MPSS	30	1518	2822
24	MPSS	45	1475	2822
24	MPSS	60	1346	2822

Table B.2: Haemocyte buffer viability raw data.

Buffer	Incubation	Count			
		CAM^+ $TP3^-$	CAM^+ $TP3^+$	CAM^-TP3^+	CAM^- $TP3^-$
ACB	15 min	9712	4	8	15
ACB	15 min	9723	13	5	4
ACB	15 min	9574	7	6	1
ACB	15 min	9382	11	17	8
ACB	15 min	9779	24	5	3
ACB	15 min	9735	4	10	38
ACB	15 min	9746	3	9	9
ACB	15 min	9743	10	10	23
MPSS	15 min	7707	3	5	4
MPSS	15 min	6622	3	8	5
MPSS	15 min	5748	8	20	3
MPSS	15 min	10040	0	30	57
MPSS	15 min	9937	1	13	49
MPSS	15 min	9929	2	24	45
MPSS	15 min	9950	0	32	18
MPSS	15 min	9970	2	15	13
MAS	15 min	8600	1	15	8
MAS	15 min	9033	0	30	5
MAS	15 min	8340	1	9	7
MAS	15 min	8633	0	7	12
MAS	15 min	7901	2	17	3
MAS	15 min	8863	0	10	1
MAS	15 min	9133	3	17	2
MAS	15 min	8929	0	12	12
ACB	2 hours	9457	4	62	252
ACB	2 hours	9792	12	67	70
ACB	2 hours	9984	4	58	109
ACB	2 hours	1829	0	16	11
ACB	2 hours	6801	2	21	237
ACB	2 hours	4403	0	17	307
ACB	2 hours	9752	5	86	241
ACB	2 hours	9875	5	34	123
MPSS	2 hours	9276	21	12	56
MPSS	2 hours	6279	14	2	39
MPSS	2 hours	4869	3	3	43
MPSS	2 hours	4680	13	4	414
MPSS	2 hours	6174	4	0	60
MPSS	2 hours	7573	6	5	37
MPSS	2 hours	8131	25	6	103

Continued on next page

Table B.2 – continued from previous page

Buffer	Incubation	Count			
		CAM^+ $TP3^-$	CAM^+ $TP3^+$	CAM^-TP3^+	CAM^- $TP3^-$
MPSS	2 hours	8930	10	0	93
MAS	2 hours	5061	0	28	64
MAS	2 hours	4947	2	39	103
MAS	2 hours	9973	11	62	58
MAS	2 hours	6190	8	14	74
MAS	2 hours	8473	0	21	104
MAS	2 hours	9884	8	64	118
MAS	2 hours	9930	5	22	124
MAS	2 hours	9953	0	28	19
ACB	20 hours	9135	8	541	206
ACB	20 hours	7519	1	1559	341
ACB	20 hours	7383	4	994	594
ACB	20 hours	9668	7	340	285
ACB	20 hours	10054	2	143	134
ACB	20 hours	9103	27	637	118
ACB	20 hours	8198	4	896	234
ACB	20 hours	8174	2	969	328
MPSS	20 hours	9577	29	51	7
MPSS	20 hours	9277	11	371	33
MPSS	20 hours	9651	12	41	11
MPSS	20 hours	9355	22	149	12
MPSS	20 hours	9879	9	59	23
MPSS	20 hours	9736	89	69	56
MPSS	20 hours	9933	2	18	8
MPSS	20 hours	9693	6	158	32
MAS	20 hours	8025	24	523	578
MAS	20 hours	8910	3	382	210
MAS	20 hours	8502	1	453	523
MAS	20 hours	9663	4	370	417
MAS	20 hours	8959	16	1088	607
MAS	20 hours	9640	3	446	467
MAS	20 hours	8537	6	675	309
MAS	20 hours	9237	10	1033	685

Table B.3: Cytotoxicity of acidic buffer pH: raw data.

Mussel ID	Buffer	Count			
		$Apo15^{+}$ $TP3^{+}$	$Apo15^{+}$ $TP3^{-}$	$Apo15^{-}TP3^{+}$	$Apo15^{-}$ $TP3^{-}$
M1	MAS	48	692	0	9088
M2	MAS	26	896	0	8891
M3	MAS	438	722	0	8517
M4	MAS	2313	784	0	7058
M5	MAS	374	382	1	9092
M6	MAS	482	517	0	8956
M7	MAS	278	465	1	9097
M8	MAS	155	442	0	9260
M9	MAS	215	867	0	8538
M10	MAS	154	806	0	8798
M11	MAS	294	496	0	8971
M12	MAS	346	655	0	8942
M13	MAS	18	372	0	9221
M14	MAS	329	1925	0	7777
M15	MAS	260	1708	0	7853
M16	MAS	749	2520	3	6285
M17	MAS	379	346	0	4037
M18	MAS	361	277	1	4200
M19	ACB	28	8	3	9850
M20	ACB	7	9	0	9934
M21	ACB	11	4	0	9944
M22	ACB	15	59	2	9881
M23	ACB	9	5	1	9975
M24	ACB	9	5	4	9939
M25	ACB	6	3	4	9955
M26	ACB	4	22	1	9838
M27	ACB	9	0	1	9745
M28	ACB	9	60	2	8878
M29	ACB	12	5	1	9169
M30	ACB	10	11	0	9697
M31	ACB	35	36	2	8721
M32	ACB	17	26	1	9291
M33	ACB	8	3	0	9853
M34	ACB	15	2	5	9770
M35	ACB	17	3	8	9432
M36	ACB	27	20	12	9747

Table B.4: Raw data from the experimental determination of the optimal range of TO-PRO^{TM}-3 Iodide concentrations for a flow cytometric dye exclusion test of membrane integrity. The table lists the TO-PRO^{TM}-3 concentrations tested (µM), incubation length (min), the mean fluorescent intensity (MFI) of viable (ToPro^{-}) and MeOH-killed haemocytes (ToPro^{+}) and the difference between the two ($MFI_{ToPro3^{+}}$ - $MFI_{ToPro3^{-}}$). Samples were analyzed on a BD Accuri C6 Plus flow cytometer (BD Biosciences, California, US) and MFI's were calculated using FlowJo^{TM} v10.8 Software (BD Life Sciences).

TO-PRO^{TM}-3 Iodide (µM)	Incubation (min)	Mean Fluorescent Intensity ToPro3^{+}	ToPro3^{-}	$MFI_{ToPro3^{+}}$ - $MFI_{ToPro3^{-}}$
0	15	764	554	210
0.03	15	867000	6750	860250
0.06	15	865000	6488	858512
0.1	15	2670000	19378	2650622
0.3	15	3710000	43720	3666280
0.2	15	3750000	41441	3708559
0.6	15	5920000	62519	5857481
0.6	15	5330000	40903	5289097
1.2	15	7700000	103179	7596821
2	15	8550000	298543	8251457
4	15	9240000	352373	8887627
8	15	9550000	456001	9093999
0.1	30	2470000	28374	2441626
0.2	30	3860000	48720	3811280
0.3	30	3640000	68309	3571691
0.6	30	5690000	94568	5595432
0.6	30	5320000	60620	5259380
1.2	30	7580000	155710	7424290
2	30	8710000	486028	8223972
4	30	9410000	577181	8832819
8	30	9670000	713160	8956840

Table B.5: Data set from the parallel determination of percent eosinophilic granulocytes from univariate log Eosin Y fluorescence (533/15 nm) measurements on the BD Accuri C6 Plus flow cytometer (FCM) and by 1000-cell differential counts of Giemsa-smears on a *Nikon Ni-U* upright microscope equipped with a *DeltaPix 4KHDMI* microscope camera.

Mussel ID	Eosinophilic granulocytes (%)	$Eosin^{bright}$ events (%)
M1	54.0	53.4
M2	75.0	71.3
M3	68.9	65.4
M4	67.6	65.2
M5	61.5	61.4
M6	29.4	30.8
M7	19.3	19.7
M8	50.8	51.3
M9	55.6	59.7
M10	54.8	55.2

Table B.6: Validation of flow cytometric differential haemocyte count gating strategy. Raw count data of small blast-like basophils (BB), basophilic granulocytes (BG) and eosinophilic granulocytes (Eo) from 1000-cell 10.000-cell differential haemocyte counts performed by microscopy and flow cytometry (FCM), respectively.

Method	Mussel ID	Count			
		BB	BG	Eo	Total
Microscopy	M1	34	338	629	1001
Microscopy	M2	53	338	687	1078
Microscopy	M3	35	309	732	1076
Microscopy	M4	111	497	523	1131
Microscopy	M5	126	489	385	1000
Microscopy	M6	45	381	597	1023
Microscopy	M7	64	520	416	1000
Microscopy	M8	55	396	549	1000
Microscopy	M9	16	208	776	1000
Microscopy	M10	45	584	371	1000
Microscopy	M11	115	441	444	1000
Microscopy	M12	40	506	454	1000
Microscopy	M13	37	596	367	1000
Microscopy	M14	44	514	442	1000
Microscopy	M15	34	246	720	1000
Microscopy	M16	25	942	60	1027
Microscopy	M17	39	511	450	1000
Microscopy	M18	154	704	218	1076
Microscopy	M19	87	428	485	1000

Continued on next page

Table B.6 – continued from previous page

Method	Mussel ID	Count			
		BB	BG	Eo	Total
Microscopy	M20	9	194	833	1036
FCM	M1	339	3370	6045	9754
FCM	M2	565	3969	5386	9920
FCM	M3	215	3174	6406	9795
FCM	M4	886	4108	4690	9684
FCM	M5	930	5263	3508	9701
FCM	M6	564	3309	5904	9777
FCM	M7	853	5203	3944	10000
FCM	M8	655	4180	5082	9917
FCM	M9	197	2167	7275	9639
FCM	M10	557	6078	3334	9969
FCM	M11	1061	4730	4419	10210
FCM	M12	422	5134	4342	9898
FCM	M13	408	6178	3303	9889
FCM	M14	464	5185	4303	9952
FCM	M15	385	3510	6037	9932
FCM	M16	258	8908	580	9746
FCM	M17	446	5437	4070	9953
FCM	M18	1484	6552	1888	9924
FCM	M19	924	4708	4305	9937
FCM	M20	186	2514	7283	9983

Table B.7: Raw data from epifluorescent microscopy cross-validation of flow cytometric gating strategy for scoring of necrotic haemocytes based TO-PRO^{TM}-3 Iodide (TP3) and Calcein (CAM) fluorescence. Samples were analyzed on a *BD Accuri C6 Plus* flow cytometer and a *Nikon 90i* upright microscope equipped with a *Digital Sight Fi1c* microscope camera. B-2A and LED-Cy5-A filtercubes were used for collection of Calcein and dsDNA-bound TO-PRO^{TM}-3 Iodide fluorescence, respectively.

Scoring method	Slide ID	Count			
		CAM^+ $TP3^-$	CAM^- $TP3^+$	CAM^+TP3^+	CAM^- $TP3^-$
FCM	M1	12056	882	14	8
FCM	M2	8464	1339	53	8
FCM	M3	4670	4926	19	51
FCM	M4	2563	6790	59	73
FCM	M5	1484	8604	32	14
FCM	M6	346	9800	16	15
FCM	M7	4118	5560	9	104
FCM	M8	0	9422	0	10
FCM	M9	10701	5	13	9
FCM	M10	14500	6952	42	34
Microscopy	M1	149	6	0	0
Microscopy	M2	248	45	1	0
Microscopy	M3	68	75	2	0
Microscopy	M4	42	92	0	0
Microscopy	M5	64	295	0	0
Microscopy	M6	5	167	0	0
Microscopy	M7	108	193	2	0
Microscopy	M8	0	247	0	3
Microscopy	M9	252	1	0	4
Microscopy	M10	222	132	0	0